MAINTAINING NITROGEN-LIMITED BALANCED-GROWTH STATES IN A CYCLO-TURBIDOSTAT

By

DYLAN FRANKS

Bachelor of Science in Chemistry & Biochemistry
Colorado School of Mines
Golden, CO
2012

Submitted to the Faculty of the
Graduate College of the
Oklahoma State University
in partial fulfillment of
the requirements for
the Degree of
DOCTOR OF PHILOSOPHY
May 2023

MAINTAINING NITROGEN-LIMITED BALANCED-GROWTH STATES IN A CYCLO-TURBIDOSTAT

Dissertation Approved:

Dr. William Henley

Dissertation Adviser

Dr. Ming Yang

Dr. Rob Burnap

Dr. Andy Dzialowski

ACKNOWLEDGEMENTS

I would like to dedicate this dissertation to my family and fiancé. I could not have endured the tribulations of my doctorate without their love and support.

Name: DYLAN FRANKS

Date of Degree: MAY 2023

Title of Study: MAINTAINING NITROGEN-LIMITED BALANCED-GROWTH STATES IN A CYCLO-TURBIDOSTAT

Major Field: PLANT SCIENCE

Abstract:

This dissertation presents two separate studies on the green microalga *Picochlorum oklahomense*. The first study investigates the minimum nitrogen cell quota required to support maximum growth rate and the effects of nitrogen limitation on cycloturbidostat cultures under steady-state, balanced growth conditions. This study introduces the concept of the threshold of nitrogen cell quota necessary to support maximum growth rate denoted as $Q_{N,T}$. The second study provides empirical evidence of multiple fission in *Picochlorum oklahomense* grown in light-saturated turbidostats and in semi-continuous cultures. We present evidence that *Picochlorum oklahomense* is an autosporic species and produces 2 to 4 daughter cells per mother cell via a multiple fission pathway. Additionally, the paper discusses the utility of turbidostats in experimental phycology and provides an outline of cycloturbidostat fundamentals. Lastly, this dissertation uses unpublished data from preliminary trials to describe potential issues encountered when utilizing cycloturbidostats in the laboratory, particularly in nutrient-limitation studies. The study highlights the importance of microalgae in understanding algal biology and building valuable year-round supply chains.

TABLE OF CONTENTS

Chapter Page

I. Minimum Nitrogen Cell Quota for Maximal Growth Rate in Cycloturbidostat Cultures of *Picochlorum oklahomense* 1

*Introduc*tion.....2
Methods.....5
Results.....11
Discussion.....23
Conclusion 35
Supplemental Figures.....36

II. Evidence of multiple fission in asynchronous continuous cultures of *Picochlorum oklahomense suggest clu*stered rounds of DNA replication.....42

Introduction.....43
Methods.....44
Results.....49
Discussion.....58
Conclusion 64
Supplemental Figures.....64

III. Lessons from the lab: The utility of cycloturbidostats in microalgal biotechnology 70

Introduction.....70
Lessons from repeated cycloturbidostat cultures.....76
Conclusion 85

REFERENCES 86

LIST OF TABLES

Table Page

1 Symbols, equations, and abbreviations.....11
2 Two-Factor ANOVA of morning vs. evening flow cytometry samples.....21
3 Growth summary of semi-continuous growth experiment 52

LIST OF FIGURES

Figure Page

1 Model of steady-state relationship between N cell quota and growth rate 2
2 Growth chronology of $[NO_3]_{inf}$ stepdown study 15
3 N cell quota for different $[NO_3]_{inf}$ treatments; Chl content vs. $Q_{N, cell}$ 16
4 Growth chronology of $[NO_3]_{inf}$ transition study 18
5 Replete vs. limited physiological parameters in replicate cultures 20
6 Comparative flow cytometry characteristics 21
7 Comparative biomass composition in replete and limited cultures 23
8 Merged cytograms showing the spread of phenotypes 28
9 Epifluorescence micrographs showing *P. oklahomense* cells 29
10 Replete vs. limited cell cycle patterns using built-in models 50
11 Evidence of multiple fission in N-limited cultures using custom gates 51
12 Cell cycle patterns in semi-continuous cultures using built-in models 53
13 Cell cycle patterns in semi-continuous cultures using custom gates 54
14 Epifluorescence images showing SYBR Green stained *P. oklahomense* cells 56
15 DIC image showing broken mother cell wall debris 57
16 DIC images of cells showing evidence of multiple fission 57
17 Contour plot showing hypothesized multiple fission cell cycle trajectories 61
18 Turbidity sensor calibrations over four experiments 76
19 Difference in predawn F_v/F_m and $rETR_{max}$ due to irradiance discrepancies 78
20 Erratic growth parameters in replicate cycloturbidostats 79
21 Vulnerability of cycloturbidostats under near-limiting nitrate supply rates 80
22 Slow growth of *T. pseudonana* cultivated in cycloturbidostats 83

CHAPTER I

Minimum Nitrogen Cell Quota for Maximal Growth Rate

in Cycloturbidostat Cultures of *Picochlorum oklahomense*

Abstract:

Replicate cycloturbidostats cultures of *Picochlorum oklahomense were manipu*lated to quantify the minimum nitrogen cell quota supporting maximum growth rate and to study the effects of nitrogen limitation on cycloturbidostat cultures growing at near-μ_{max} under steady-state, balanced growth conditions. Results show that cyclical diurnal neutral lipid accumulation and ultradian growth are not mutually exclusive, and that cycloturbidostat cultures may be maintained near or at the threshold of N-limitation to control cell composition and modulate biomass productivity. Using this novel approach, we have identified the threshold of N limitation in *P. oklahomense* and investigated the effects of N limitation on replicate cycloturbidostat cultures. Mildly N-limited cultures grew rapidly (87% μ_{max}) and maintained near-optimal physiology, while accumulating moderate levels of neutral lipids during the photoperiod. Flow cytometry revealed differences in temporal patterns between treatments, demonstrating the importance of the cell-based approach in manipulating microalgal cultures. This study highlights the utility of turbidostats in experimental phycology and defines a scantly explored concept in the study of N limitation, the threshold of N cell quota necessary to support μ_{max}, below which cells are forced to re-allocate resources and slow growth, denoted $Q_{N,T}$.

Keywords: continuous culture, balanced growth, N-limitation, metabolic uncoupling

1.0 Introduction:

Algal growth dynamics have classically been described using cell nutrient quotas, which evaluate the amount of a particular nutrient needed to synthesize a new cell and maintain a particular growth rate [1-3]. These quotas may be based on measured cellular composition or derived by mass balance from nutrient supply and cell division rates. The maximum quota attainable in a species is denoted Q_{max}, and the minimum quota for survival or subsistence, Q_{min} . While some nutrients such as phosphorus can be stored in an inorganic form within the cell, there is no inorganic storage mechanism for nitrogen, making the cellular N quota an important aspect of algal physiology. One poorly studied aspect of N cell quota ($Q_{N, cell}$) is the level necessary to maintain maximum specific growth rate (μ_{max}) denoted here as $Q_{N, T}$, below which growth rate decreases, and cells transition to new metabolic states. The relationship between N cell quota and growth rate is shown in Fig. 1, along with minimum, maximum, and transition levels indicated.

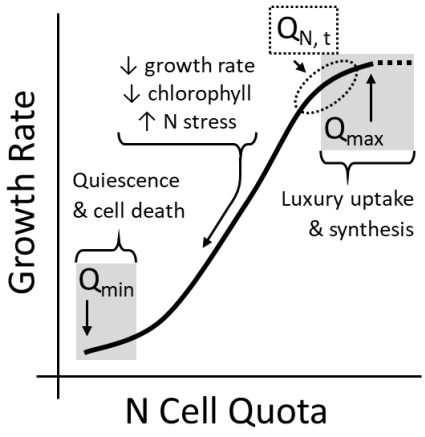

Fig. 1: Conceptual model of steady-state relationship between N cell quota and growth rate. Q_{MAX}: no increase in growth rate above this N cell quota, though quota may continue to increase. Q_{MIN}: no growth below this N cell quota, cells die or enter quiescence. $Q_{N, T}$: N cell quota transition point below which cells are forced to re-allocate resources and slow growth. Moving down in N cell quota, cells experience increasing levels of N stress. Modified from [3].

The well-known concept of nitrogen (N) limitation-induced lipid accumulation is typically studied in batch culture, where nutrients are depleted over time or abruptly removed from the growth media via centrifugation and resuspension, generating limitation and starvation responses, respectively. N starvation leads to the cessation of cell division and the subsequent hyper-accumulation of storage products including starch and/or lipid; N limitation supports sub-maximal cell division, and its physiological effects are more species-specific and complex [4, 5]. In any case, culture conditions in these contexts induce transient physiological states, which preclude the control and measurement of cell quota. Moreover, few N limitation studies focused on biocommodity production employ a cell-based framework, opting instead for biomass-specific measures and areal productivities [6-8].

As an alternative, continuous culture is used to maintain stable growth rate and nutrient supply via frequent replacement of culture volume with fresh media. This is classically achieved using either a turbidostat or a chemostat; a cyclostat refers to the operation of these culture modes under a photoperiod. Chemostats supply media at a constant rate to set an experimentally fixed growth rate, and equilibrium cell/biomass density decreases with increasing dilution rate. In contrast, turbidostats use an arbitrary turbidity setpoint to maintain a constant turbidity at the nutrient-replete growth rate (μ_{max}) of the organism under the given experimental conditions [9-11]. Individual turbidostat systems will exhibit different equilibria as biomass density is determined by an arbitrary turbidity setpoint. This, along with light and nutrient levels, temperature, and species all work to determine the equilibrium-state of the system and thereby the operating cell quota under balanced growth.

In continuous cultures supplied with continuous light, cells constantly fix and metabolize photosynthate, maintaining equilibrium biomass density and physiology [12]. However, cyclostat cultures respire photosynthate at night, thereby decreasing biomass density before returning to their equilibrium after accumulating biomass the following morning [9-11]. In this dynamic steady-state, cultures are in physiological balanced growth, where growth rate and the internal concentration of biomass constituents are relatively stable at any given point in the diurnal photoperiod [1, 9-11, 13].

N limitation decreases growth rate, resulting in no net increase in lipid productivity [5-7]. However, insufficient N supply decreases flux through N assimilation, leading to the uncoupling of N and carbon metabolism, whereby healthy cells accumulate carbohydrates and/or lipids [14-16]. Thus, we hypothesize that supplying levels of N slightly less than Q_{max} to cultures in a balanced-growth state may yield high relative growth rate with elevated lipid content.

Little work on the threshold of nitrogen limitation, i.e., $Q_{N,T}$, where μ falls below μ_{max}, is present in the literature, though some studies have made strides in understanding the dynamics of N limitation in various species [4, 12, 13, 15, 17, 18]. By design, turbidostats operate at sustained μ_{max} at a fixed biomass density without the risk of washout, unlike in chemostats. In this way, turbidostats are controlled by the growth rate of the organism, not by the operator. This allows for the study of N limitation on whole-cell physiology at near-μ_{max}.

Previous studies have shown that cultures supplied insufficient levels of nitrogen in turbidostat culture and continuous light may accumulate lipid under supersaturating but non-photoinhibitory light levels [4, 12, 15, 16]. Some studies utilizing continuous culture have reported lipid productivities higher than those previously achieved in batch culture, without compromising growth [12, 13, 15, 17]. Continuous culture may even outpace batch culture in terms of gross lipid productivity even though cells exhibited lower lipid content than in stationary phase of batch culture [17].

This is commonly achieved by supplying decreasing levels of N until a limiting level is identified, then iterating until lipid accumulation is induced [12, 16, 17]. However, these studies share some common limitations. The values of N supply were normalized to culture volume or total biomass, not cells, which is more relevant to whole-cell physiology [12, 17]. In some cases, use of continuous light limits application to outdoor culture, as lipid content and other physiological metrics exhibit diel cycles [12, 14, 16, 17]. Photoperiod may have other species-specific effects, as nocturnal respiration [19], cell cycle dynamics [20, 21], and the synthesis rates of different biomass constituents may vary among species/strains, leading to different operational diel cycles in cyclostat culture [4, 15]. To our knowledge, no study utilizing continuous culture reports using more than duplicates, thus a study

utilizing replicate continuous cultures subjected to a photoperiod and focused on whole-cell physiology would help to elucidate the ways that algae may be grown at near-μ_{max} while triggering lipid accumulation.

Here we focus on a poorly studied physiological transition between N replete and incipient N-limitation. In batch cultures this transition is progressive, such that any physiological transition is confounded by other variables and cannot be easily characterized. We manipulated steady state cycloturbidostat cultures of *Picochlorum oklahomense* by stepwise reductions in influent nitrate concentration ($[NO_3]_{inf}$). This allowed us to quantify the minimum nitrogen cell quota supporting maximum growth rate ($Q_{N,T}$) and study the effects of nitrogen limitation on cycloturbidostat cultures growing at near-μ_{max} under steady-state, balanced growth conditions. This type of continuous culture mode has been loosely termed a manipulated steady state, wherein cultures held in a balanced growth state are perturbed or shifted to a new state to alter biochemical composition [4, 9]. Using this novel approach, we have identified the threshold of N limitation in *P. oklahomense* and investigated the effects of N limitation on replicate cycloturbidostat cultures to control cell composition.

2.0 Methods:

2.1.1 Growth conditions and culture maintenance:

Stock cultures of *Picochlorum oklahomense* (Trebouxiophyceae; CCMP 2329/UTEX 2795) were maintained in artificial saltwater (AS) containing 20 g NaCl L^{-1} (2% w/v), 5 mM $NaHCO_3$, 825 μM Tris buffer, f/2 vitamins, and a trace metals mix [13]. Cultures were maintained in 0.5-L bottles, sparged with air, and stirred at 100 rpm under 150 μmol photons m^{-2} s^{-1} of illumination provided by 400-W metal halide lamps on a 14:10 h L:D cycle.

2.1.2 Turbidostat experiments:

The turbidostat setup consisted of 1-L wide-mouth Teflon FEP culture bottles, OASBF fiber optic opposed-mode pulse-modulated turbidity sensors (880 nm; Banner Engineering Corp., Plymouth

MN), peristaltic pumps and a microcontroller system. Culture bottles were topped with silicone stoppers fitted with flint glass tubing for media input and culture withdrawal, an air inlet with a 0.22-μm disk filter, an air vent covered with cotton, and a sample port. Dual-channel Anko 860 peristaltic pumps (ANKO Products, Bradenton, FL) simultaneously moved media from refrigerated 2 L bottles into the culture bottle and culture effluent into refrigerated 1-L cubitainers. The pumps were connected to a custom-programmed CR10X microcontroller/data logger and AM16/32B multiplexer (Campbell Scientific, Logan, UT), which connected to a computer and the user interface. A diagram and annotated image of the system is provided in Supp. Fig. 1. The system maintained a constant biomass density by averaging the turbidity signal at 15 sec intervals over a 5-minute period and triggering 1-minute pump cycles at a flow rate of 10 mL min^{-1} when the signal exceeded an arbitrary set-point voltage; this replaced approximately 3% of the 300 mL culture volume per pump cycle. The Banner Instruments OASBF turbidity sensors were calibrated using a two-point calibration with neutral density filters and deionized water. These optical sensors give a voltage (mV) reading according to turbidity as measured at a wavelength of 880 nm, which measures light scattering; a summary of calibrations across experiments and units is provided in Supp. Fig. 2.

This setup was housed in a temperature-controlled growth room maintained at 25 ± 3 °C. Light was provided by two metal halide lamps at *ca.* 450 – 550 μmol photons m^{-2} s^{-1} incident illumination for experiment 1, and two PhytoMAX 400W LED light banks (PhytoMAX 400, Black Dog LED, Niwot, CO) at *ca.* 750 – 850 μmol photons m^{-2} s^{-1} incident illumination for experiment 2 and 3. All three experiments were conducted on a 14:10 L:D cycle. Each culture was stirred at ~120 rpm and sparged continuously with air at ~10 mL min^{-1} and 1.0% CO_2 in air during the photoperiod. Fresh media was made in 2-L batches, fitted to luer-lock connections for the corresponding cultures, and stored at 4˚C. Culture effluent volume was measured each morning to determine dilution rate over the previous day.

We altered $Q_{N,\,cell}$ by changing $[NO_3]_{inf}$ without altering $[PO_4]$, such that the N:P ratios fell with decreasing $[NO_3]_{inf}$. In summary, $[NO_3]_{inf}$ levels ranged from 400 to 250 μM and $[PO_4]_{inf}$ levels were kept at 80 μM throughout all experiments giving N:P values from 5 to 3.125.

In a turbidostat, specific growth rate (μ, d^{-1}) equals the dilution rate (D) as determined by measures of effluent volume from the previous day. We calculated N cell quota according to the following equation:

$$Q_{N,cell} = \frac{\mu \times [NO_3]_{inf} \times \text{culture vol.}}{\text{cell\#} \times \mu \times \text{culture vol.}} = \frac{\mu\text{mol d}^{-1}\,\text{L}^{-1}}{\text{cells mL}^{-1}\,\text{d}^{-1}\,\text{L}^{-1}} = \frac{\text{pmol}}{\text{cell}},$$

where $Q_{N,\,cell}$ is equal to the product of μ and $[NO_3]_{inf}$ divided by the product of pre-dawn cell count and μ, which gives a cell-specific figure with reduced units of pmol $cell^{-1}$.

Cultures intended for inoculation of all experiments were maintained in semi-continuous mode at 0.5 d^{-1} by replacing half the culture volume at the beginning of each day with fresh 2% AS medium and acclimated to the appropriate experimental lighting for at least 3 days before inoculation. Experimental cultures for expt. 2 and 3 were inoculated by mixing 50 mL of inoculum from equilibrated cultures with 250 mL of fresh 2% AS media (200 mL in expt. 1 for a total of 250 mL) modified to contain 120 μM nitrate, 24 μM phosphate, 10 mM initial $NaHCO_3$ and no ~~Tris~~ buffer. This yielded a turbidity level less than half of the setpoint.

2.1.3 Growth and physiological characterization:

Each day prior to the onset of the photoperiod, a 10 mL sample was withdrawn from each culture and used for pre-dawn measurements. Measurements of cell density were carried out on a hemocytometer for expt. 1 and a Nexcelom Auto X4 automated cell counter with SD100 slides (Nexcelom Bioscience, Lawrence, MA) for expt. 2 and 3. Chlorophyll content in expt. 1 was determined by filtering 5 mL culture samples onto GF/F filters and extracting with 2 mL of N,N-

dimethylformamide (DMF). Calculations for the determination of total chlorophyll content were carried out according to [22] and normalized to cell density.

Rapid light curves (RLC) were gathered using a fiber optic Phyto-PAM EDF fluorometer (Heinz Walz GmbH, Effeltrich, Germany) to measure maximum quantum yield (F_v/F_m) and maximum relative electron transport rate ($rETR_{max}$) through PSII. All measures are reported as means ± standard deviation.

2.1.4 Flow cytometry

Flow cytometry for experiment 3 was performed by gathering 1 mL culture samples at designated time-points from pre-dawn through late photoperiod in ca. 3-hour increments. Evening timepoints were taken 9 hours into the photoperiod (5 hours prior to the onset of the dark period) with the final sample taken 30 minutes after the onset of the dark period. Samples were transferred to 1.7 mL centrifuge tubes and centrifuged at 12,000 x rpm for 3 min. The supernatant was removed and saved for residual NO_3 analysis.

Pelleted cells for neutral lipid staining and flow cytometry were aspirated and frozen at -20˚C. On the day of analysis, samples were thawed and resuspended in 2 mL PBS buffer with 0.010% (v/v) Triton X-100 and 0.1% (v/v) DMSO. Samples were incubated at room temperature for 10 minutes before analysis. Each sample was processed unstained at the low flow setting (12 µL/sec). Then samples were stained with 8 µL of BODIPY 495/503 (Thermo-Fisher, Waltham, MA) (diluted to 500 µg/mL in DMSO), vortexed for 30 sec and incubated in darkness for 10 min before processing [23].

Pelleted cells for cell cycle analysis were fixed in 0.2 µm filtered neutralized methanol and stored at -20˚C. On the day of analysis, samples were thawed and centrifuged at 12,000 x rpm for 5 min, re-extracted in 0.2 µm filtered methanol, and pelleted again by centrifuging at 12,000 x rpm for 5 min. This pellet was resuspended in 2 mL of PBS buffer and stained with 8 µL of SYBR Green 1 (Thermo-Fisher, Waltham, MA) (diluted to 25:1 in Tris-EDTA buffer), then vortexed for 10 seconds and incubated in darkness for 10 minutes before processing [20, 21].

The 488-nm argon laser of the FACSCalibur® (BD Biosciences, San Jose, CA) excited green BODIPY fluorescence in the presence of neutral lipids or green SYBR Green 1 fluorescence, which were detected in the FL2 channel (560 – 640 nm), and red chlorophyll fluorescence, which was detected in the FL3 channel (> 670 nm). A total of 10,000 events were gathered and cells were filtered first by size in a FSC vs. SSC gate, then by the presence of chlorophyll in a FSC vs FL3 gate. A logarithmic scale for FSC-H was chosen in order to differentiate cell size more precisely as *Picochlorum* is very small, making it difficult to distinguish between cells and debris. Determination of neutral lipid content was performed by running unstained samples prior to staining in order to obtain a median baseline value for FL2, which was then subtracted from the median FL2 value of stained sample; flow cytometer settings were constant for all samples [20, 21, 23]. All cell cycle calculations were performed via FCS Express Multicycle (De Novo Software, Pasadena, CA).

2.1.3 Biomass characterization

Turbidostat effluent was collected in a capped flask prior to the first pump cycle of the day. Fractions of effluent for biomass analysis were collected in fresh containers, and filtered onto pre-weighed GF/C filters, dried in an oven at 40˚C for 48 hours and stored in a desiccator. Ash free dry weight was determined by filtering 50 mL samples of effluent onto pre-weighed GF/F filters, drying in an oven at 40°C overnight, and combusting in a furnace at 450°C for at least 4 hours. Determination of C:N ratio was carried out on a Vario EL Cube lemental analyzer (Elementar Australia Pty Ltd, Sydney, NSW) by filtering 50 mL samples of effluent or culture onto pre-weighed GF/F filters and drying in an oven at 40°C overnight.

Total lipid content was determined via a wet-lipid fatty-acid methyl ester (FAME) method and analyzed on a GC-MS Model QP2010S system (Shimadzu, Kyoto, Japan). Briefly, 50 mL samples of culture were filtered onto pre-weighed GF/F filters and dried in an oven at 40°C overnight. These filters were weighed, placed in 4 mL glass vials and trans-esterified by first adding 400 µL of a chloroform:methanol (2:1, v/v) solution and tamping the filter with a clean glass rod before adding

600 µL of a 0.6M HCl:methanol solution; samples were sealed and vortexed for 30 seconds before incubating at 85°C for 1 hour. Samples were cooled to room temperature and 1 mL of hexane was added, then samples were shaken vigorously for 30 minutes to extract FAMEs. Sample aliquots were transferred to clean GC-MS vials with inserts and analyzed immediately [24]. All measures are reported as means ± standard deviation based on replicate cultures over multiple days.

2.1.5 Residual nitrate

Residual nitrate plus nitrite (NO_x) concentrations were determined with a micro-plate assay developed using vanadium as a reductant [25]. The supernatant from centrifuged samples intended for flow cytometry analysis was used for NO_x analysis; this included pre-dawn and evening timepoints for each culture. We constructed NO_x standard curves using 2% AS salts.

2.1.6 Microscopy

The agar pad method was utilized for epifluorescence microscopy to prevent cells from moving during imaging. Briefly, clean glass microscope slides were arranged forming a 1 cm trough between slides, with a slide below the trough and a slide above. A mixture of 1% low-melt agar was mixed with 2% AS salts and microwaved for 30 seconds. Once cool, the agar was pipetted into the trough and allowed to harden. The slides were carefully removed, and 1 cm square agar pads were cut and transferred to clean slides. Pelleted cells were thawed, washed once with PBS buffer, and resuspended in 0.5 mL of PBS buffer, then stained with 2 µL of BODIPY 495/503. Cells were incubated for 10 mins, then pipetted onto the agar pads in darkness and imaged with UV excitation.

2.1.6 Statistical analysis

Three iterative experiments are detailed here with slightly different arrangements of control and treatment groups. Experiment 1 utilized four replicate culture bottles (n = 4) where all replicates followed the same nutrient regime. Experiment #2 utilized eight total cultures in two groups (n = 4, 4)

that were inoculated identically and fed identical nutrient regimes until the treatment group was changed. Experiment #3 also utilized eight total cultures in two groups (n = 4, 4), but these groups were inoculated and operated at their respective nutrient regimes for the duration of the experiment. Groups of replicate cultures were evenly distributed in relation to the light source to control for discrepancies in photon flux.

All growth and physiological parameters are reported as mean ± standard deviation of replicate cycloturbidostat cultures (expt. 1: n = 4; expt. 2 and 3: n = 4, 4 – replete, limited). All flow cytometry parameters are reported as medians for cytogram values except when performing t-tests where means are required.

A summary of symbols, equations, and abbreviations with descriptions can be found in Table 1.

Table 1: Symbols, equations, abbreviations, and descriptions used in this manuscript.

Symbol	Equation	Description	Units
μ	effluent volume / culture volume	Volumetric specific growth rate	d^{-1}
$Q_{N, Total}$	μ x 0.3 L x $[NO_3]$	Bulk nitrate quota	$\mu mol\ NO_3\ d^{-1}$
$Q_{N, cell}$	$Q_{N, bulk}$ / (cell# x μ)	Nitrate cell quota	$pmol\ cell^{-1}$
r_x	C_x x μ	Biomass productivity	$mg\ L^{-1}\ d^{-1}$
D	μ / ln(2)	Doubling rate	d^{-1}
NL_x	r_x x [NL]	Neutral lipid productivity	$mg\ L^{-1}\ d^{-1}$

Abbreviation	Description	Units
cell#	Cell density (pre-dawn unless otherwise stated)	$cells\ mL^{-1}$
$[NO_3]_{inf}$	Nitrate concentration in the influent media	µM
$Q_{N, max/min}$	Minimum and maximum N cell quota	$pmol\ cell^{-1}$
$Q_{N, T}$	Q_N transition below which growth rate decreases	$pmol\ cell^{-1}$
μ_{max}	Maximum growth rate	d^{-1}
C_X	Ash free dry weight	$mg\ L^{-1}$
$\%G_1$	% population in G1 phase of cell cycle	%
%S	% population in S phase of cell cycle	%
F_v/F_m	Maximum photosynthetic quantum yield	unitless (0 – 1)
$rETR_{max}$	Relative maximum electron transport rate	relative
[NL]	Neutral lipid content	% or relative
[Chl]	Chlorophyll content	$fg\ cell^{-1}$ or relative
FSC	Forward scatter, approximates cell diameter	relative
SSC	Side scatter, a measure of light attenuation by cells	relative

3.0 Results:

3.1 Nitrate step-down identifies minimum $Q_{N, cell}$ for maximal growth rate (Experiment 1):

Following inoculation, cultures rapidly accumulated biomass up to the turbidity setpoint; this is a common feature of continuous culture studies [10, 11]. Next, cultures approached steady-state physiology constrained by the interplay between cell density, chlorophyll content, light availability, and nutrient supply. Multiple cycloturbidostat iterations suggest the apparent growth rate of the inoculum, along with the initial cell density and nutrient concentration of the resulting culture are important factors in determining the degree of variability in this initial phase, i.e., excess nutrients lead to high initial cellular chlorophyll concentrations and variability in the approach to steady state.

In experiment 1, cultures (n = 4) were inoculated in the late afternoon of day 0 at *ca*. 4.5 x 10^6 cells mL^{-1} (only one count was taken and assumed for all units) in media containing 400 µM NO_3. All cultures nearly reached the turbidity set-point at the end of day 1 and began cycling through the photoperiod on day 2. Mean µ from day 2 – 11 was 1.02 ± 0.31 d^{-1} (mean ± SD, n = 40, i.e., 4 cultures x 10 days). The pre-dawn cell density and chlorophyll content of replicate cultures were stable and exhibited similar patterns from day 6 – 11, respectively averaging 9.6 ± 1.8 x 10^6 cells mL^{-1} (n = 18) and 155 ± 16 fg Chl $cell^{-1}$ (n = 17) (Fig. 2B, C).

The main purpose of experiment 1 was to identify the threshold in N supply as a starting point for future experiments. Cultures reached a balanced growth state at 400 µM $[NO_3]_{inf}$, with a stable growth rate of 1.18 ± 0.15 d^{-1} (n = 28, i.e. 7 days x 4 units) from day 12 – 18 (Fig. 2A). Mean pre-dawn cell density and chlorophyll content from days 12 – 18 respectively were 10.6 ±1.0 x 10^6 cells mL^{-1} (n = 8) and 160 ± 19 fg $cell^{-1}$ (n = 8; Fig. 2B, C). No increase in growth rates, cell densities, or chlorophyll content was evident after $[NO_3]_{inf}$ was increased to 600 µM on day 19, indicating nitrate saturation at an influent concentration of 400 µM.

However, when $[NO_3]_{inf}$ returned to 400 µM on day 28, growth rate increased by 33% and chlorophyll content decreased by 32%, but cell densities did not change (Fig. 2A– C). This apparent

increase in productivity (faster growth, lower chlorophyll) may be explained by increased light penetration into the culture due to the decreased chlorophyll content. Perhaps cultures acclimated to an extent through the first *ca.* 25 days of the experiment or were slightly light limited when chlorophyll content was high. Another possibility is that a 33% drop in influent N, even at saturating levels of $Q_{N, cell}$, triggered a physiological response. No changes in aeration, stirring, CO_2 supply, or temperature were documented or apparent. Based on intermittent sampling, results up to day 28 are consistent with nitrate-replete growth at $[NO_3]_{inf} \geq 400$ μM.

Following the drop from 400 to 300 μM on day 39, growth rate and chlorophyll content decreased by 5.7% and 14.7% respectively and cell density increased by 5.7% during days 31 – 34 (Fig. 2A-C). Finally, after $[NO_3]_{inf}$ was dropped to 250 μM on day 46, chlorophyll abruptly halved to 45 ± 17 fg cell^{-1} (n = 15), while growth rate held steady for 4 days at 1.57 ± 0.27 d^{-1} (n = 14) before rapidly declining over the next five days.

Chlorophyll content remained above 107 fg cell^{-1} for the first 34 days of the experiment at $[NO_3]_{inf} \geq 400$ μM, dropping briefly to *ca.* 95 fg cell^{-1} before $[NO_3]_{inf}$ was decreased to 300 μM (Fig. 2C). Likewise, $Q_{N, cell}$ remained above *ca.* 11 pmol cell^{-1} during the same period (Fig. 3A). Diel cycling of chlorophyll content was evident with evening values often doubling their pre-dawn values; however, a clear pattern was difficult to discern due to limited sampling (Supp. Fig. 3). Over the course of the experiment including the final 250 μM $[NO_3]_{inf}$ condition, cellular chlorophyll content showed a downward trend and was strongly correlated with $Q_{N, cell}$ ($F(1,110) = 98.41$, $p < 0.001$, $R^2 = 0.4722$; Fig. 3B). However, nearly all values for the 250 μM $[NO_3]_{inf}$ treatment fall below the trendline, indicating uncoupling of this relationship once $Q_{N, cell}$ fell below 7.05 pmol cell^{-1}. This value is the median of the 250 μM treatment and coincidentally the lower bound of the first quartile for 300 μM treatment. Presumably, this is the $Q_{N, cell}$ threshold to support μ_{max}, denoted $Q_{N, T}$. The spread of $Q_{N, cell}$ values across the $[NO_3]_{inf}$ treatments decreases and approaches a low asymptotic value, which presumably corresponds to $Q_{N, T}$.

While $Q_{N, cell}$ never fell below 5.16 pmol cell^{-1} even with decreasing growth rate under the 250 μM $[NO_3]_{inf}$ treatment, chlorophyll content continued to fall, indicating that cells continued to divide by sacrificing the synthesis of chlorophyll, instead allocating more assimilated N to maintenance metabolism. A regression including only $[NO_3]_{inf}$ conditions ≥ 300 μM exhibited a lower slope (R^2 = 0.3538, $F(1,83) = 45.45$, $p < 0.001$).

More sporadic measurements provide additional insights. Dry biomass was 80 ± 4.1 mg L^{-1} (n = 4) on the final day of the 300 μM treatment and fell slightly to 69 ± 8.7 mg L^{-1} (n = 4) on day 49, the final day with mean growth rate ≥1.0 d^{-1}. Dry biomass fell further to 55.5 ± 6.0 mg L^{-1} (n = 4) on day 50 when growth rate fell below 1 d^{-1}. C:N molar ratio was 6.6 ± 0.58 (n = 4) on the final day of the 300 μM treatment and fell slightly to 6.3 ± 0.51 (n = 4) on day 50. Pre-dawn turbidity, which tracks biomass density, was relatively consistent but trended downward over the course of the experiment, with 3-day rolling coefficients of variation rarely exceeding 5%. Pre-dawn turbidity from days 2–53 was 945 ± 102 mV (n = 208; Supp. Fig. 4). These supporting data further illustrate that our turbidostat cultures were in a stable and reproducible balanced growth state when held at constant $[NO_3]_{inf}$.

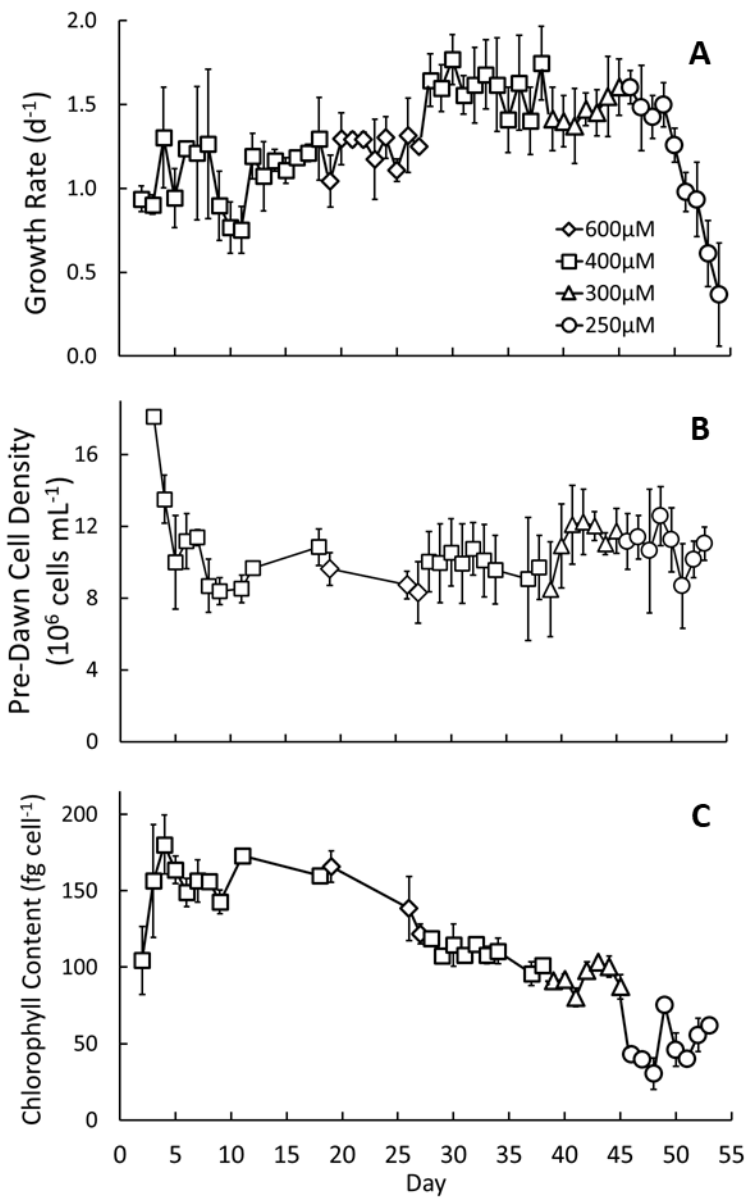

Fig. 2: Growth chronology of $[NO_3]_{inf}$ stepdown study (expt. 1). A) growth rate, B) pre-dawn cell density of individual cultures, and C) pre-dawn [Chl]. Symbols indicate $[NO_3]_{inf}$ treatment. Means ± SD (n = 4); some error bars are smaller than symbols.

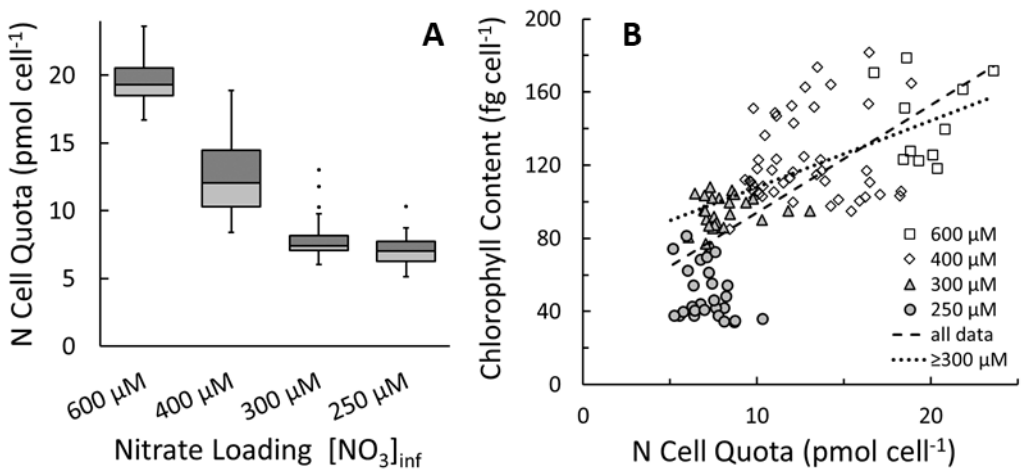

Fig. 3: A) Box plots with quartiles and outliers of N cell quota ($Q_{N, cell}$) for different $[NO_3]_{inf}$ treatments (expt. 1). B) Chl content vs. $Q_{N, cell}$ (expt. 1). Each point represents a single culture on a given day. Symbols indicate $[NO_3]_{inf}$. Two linear regressions are shown, one including all data (- - -; $F(1,110) = 98.41$, $p < 0.001$, $R^2 = 0.4722$), and one including only $[NO_3]_{inf}$ conditions ≥ 300 µM (**....**; $F(1,83) = 45.45$, $p < 0.001$, $R^2 = 0.3538$).

3.2 Transition from replete to limited $[NO_3]_{inf}$ triggers physiological symptoms (Experiment 2):

Experiment 2 incorporated several improvements in the culture system including 4 more units (n = 8), new dual-channel pumps, spatially uniform LED lighting at *ca.* 150% PFD of previous lighting, and improved inoculation protocols. These improvements increased the stability of and reduced inherent variability in our cycloturbidostat cultures, which improves reproducibility.

In experiment 2, cultures (n = 8) were inoculated in the late afternoon of day 0 at 300 µM NO_3 (n = 8), which was chosen as the replete treatment from the results of exp 1 and other preliminary trials. Initial cell densities ranged from 11.9 to 13.5 x 10^6 cells mL^{-1}, with one outlier of 18.2 x 10^6 cells mL^{-1}; all cultures reached the setpoint near midday on day 1. During the first three days of cycling, growth rate increased to their steady-state values of *ca.* 1.5 d^{-1}. Cell densities spiked on day two, before settling into their steady-state values of *ca.* 14.5 x 10^6 cells mL^{-1}. Less variability in growth

rate and cell density was evident as compared to experiment 1, but pre-dawn F_v/F_m fluctuated widely at first (Fig. 4), indicating that steady state physiology had not yet been reached.

Cultures maintained steady-state from day 6 – 12 at 300 µM $[NO_3]_{inf}$ with a growth rate of 1.60 ± 0.25 d^{-1} (n = 56, i.e., 8 units x 7 days), pre-dawn cell density of 15.9 ± 4.5 x 10^6 cells mL^{-1} (n = 56), and $Q_{N, cell}$ of 6.01 ± 1.27 (n = 56; Fig. 4A–C). The pre-dawn maximum photosystem II quantum yield (F_v/F_m) varied moderately over the first 12 days of growth (0.47 ± 0.05, n = 31), despite the relative consistency of growth rate and $Q_{N, cell}$; mean relative maximum electron transport rate ($rETR_{max}$) was 28.2 ± 7.0 (n = 31) from days 6 – 12 (Fig. 4D, E).

Growth metrics were stable from day 13 – 26 with a growth rate of 1.73 ± 0.18 d^{-1} (n = 120), pre-dawn cell density of 17.0 ± 3.75 x 10^6 cells mL^{-1} (n = 80), and $Q_{N, cell}$ of 5.52 ± 0.99 (n = 80; Fig. 4A-C). Pre-dawn fluorescence parameters were also stable with an F_v/F_m of 0.55 ± 0.04 (n = 78; Fig. 4D) and a $rETR_{max}$ of 30.1 ± 2.67 (n = 78; Fig. 4E) from days 13 – 26.

On day 27, we decreased $[NO_3]_{inf}$ for half of the cultures (n = 4) from 300 µM to 250 µM $[NO_3]$, while half remained at 300 µM $[NO_3]$. Growth rates diverged by 16.9% during days 32 – 37, and as a result pre-dawn cell density on the same days averaged 18% higher in the 250 µM treatment than in the 300 µM treatment and $Q_{N, cell}$ was 31% lower in the 250 µM treatment than in the 300 µM treatment. While the $rETR_{max}$ was 10.8% lower in the 250 µM treatment than in the 300 µM treatment, F_v/F_m was unchanged (Fig. 4D).

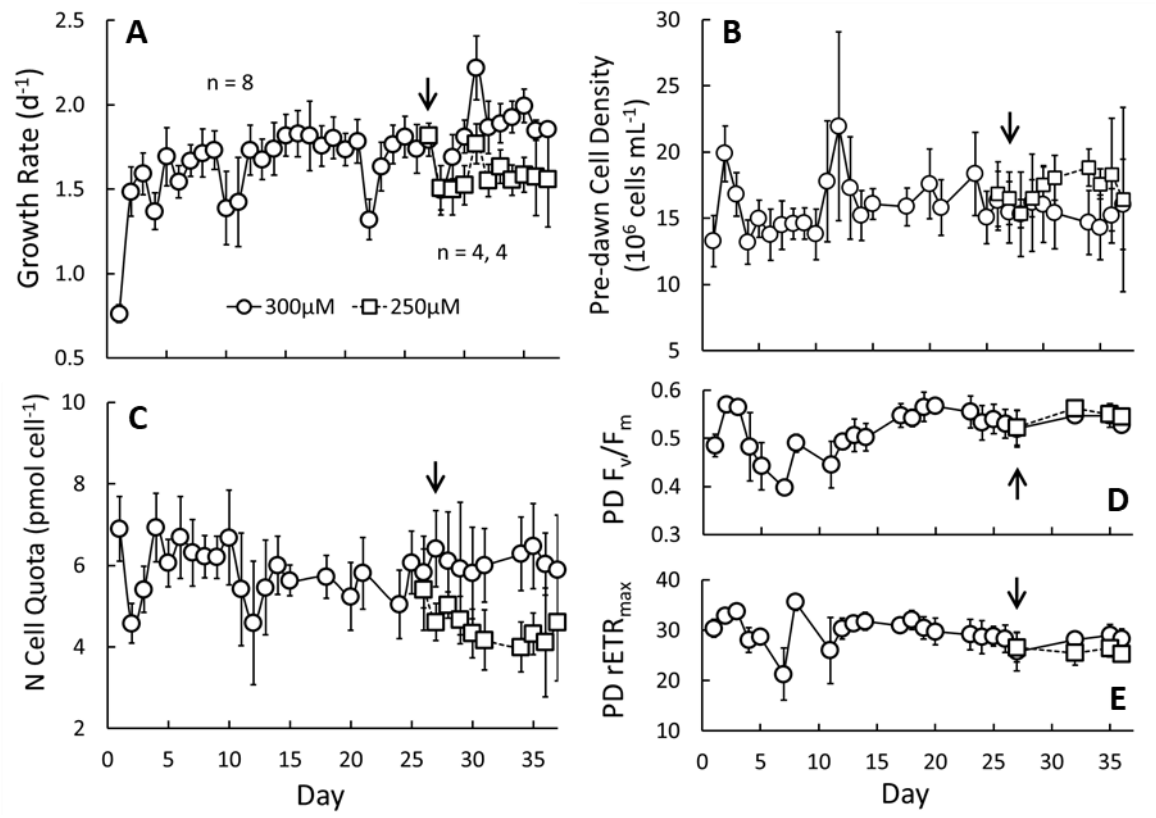

Fig. 4: Growth chronology of $[NO_3]_{inf}$ transition study (expt. 2). A) specific growth rate, B) pre-dawn cell density, C) $Q_{N, cell}$, D) pre-dawn F_v/F_m and E) pre-dawn $rETR_{max}$. Symbols indicate $[NO_3]_{inf}$ treatment. Means ± SD; (n = 8) until day 27 (indicated by arrows) when $[NO_3]_{inf}$ was switched to 250 µM (n = 4, 4).

Residual $[NO_3]$ in the cultures was monitored during pre-dawn sampling from days 11 – 37 and was less <5 µM for 69.4% of the 160 samples, and >30 µM for only 10.6% of the samples; this shows that residual $[NO_3]$ in the culture was low and most of the N supplied through the day was assimilated (Supp. Table 1).

Mean ash free dry weight was 96.0 ± 2.5 mg/L (days 21 – 25) (n = 20). Pre-dawn turbidity from days 5 – 37 was consistent (878 ± 32 mV) across the experiment and was not correlated with growth rate or affected by the change in $[NO_3]_{inf}$ (Supp. Fig. 4). Having shown that our turbidostat cultures

are not limited by N at 300 μM $[NO_3]_{inf}$ but exhibit symptoms of N limitation at 250 μM $[NO_3]_{inf}$, such as decreased growth rate and chlorophyll content, and depressed fluorescence parameters, we will now refer to the 300 and 250 μM $[NO_3]_{inf}$ treatments as replete and limited, respectively.

3.3 Limiting $Q_{N, cell}$ alters diurnal physiological patterns (Experiment 3):

The purpose of experiment 3 was to further characterize physiological differences between replete and limited cycloturbidostat cultures. In this experiment, half of the cultures were initiated at 300 and half at 250 μM $[NO_3]_{inf}$. A time-course of growth is shown in Supp. Fig. 5.

All cultures (n = 8) were inoculated 4 hrs into the photoperiod on day 0 with identical media containing 200 μM NO_3. Cultures grew in batch mode with six cultures reaching the turbidity setpoint by the end of the photoperiod on day 0. Turbidostatic growth began on day 1 with all cultures supplied with their respective media treatments (300 and 250 μM $[NO_3]_{inf}$; n = 4, 4). During the first three days of dilution, the limited treatment demanded marginally smaller $Q_{N, cell}$ rates than the replete treatment, resulting in lower pre-dawn cell densities and lower specific growth rates by day 3 in the limited cultures. However, this decrease in dilution led to increased cell densities and lower $Q_{N, cell}$ in limited cultures on day 4, which coincided with lower pre-dawn F_v/F_m and $rETR_{max}$. Nevertheless, both treatments achieved steady-state balanced growth by day 6 (Figs. 5 – 7; Suppl. Fig. 5).

Steady state growth rate from day 7 – 11 was 13.1% lower in the limited compared to the replete $[NO_3]_{inf}$ treatment (n = 20; $t_{2,38} = 4.72$, $p < 0.001$; Fig. 5A). Pre-dawn cell density was 9.1% higher in the limited than in the replete $[NO_3]_{inf}$ treatment ($t_{2,38} = -2.48$, $p = 0.018$; Fig. 5B). Mean $Q_{N, cell}$ from day 7 – 11 was 23.5% lower in the limited than in the replete $[NO_3]_{inf}$ treatment ($t_{2,38} = 7.87$, $p < 0.001$; Fig. 5C). Mean pre-dawn F_v/F_m and $rETR_{max}$ from days 7 – 11 Figs. 5D, E) did not differ significantly between the limited and replete treatments. Details on two-tailed t-test results from data in Fig. 5 are given in Supp. Table 2.

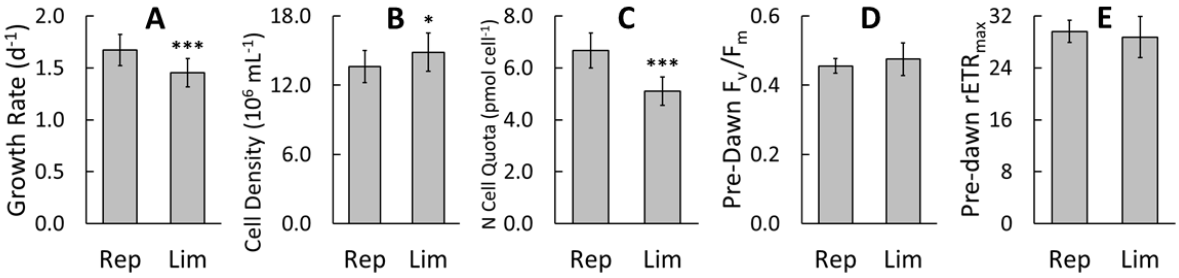

Fig. 5: Comparative physiological parameters from days 7 – 11 in replicate cultures (n = 4, 4) (expt. 3). A) mean growth rate, B) mean pre-dawn cell density, C) mean $Q_{N, cell}$, D) mean pre-dawn yield (F_v/F_m), E) mean maximum relative electron transport rate ($rETR_{max}$). Error bars represent standard deviation. Significant differences are indicated by * ($p < 0.05$) and *** ($p < 0.001$) (Supp Table 2).

We employed flow cytometry to characterize the distribution of individual cellular properties over the course of the photoperiod in individual cultures under both the replete and limited treatments over a 5-day period. Cell size as indicated by FSC increased through the course of the photoperiod and while cell size at dawn was roughly equal between treatments, the median cell size in the N-limited cultures was less than the replete cell size by the end of the photoperiod, but this difference was not significant ($n = 5$; $t_{2,8} = 1.99$, $p = 0.081$; Fig. 6A). SSC was significantly higher in the limited culture at dawn ($n = 5$; $t_{2,8} = 3.81$, $p = 0.005$), but showed no difference between treatments at the end of the photoperiod ($n = 5$; $t_{2,8} = 0.70$, $p = 0.505$; Fig. 6B). Chlorophyll content was equal in pre-dawn samples and increased over the course of the photoperiod, with the limited treatment reaching only half the replete treatment by the evening sample ($n = 5$; $t_{2,8} = 4.97$, $p = 0.001$; Fig. 6C). Neutral lipid (NL) content was significantly higher in the limited treatment at the evening timepoint ($n = 5$; $t_{2,8} = 3.68$, $p = 0.006$), despite being equal at dawn (Fig. 6D). Neutral lipid content increased over the course of the photoperiod in the limited treatment but did not increase in the replete culture. Supp. Fig. 6 shows a time course of cellular properties in two individual cultures under each treatment over days 9 – 13; samples were taken mid-photoperiod to better resolve phenotypic patterns. T-tests were performed on daily median values ($n = 5$) from pre-dawn and evening sample cytograms with

significant differences indicated in Fig. 6; a summary of these t-test results is given in Supp. Table 3. Furthermore, two-way ANOVAs were performed for each of the flow cytometry measures with replete vs. limited and pre-dawn vs. evening as the two factors. A significant difference between pre-dawn and evening measures was found for all measured characteristics, with significant differences between the replete and limited treatments for both chlorophyll and neutral lipid content. A significant interaction was found for all measures except SSC. A summary of these ANOVA results is given in Table 4.

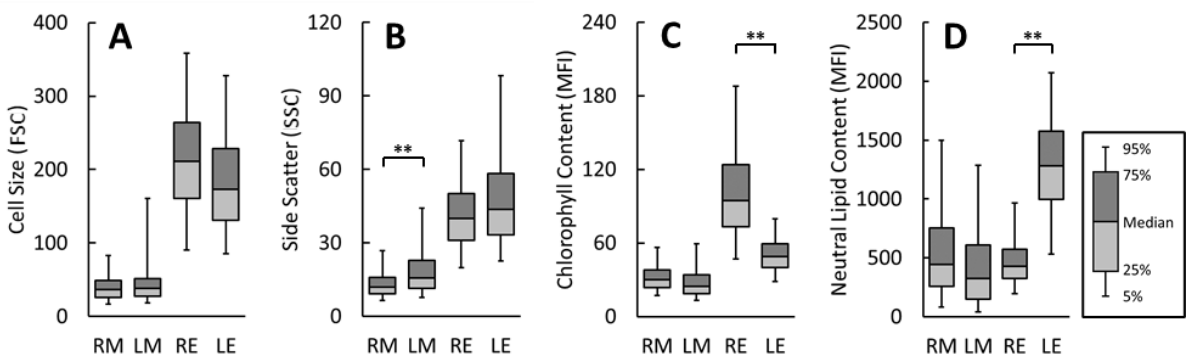

Fig. 6: Comparative flow cytometry characteristics from days 7 – 11 in two individual cultures (expt. 3). MFI = median fluorescence intensity; RM = replete pre-dawn; RE = replete evening; LM = limited pre-dawn; LE = limited evening. At least two replicate cytograms from each sample were merged to increase sample size. Significant differences were calculated using two-tail t-tests assuming equal variances and are indicated by ** ($p < 0.01$). (Supp Table 3).

Table 2: Results of two-Factor ANOVA tests with replication (Expt. 3, Fig. 6, Supp. Table 3). M = morning (pre-dawn), E = evening, Rep = replete, Lim = limited.

	Cell Size (FSC)		Side Scatter (SSC)		Chl Content (MFI)		NL Content (MFI)		
	F calc	*P-value*	*F calc*	*P-value*	*F calc*	*P-value*	*F calc*	*P-value*	*F crit*
M vs E	392.8	1.10 E-12 ***	71.7	2.63 E-07 ***	93.1	4.51 E-08 ***	13.1	0.002 **	4.49
Rep vs Lim	3.82	0.07 -	1.64	0.218 -	27.4	8.23 E-05 ***	4.55	0.049 *	4.49
Interaction	5.56	0.03 *	0.009	0.925 -	18.2	0.0006 ***	10.2	0.0057 **	4.49

Flow cytometry was also employed to monitor the progression of the cell cycle over the course of three consecutive days in two individual cultures, one each under the replete and limited treatment. The replete treatment showed phased cell division beginning late in the photoperiod with peak S-phase populations and the lowest %G1 occurring just after the onset of the dark period. In contrast, the limited treatment showed peak S-phase populations and the lowest %G1 occurring ca. 9 hrs into the 14 hr photoperiod. Notably, the G2 population never fell below 11% in the replete culture, but the G2 population fell to near-zero in the limited culture 9 hrs into the photoperiod. These data are not shown but will be presented in another manuscript.

Residual [NO_3] in the media was monitored at both pre-dawn and evening timepoints and was less than 5 µM for the majority of the samples taken (Supp. Table 4). No obvious difference in residual [NO_3] was evident between pre-dawn and evening timepoints, or between $[NO_3]_{inf}$ treatments. Sampling across multiple pump cycles and cultures showed that [NO_3] in the culture would routinely reach up to 20 µM directly after pump cycles before decreasing to undetectable levels in the *ca.* 20 min before the next pump cycle (data not shown).

Ash free dry weight from days 7 – 10 was 127 ± 14 mg L^{-1} (n = 32, i.e., 8 cultures x 4 days). Pre-dawn turbidity was consistent across the experiment at 863 ± 23 mV and was not correlated with growth rate (Supp. Fig. 4). No difference in ash free dry weight or pre-dawn turbidity was evident between treatments. On days 10 – 11 at the end of the photoperiod, *ca.* 50 mL samples were withdrawn from all 8 cultures and filtered onto glass-fiber filters for biomass analyses. FAME total lipid analysis showed no difference in total lipid content at evening timepoints on days 10 – 11 (n = 16; $t_{2,14}$ = -0.18, p = 0.86; Fig. 7A, B) or fatty-acid profile between the replete and limited $[NO_3]_{inf}$ treatments. C:N ratio at evening timepoints also did not differ on days 10 – 11 (n = 16; $t_{2,30}$ = -0.36, p = 0.73; Fig. 7C) between $[NO_3]_{inf}$ treatments (Fig. 7C).

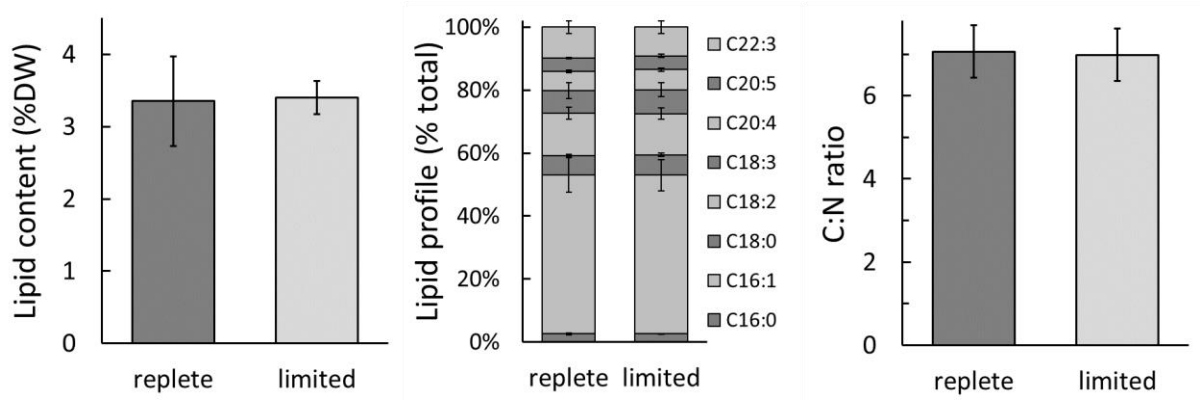

Fig. 7: Comparative biomass composition from replete and limited replicate cultures (n = 4, 4) (expt. 3). A) total lipid content (%DW), B) lipid profile, and C) biomass C:N molar ratio. Means ± standard deviation (n = 8, 8) (n = 4 cultures over 2 days).

4.0 Discussion

4.1 Manipulating $Q_{N, cell}$ in cycloturbidostats

Here we demonstrate that cycloturbidostat cultures of *Picochlorum oklahomense* may be maintained near or at the threshold of N-limitation without washout or cell death. We identified the $Q_{N, cell}$ threshold via an empirical N-step down approach and confirmed that threshold in subsequent experimental trials. We show that that mildly N-limited cells in cycloturbidostats grow rapidly (87% μ_{max}) and maintain near optimal physiology, while accumulating moderate levels of neutral lipids (BODIPY fluorescence) during the photoperiod. Using this novel approach, we identified the threshold of N limitation in *P. oklahomense* and investigated the effects of N limitation on replicate cycloturbidostat cultures of *P. oklahomense*. Turbidostats are under-represented in the literature especially in the context of cyclostat culture, and multiple replicate cycloturbidostats are rarely utilized in this particular way to demonstrate reproducible results across units [9-13, 15, 17, 20, 26].

Results from experiment 1, the N-step down trial, show that chlorophyll and $Q_{N, cell}$ exhibit a roughly linear relationship above $Q_{N, cell}$ >7 pmol cell^{-1}, which we designate $Q_{N, T}$, the threshold to support μ_{max}. This indicates that once $Q_{N, cell}$ fell below $Q_{N, T}$ (Fig. 1) cells were no longer able to

maintain homeostasis/equilibrium and the ratio of functional biomass to photosynthetic capacity changes to focus on maintenance metabolism, with less investment in light harvesting, leading to decreased growth rate and chlorophyll content. Coincidentally, this $Q_{N,T}$ value is the median of the 250 μM treatment and the lower bound of Q1 for 300 μM treatment. Furthermore, turbidostat failure did not occur until 3 days after the drop to the 250 μM treatment, probably due to chlorophyll-protein 'buffering' of N quota related to the depletion of internal N reserves for maintaining cellular function [3, 4, 10, 11, 13, 15, 27-29].

Experiments 2 and 3 showed that N-limited cycloturbidostat cultures were characterized by marginally lower growth rate and much lower late-photoperiod chlorophyll content, with negligible reduction in F_v/F_m and $rETR_{max}$ at balanced-growth. Flow cytometry phenotyping in experiment 3 indicated the cells in the limited treatment held more neutral lipid than cells in the replete treatment late in the photoperiod. However, C:N and total lipids were identical both pre-dawn and late in the photoperiod. No difference in cell size was evident at pre-dawn timepoints, but N-limited cells were smaller than N-replete cells at the end of the photoperiod. Note that FAME total lipid results are normalized to DW while flow cytometry lipid results are per cell; the slightly larger replete cells at the end of the photoperiod could explain the higher BODIPY lipid content in smaller limited cells, despite no apparent difference based on FAME. Side scatter was lower in the N-limited cells at pre-dawn timepoints, potentially indicating less storage compounds, i.e., starch and lipid. Lower chlorophyll content and decreased cell size in the limited treatment at the end of the photoperiod reflects the decrease in $Q_{N,cell}$, and given the rapid growth rate and comparable F_v/F_m and $rETR_{max}$, this shows a metabolic reconfiguration around N and the ratio of functional biomass to light harvesting capacity [13, 15, 16, 18, 20, 21, 23].

While $[NO_3]_{inf}$ in the replete treatment exceeded that in the limited treatment, our turbidostats are not ideal closed systems, meaning some N may leave the system in the culture effluent without being assimilated and introduce some error in the calculated $Q_{N,cell}$ values; this could result in a smaller or negligible change on C:N between treatments. In other words, the replete treatment always has N

available when needed but the limited treatment does not, leading to a physiological change due to incipient N limitation but a negligible change in C:N ratio. Instead, cell size and division rate both decrease slightly. This is a precipitous balance, with further reduction in $[NO_3]_{inf}$ causing culture washout as cells cannot obtain sufficient N to divide.

There may be small discrepancies in the calculated $Q_{N, cell}$ between our replicate experiments, but the benchmark of 7 pmol cell^{-1} is an estimate of $Q_{N, T}$ for *P. oklahomense*. The low bound for $Q_{N, T}$ in each experiment was 5.16, 4.26, and 5.11 pmol cell^{-1} for experiments 1, 2, and 3, respectively; and the $Q_{N, cell}$ value for the replete treatments in experiments 2 and 3 was 6.17 and 6.68 pmol cell^{-1}, respectively. This is to say that when $Q_{N, cell}$ falls below 7 pmol cell^{-1} cells are no longer able to maintain maximum specific growth rate.

This can be seen in Fig. 3A where an asymptotic limit is evident around 7 pmol cell^{-1}. This calculated value is an approximation and is influenced by the estimation of both growth rate and cell density measurements, which were performed differently across experiments (hemocytometer vs Nexcelom). Furthermore, periodic residual NO_3 measurements of freshly made media showed lower $[NO_3]$ than the nominal values (300 μM = 258.0 ± 34.4 (n = 15) and 250 μM = 213.4 ± 27.9 (n = 17), which constitutes 82.7% of the replete $[NO_3]$), but the proportional difference between treatments was unchanged. Thus, $Q_{N, cell}$ is likely lower than the reported values, which are based on nominal concentrations. Other possible causes of error include differences in any combination of the following from one experiment to another: (i) culture volume; (ii) pump cycle duration or volume; (iii) light; (iv) set-point or actual cell density; (v) N concentration variations among batches of media; (vi) steady state μ; (vii) $[CO_2]$, pH, bubbling rate, stirring speed, etc.

It is important to reiterate that these $[NO_{3inf}]$ treatments are specific to our turbidostat setup and arbitrary set-point (which controls cells mL^{-1}) as well as the particular physiology of our study organism. It is equally important to note that the ambient $[NO_3]$ experienced by cells is exceedingly low as compared to the influent medium, and extremely low as compared to batch cultures in early log phase. In turbidostats, N is supplied in small doses on demand, resulting in very low residual N.

This dynamic is illustrated by our residual [NO_3] data, showing that [NO_3] is typically low late in the photoperiod, but can be elevated in particular situations where rapid growth and the onset of the dark-period cause cultures to enter the S-phase of the cell cycle, thereby leaving un-assimilated N in the culture overnight (Supp. Tables 1 and 4) [3, 4, 10, 11, 15, 19, 20, 30].

4.2 Diurnal uncoupling of N & C metabolism

Unlike phosphorus or iron, N cannot be stored in inorganic form, giving the N quota curve a near-curvilinear form (Fig. 1) [1, 2, 3]. Moreover, glutamine synthase within the GS-GOGAT cycle, utilizes ketoacid skeletons from central carbon metabolism to manufacturing amino acids from inorganic N, i.e., N assimilation requires a supply of C skeletons for amino acid synthesis; this is the reason N and C metabolism are so tightly coupled [1, 2, 10, 27, 29].

Mildly N-limited *Picochlorum* cells in turbidostat mode, while dividing rapidly and not significantly stressed, may be forced to place C skeletons in temporary storage during the photoperiod until sufficient N is available. This is in contrast to the classic acclimation response, where previously assimilated N may be redirected and used for functional biomass, sacrificing chlorophyll and photosynthetic antennae to maintain cellular function essentially modifying the ratio of functional biomass (protein) to photosystems or photosynthetic capacity [3, 27, 29].

Flow cytometry offers the ability to compare merged cytograms from samples taken across days and photoperiod timepoints, i.e., we can pool cell samples to compare the full diel range of phenotypes present in our cycloturbidostat cultures. Fig. 8 shows pooled populations for two individual cultures, one under the replete (Fig. 8A,D) and one under the limited treatment (Fig. 8B,E). Time is implicit – as cells increase in size over the day, they follow a lower left to upper right 'trajectory' with the most common routes to division shown by the densest regions in red.

Replete cells show a single trajectory, where chlorophyll increases in a quasi-liner fashion with cell size. In contrast, panel B shows multiple dense regions or possible trajectories, some high chlorophyll and some low. This implies that cells, depending on their life history, are forced to take

different trajectories to successful cell division, suggesting heterogeneous routes to division in the limited treatment. The overlapping contour map in Fig. 8C shows that the phenotypes present in our respective cultures differ in their average chlorophyll content late in the photoperiod, i.e., when cells are large, as confirmed by the analyses above (Fig 6, Table 4, Supp. Table 3). Chlorophyll vs. neutral lipid content plots reveal further differences between N-replete and N-limited cells. The densest regions in the replete plot (Fig. 8D) fall below the 10^3 mark for [NL] where the limited plot (Fig. 8E) shows dense regions above the 10^3 mark when cells are large. In contrast, replete cells exhibit high [Chl] but dense regions in the limited plot fall below the 10^3 mark (Fig 8D,E). Panel F shows that the densest regions in the replete and limited plot do not overlap, except when the limited culture exhibits relatively high [Chl]. This suggests that heterogeneous routes to division in the limited treatment allow for a small subset of cells to follow a diurnal trend similar to replete cells; presumably, these cells do not exhibit the replete-like high lipid and low chlorophyll characteristic because they were able to assimilate an adequate amount (i.e. > $Q_{N,T}$) of N through the photoperiod. An epifluorescence micrograph of *P. oklahomense* shows that cells may contain multiple lipid droplets and multiple chloroplasts per cell – this gives added validity to the flow cytometry data presented here (Fig. 9).

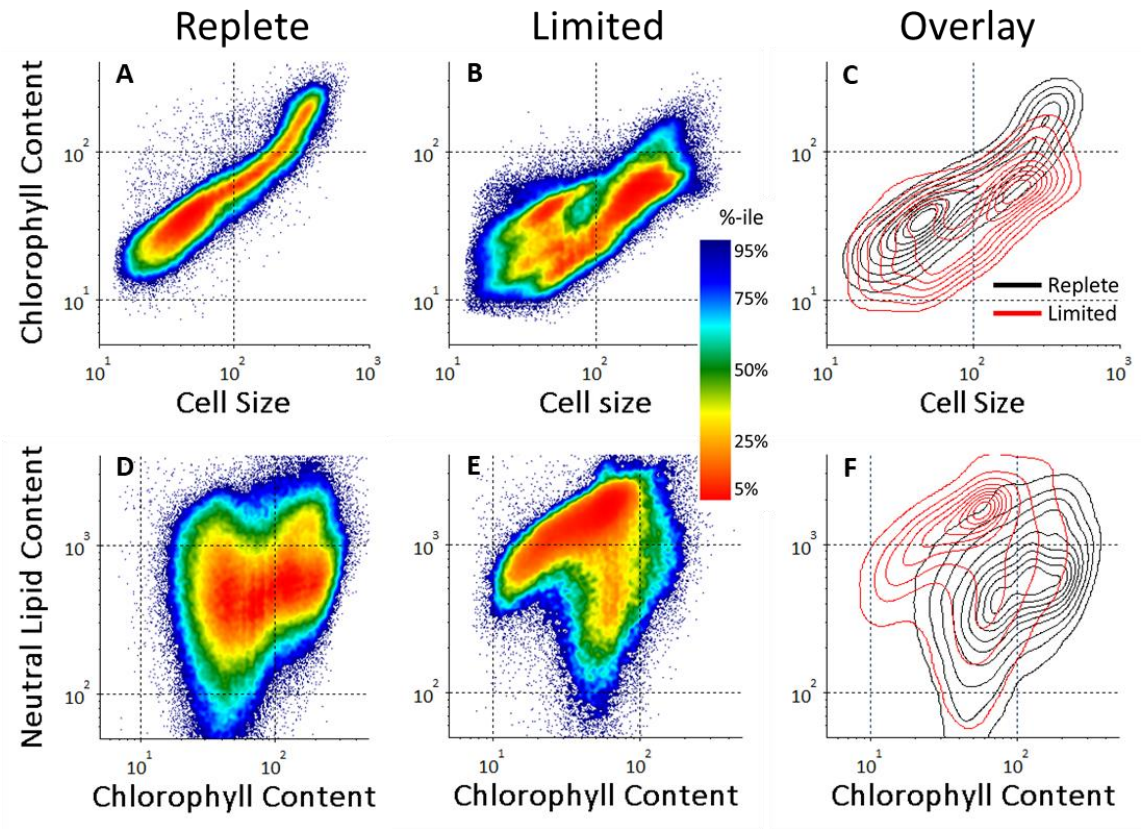

Fig. 8: Merged cytograms showing the spread of phenotypes present in samples across days and timepoints (expt. 3). A) replete [Chl] vs cell size, B) limited [Chl] vs cell size, C) contour map showing overlay of A and B, D) replete [NL] vs. [Chl], E) limited [NL] vs. [Chl], F) C) contour map showing overlay of D and E. Colors in A, B, D, E represent percentile of population with the most dense areas shown in red. Contour maps C and F are based on the same population percentiles with eight levels shown; replete cultures are shown in black, limited in red. Data shown here are the same as in Fig. 6 with mid-day samples included.

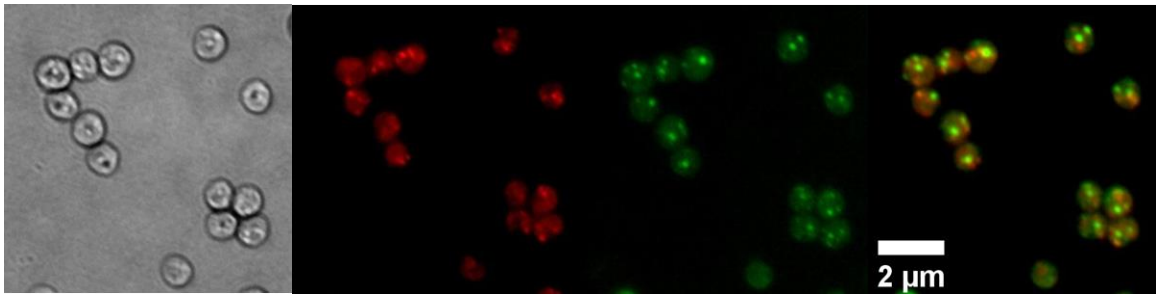

Fig. 9: Epifluorescence micrographs showing *P. oklahomense* cells from an early stationary-phase batch culture with individual channels and an overlay showing chlorophyll fluorescence in red and BODIPY stained neutral lipid bodies in green. Scale bar is 2 µm.

These results suggest that net daily N and C assimilation rates are proportionally equal in replete and limited cells, but due to the decrease in growth rate (13.1%) along with the decrease in $[NO_3]_{inf}$ (17.3%) and $Q_{N,\,cell}$ (23.5%), there is no difference in C:N. A transient uncoupling between C and N assimilation rates occurs over the course of the photoperiod, hence the increased NL fluorescence in limited cells. However, not enough time passes with cells in this uncoupled state to alter C:N ratio as N sufficient for cell division is continually supplied, i.e., cells are not N-limited to the point of cell cycle arrest. We assert that, although cells are N-limited they are not stressed to the point of major, slowly reversible metabolic rearrrangement (i.e., acclimation). Instead, N-limited cells transiently uncouple C and N metabolism to maintain C fixation throughout the photoperiod before cells return to their 'replete-like' phenotype at pre-dawn. However, while neutral lipid content is elevated late in the photoperiod in limited cultures as compared to replete, stored lipids are likely re-distributed to synthesize new membranes in support of cell division at night [5, 14, 15, 19-21].

It is important to emphasize that these daily adjustments are hypothesized to be distinct from the canonical acclimation response to a stressor involving long-lasting, metabolism-wide changes – these would be made in the approach to steady-state as cultures reach a dynamic balanced-growth state.

Cells in the slower growing limited treatment make less chlorophyll, likely reallocating N resources to maintain essential cellular functions. Despite this decrease in light harvesting capacity,

limited cultures grew nearly as fast as replete cultures – a slight increase in F_v/F_m suggests these cells are forced to be more efficient light harvesters. However, they still experience an uncoupling and opt to temporarily store C skeletons. We posit that cells in our limited treatment have at the least initiated lipid droplet formation in contrast to the replete treatment – either the replete cells have not initiated the formation of or are not actively growing their lipid bodies. This occurs despite minimal decrease in cell division rate and no change in C:N ratio, which implies that cells can effectively sense incipient limitation and adjust physiology in real-time in order to maintain homeostasis.

4.3 Cycloturbidostat Dynamics and Inherent Variability

Turbidostats are designed to operate only at nutrient-replete μ_{max} for the given organism and conditions, and since turbidostats maintain a constant biomass density, $Q_{N,\,cell}$ can be manipulated by changing $[NO_3]_{inf}$ and a growth rate < μ_{max} could be maintained. As stated, if $Q_{N,\,cell}$ falls below $Q_{N,\,T}$ a cycloturbidostat culture may fail due to its inability to recover night-time respiratory losses and maintain growth. This is not as relevant an issue in turbidostats under continuous light as turbidity never decreases due to dark respiration – however, cultures could still crash if supplied too little N, but this would likely occur at a lower $[NO_3]_{inf}$ than on a L:D cycle.

In contrast, equilibrium biomass density varies directly with $[NO_3]_{inf}$ in chemostats, and thus may not be independently controlled [9-11]. Chemostats are also constrained by the risk of washout, which may occur at high μ/μ_{max}, i.e., 90% of μ_{max}. Thus, turbidostats are distinct from chemostats in two important ways: biomass density is uncoupled from $[NO_3]_{inf}$, and they operate at μ_{max} without the risk of washout. This however adds complexity as biomass density, light and nutrient availability, and growth rate are inter-related; chemostats in comparison are simpler and less variable. For these reasons, nutrient limited balanced-growth states in turbidostats are difficult to maintain under near-limiting conditions.

Cycloturbidostats in particular have this added complexity, thus show increased variability from culture-to-culture and day-to-day. In order to minimize this variability, turbidity sensors were

calibrated before each experiment, inoculum was grown under experimental lighting with minimal nutrients, and measures were taken to minimize human error, e.g., loss of media flow, sampling perturbance, etc. This inherent variability makes the interpretation of these results difficult as evidenced by subtle differences between the iterative experiment herein. In particular, that growth rate declined precipitously after the drop to 250 μM in experiment 1 but not in experiment 2 points to this variability. However, these differences could simply be explained by subtle discrepancies in cell density, light intensity, and media supply altering the dynamics of the system, i.e., the 'cliff' of nitrogen limitation is more clearly illuminated by cell-based measurements rather than bulk nitrogen supply or overall growth characteristics.

In order to determine when cultures are in steady-state, Klok et al. set an arbitrary benchmark of 10% change over a 3-day period in growth rate, cell count, and chlorophyll content; however, they utilized continuous light, which likely decreases the variability in growth parameters [12]. While the coefficients of variation of mean growth rates and cell counts for replicate culture units in our experiments were above the arbitrary benchmark of 10% change over a 3-day period, 3-day rolling coefficients of variation within each culture unit remained below 10% for most of the experiment. The highest variability occurred in the first ca. 12 days of the experiment, following changes in $[NO_3]_{inf}$, and at the lowest $Q_{N,\ cell}$ rates (Supp. Fig. 7).

It seems pertinent to note that different growth rates may result in different degrees of asynchrony, in theory. Given that doubling rate (D) is equal to μ divided by ln(2), a μ of 1.67 d^{-1} in our replete treatment would equal a D of 2.41 d^{-1}, and a μ of 1.45 d^{-1} in our limited treatment a D of 2.09 d^{-1}. Thus, the heterogeneity exhibited in our limited treatment may be explained in part by the asynchrony driven by the apparent growth rate. In other words, cells that have a life-history depending on the timing of their individual cell cycle events relative to the photoperiod or other cyclical phenomena like nitrate uptake and assimilation. Anecdotally, a higher degree of asynchrony was evident in the limited treatment where pre-dawn samples showed more cells yet undivided. The heterogeneous

population dynamics exhibited here by partially-synchronized cyclostat cultures could be considered an emergent property that highlights the need to understand both whole-cell physiology and system-level population dynamics.

4.4 Lessons for Future Studies in Microalgal Biotechnology

We sought to identify and characterize a poorly studied physiological transition state between N-replete and incipient N-limitation. In batch cultures this transition is progressive such that any physiological transition is confounded by other variables and cannot be easily characterized. We employed cyclo-turbidostats to 'trick' cells into a state of incipient N-limitation. This was achieved without the use of genetic engineering, using only precise control of limiting nutrient supply, and likely could not be observed in batch or chemostat culture - physiology is non-steady state in batch, and chemostats at different dilution rates force different growth rates and biomass density.

While *P. oklahomense* typically exhibits low percent lipid content, several *Picochlorum* strains have received considerable attention due to their rapid growth, wide salinity tolerance, and high light and temperature tolerance [26, 31-34]; Figure 9 shows a micrograph of *P. oklahomense* cells from an early stationary-phase culture with red chlorophyll fluorescence and multiple green BODIPY stained neutral lipid bodies. Given a growth rate of 1.67 d^{-1} and a dry biomass concentration of 127 mg L^{-1} in our cycloturbidostat cultures, we obtain a biomass productivity of 212.1 mg L^{-1} d^{-1} and a lipid productivity of 6.4 mg L^{-1} d^{-1}. However, the estimation of overall lipid productivity may not capture the difference in cellular lipid content as evidenced by the flow cytometry results herein. There is little evidence for widespread cell death following lipid-accumulation as cell densities and growth rates indicate that the majority of cells persist to grow the following day. Thus, a portion of the population induces the accumulation of carbon reserves during the photoperiod and re-allocates those stored resources during the scotoperiod and the following day. It should be noted that this system was not optimized for production and could be improved if that was the goal.

Although the lipid content values reported here are low, *Picochlorum* is not known to be a high lipid accumulator and seems to prefer carbohydrate storage over lipids [31, 32, 34]. A lipid content of 11% of dry weight was attained in *P. oklahomense* growing at 0.2 d^{-1} in a two-stage turbidostat [13], and other studies focused on this genus have reported lipid content values below 10% and up to 20% of dry biomass in the stationary phase of batch growth [31, 32, 34]. We chose this strain because of its optimal behavior in turbidostats (doesn't sink or stick) rather than its tendency to accumulate lipids. Nevertheless, it still moderately accumulated lipids while growing rapidly, contrary to current dogma. While results did not show hyper-accumulation of lipids to a biotechnologically relevant level, the findings and conclusions herein offer new conceptual physiological insights to support future studies. Repeating similarly designed experiments using strains known to hyperaccumulate lipids would be a worthy endeavor.

This study expands on other studies utilizing continuous cultures with the intention of leveraging the control N supply to enhance biomass and lipid productivity [4, 12, 13, 15-17]. These studies demonstrate that TAG accumulation is related to both N-supply and light, i.e., reducing power. The various species used in these studies have varying physiologic characteristics which have pronounced effects on the dynamics of continuous cultures, i.e., preference for NO_3 or NH_4, N:P ratio, capacity for mixotrophic growth, respiration rates, cell sizes, etc. The study conducted by Klok et al. showed that cells in their turbidostats uncoupled N and C metabolism when supplied with excess reducing power relative to their N supply [12]. Likewise, Wen et al. posit that continuous culture can outpace batch cultures if lipid production is optimized for specific N supply [17]. However, these studies used continuous light and simply provide the understanding that when reducing power exceeds the needs of the cell and given that irradiance does not exceed the point of photoinhibition, cells will uncouple N and C metabolism and increase C stores. The twin studies of Lacour et al. demonstrated the effects of different N limitation regimes (N-limited vs. and N-starved) under continuous light and illustrated the effects of the photoperiod on neutral lipid content [15, 16].

Those studies employed carbon or biomass-based analyses and did not quantify cell-specific N supply ($Q_{N, cell}$). Our study takes a cell-based approach, which stands in contrast to both the biomass-based approach of biofuel engineers, and the carbon-based approach of oceanography and limnology (where the assemblage of algae is mixed and often unknown). Our approach shows a potential for enhanced productivity in terms of chlorophyll per biomass, as we show reduced chlorophyll content in limited cycloturbidostats, which by definition maintain equal biomass concentrations day-to-day and calibrated culture-to-culture. No previous continuous culture study used more than duplicate cultures. Studies investigating $Q_{N, T}$ and related concepts while utilizing continuous cultures may help elucidate the ways that algae may be grown at near-μ_{max} or under near-limiting conditions while maintaining stability and a predictable dynamic balanced growth state. Combining manipulated steady state culture with genetic approaches could be a powerful strategy to improve productivity of biomass and desired biochemical components. In principle, this approach could be optimized to manipulate other biochemical components.

Controlling $Q_{N, cell}$ in large tubular photobioreactors or open pond raceway systems will be a difficult task. However, taking the difficult steps to understand and minimize variability in cell-specific N supply will increase both the economic and photosynthetic efficiency of cultivation systems by minimizing the need for N supply, increasing light penetration via reduced chlorophyll content, and priming cells for hyper-accumulation of carbon storage products. There is no doubt that nutrient management will be an essential agronomic tool utilized by all large-scale algal farms [4, 6-8, 19, 35-37].

5.1 Conclusion

These results show that cyclical diurnal neutral lipid accumulation and ultradian growth are not mutually exclusive, and that cycloturbidostat cultures of *Picochlorum oklahomense* may be maintained near or at the threshold of N-limitation to control cell composition and modulate biomass productivity. This is a technically challenging, labor-intensive feat, necessitating experiments

addressing subtle changes in a physiological transition zone that has scantly been explored. This is only possible in cycloturbidostats (not in batch, semi-continuous, or chemostat cultures), due to their sensitivity and unique dynamics. Using this novel approach, we have identified the threshold of N limitation in *P. oklahomense* and investigated the effects of N limitation on replicate cycloturbidostat cultures. Mildly N-limited cycloturbidostat cultures grew rapidly (87% μ_{max}) and maintained near optimal physiology, while also accumulating neutral lipids during the photoperiod. Flow cytometry revealed differences in temporal patterns between treatments, demonstrating the importance of the cell-based approach in manipulating and monitoring microalgal cultures. This study highlights the utility of turbidostats in experimental phycology and defines a scantly explored concept in the study of N limitation, the threshold of N cell quota necessary to support μ_{max} below which cells are forced to re-allocate resources and slow growth, denoted $Q_{N,\,T}$. Given the reduction in cost and widespread adoption of microcontrollers, turbidostats are becoming more affordable and easier to build. Coupled with advancements in molecular biology and mathematical growth modelling, turbidostats seem primed to bring significant discoveries in microalgal research. Revisiting the canons of the phycological heyday of the late 20th century armed with the tools of today will surely bring new answers and many more questions.

Funding:

This research was conducted in partial fulfillment of the requirements for the degree of Doctor of Philosophy (Ph.D.) in the Department of Plant Biology, Ecology, and Evolution (PBEE) at Oklahoma State University on behalf of Dylan Franks (DF). The research results discussed in this publication were made possible in total or in part by funding through the award for project number PS16-003, from the Oklahoma Center for the Advancement of Science and Technology, as well as the J.K. McPherson Memorial Fund of the PBEE department, and the Graduate and Professional Student Government Association at Oklahoma State University.

Supplemental Figures:

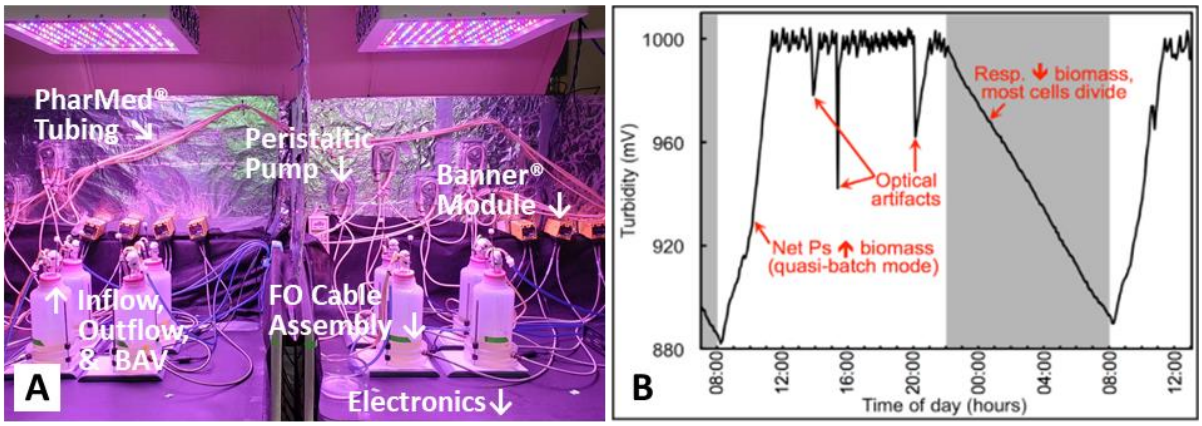

Supp. Fig. 1: A) Image of cycloturbidostat setup with tubing, pumps, optical sensor modules, in/outflow, and biological air valve (BAV), fiber optic (FO) assemblies, and electronics labelled. Media and effluent refrigerators not pictured. B) Turbidostat trace throughout a steady state period for one replicate cultures.

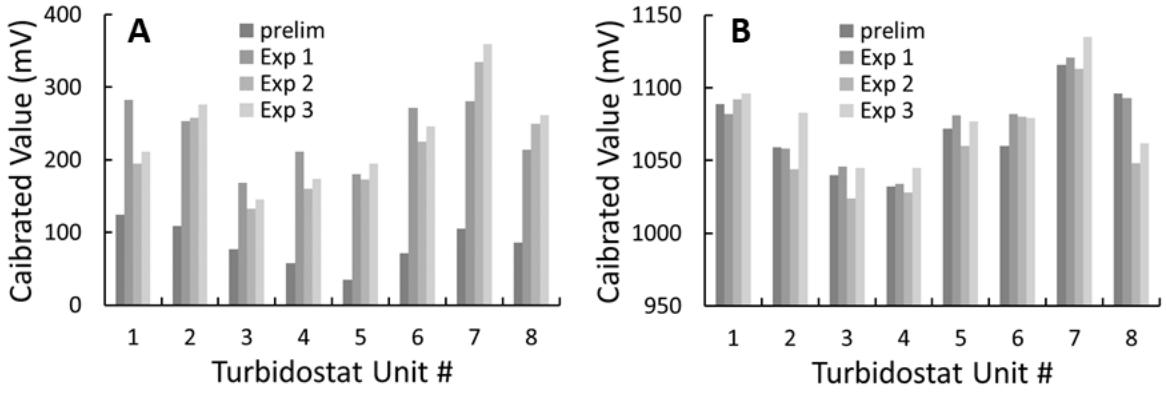

Supp. Fig. 2: Calibrated turbidity values across different experiments. Sensors were calibrated with DI water (A) and a neutral density filter (B).

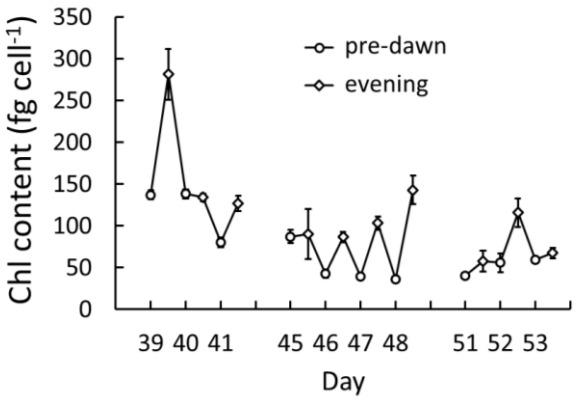

Supp. Fig. 3: Diel cycling of chlorophyll in experiment 1. Data points represents means ± SD of 4 replicate cultures at pre-dawn and evening time-points.

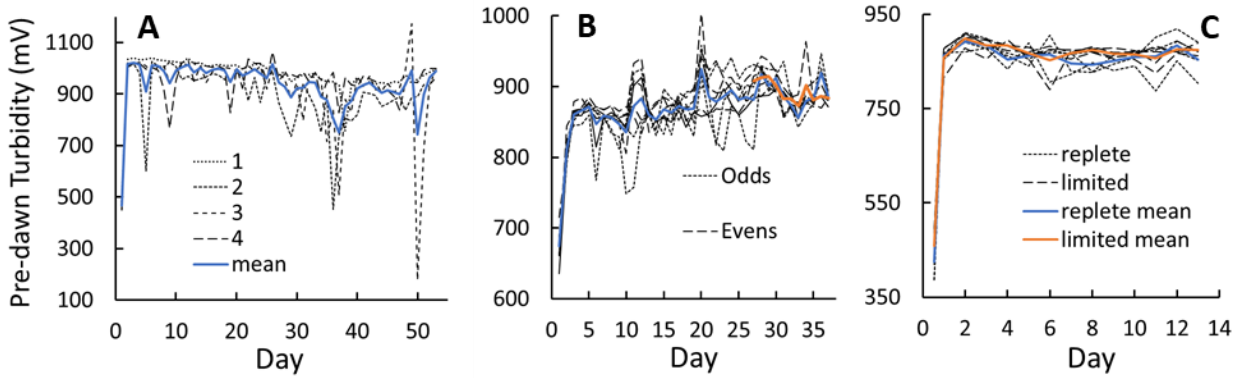

Supp. Fig. 4: Pre-dawn turbidity for individual cultures and relevant means from A) experiment 1, B) experiment 2, and C) experiment 3.

Supp. Table 1: Residual NO_3 present in pre-dawn samples (Exp 2).

NO_x Bin	*Frequency (count, % total)*	
≤ 5 µM	80	50.0%
5–10 µM	31	19.4%
10–30 µM	7	4.4%
30–100 µM	25	15.6%
> 100 µM	17	10.6%
	n = 160	

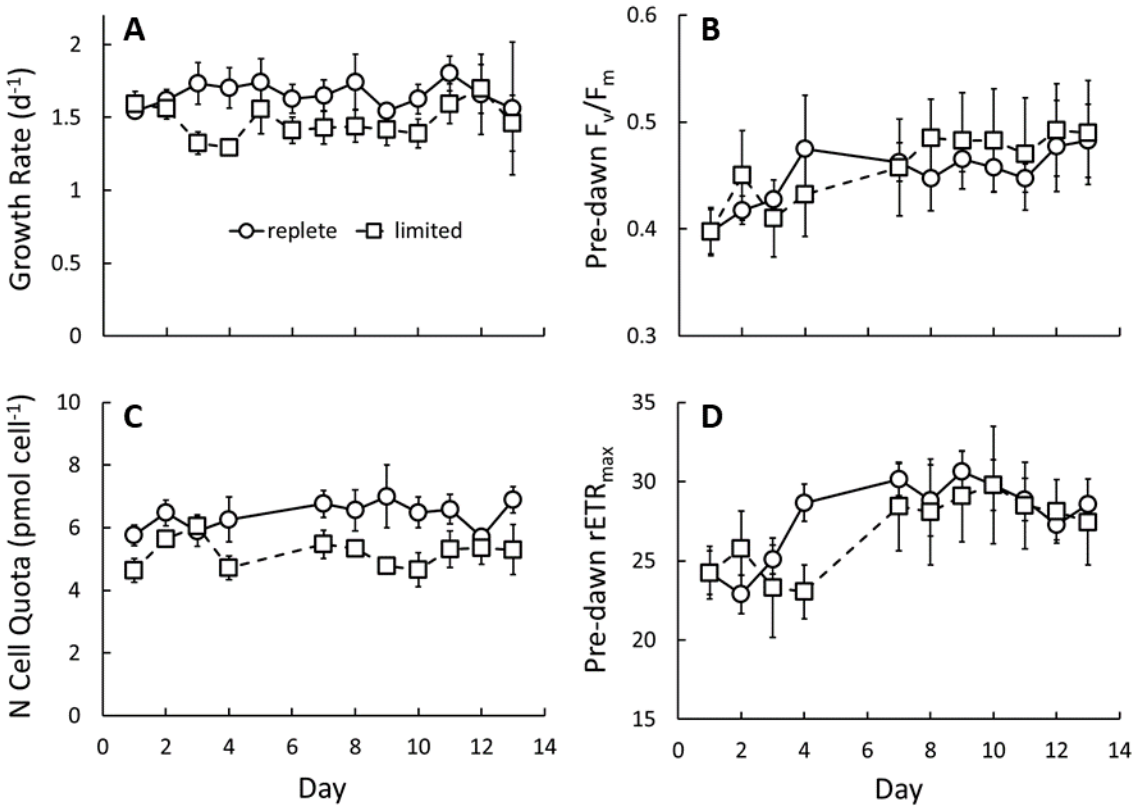

Supp. Fig. 5: Growth chronology of $[NO_3]_{inf}$ comparative study (expt. 3). A) specific growth rate, B) pre-dawn F_v/F_m, C) cell N quota, and D) pre-dawn $rETR_{max}$ of individual cultures. Symbols indicate $[NO_3]_{inf}$ treatment. Means ± SD, (n = 4).

Supp. Table 2: Two-tailed t-test results from data in Fig 5: Comparative physiological parameters from days 7 – 11 in replicate cultures (n = 4, 4) (expt. 3).

	Growth rate (d^{-1})		Cell Density (10^6 mL)		$Q_{N, cell}$ (pmol $cell^{-1}$)		F_v/F_m		ETR_{max}	
	Rep	Lim	Rep	Lim	Rep	Lim	Rep	Lim	Rep	Lim
mean	1.67	1.45	13.6	14.9	6.68	5.11	0.46	0.48	29.6	28.8
SD	0.15	0.13	1.40	1.66	0.67	0.55	0.02	0.05	1.71	3.17
Var.	0.024	0.019	2.06	2.90	0.47	0.32	0.0005	0.0023	3.1	10.5
N	20	20	20	20	20	20	20	20	20	20
df	38		38		38		38		38	
%Δ	-13.1%		9.1%		-23.5%		4.3%		-2.9%	
t Stat	4.72		-2.48		7.87		-1.65		1.05	
p	3.2E-05		0.018		1.7E-09		0.108		0.29	
t Crit	2.02		2.02		2.02		2.02		2.02	

Supp. Table 3: Two-tail t-tests assuming equal variances on median values of comparative flow cytometry characteristics from Fig. 6 (expt. 3). Data includes days 7 – 11 in two individual cultures.

	Cell Size (FSC)				Side Scatter (SSC)				Chl Content (MFI)				NL Content (MFI)			
	RM	LM	RE	LE	RM	LM	RE	LE	RM	LM	RE	LE	RM	LM	RE	LE
Mean	46.7	49.9	226.9	191.8	14.0	19.0	49.3	55.1	34.2	28.6	114.2	59.6	666.4	541.8	716.2	1343
SD	2.7	1.9	25.8	19.5	0.5	2.6	10.2	13.1	1.4	6.6	21.6	4.0	244.0	214.4	330.1	84.6
Var.	9.0	4.6	834	474	0.3	8.3	130	215	2.5	54.8	585	19.7	74399	57450	136211	8943
N	5		5		5		5		5		5		5		5	
df	8		8		8		8		8		8		8		8	
%Δ	7.0%		-15.4%		35.5%		11.8%		-16.2%		-47.8%		-18.7%		87.5%	
t Stat	-1.99		2.17		-3.81		-0.70		1.64		4.97		0.77		-3.68	
P	0.081		0.062		0.005		0.505		0.140		0.001		0.465		0.006	
t Crit	2.31		2.31		2.31		2.31		2.31		2.31		2.31		2.31	

Supp. Table 4: Residual NO_3 present in culture samples. (expt. 3)

NO_x Bin	Replete Pre-Dawn		Limited Pre-Dawn		Replete Evening		Limited Evening	
	Frequency (count, % total)							
0 µM	43	76.8%	36	64.3%	19	79.2%	20	83.3%
≤ 5 µM	5	8.9%	2	3.6%	0	0.0%	0	0.0%
5–10 µM	1	1.8%	0	0.0%	1	4.2%	1	4.2%
10–30 µM	1	1.8%	4	7.1%	2	8.3%	1	4.2%
30–100 µM	0	0.0%	8	14.3%	2	8.3%	1	4.2%
> 100 µM	6	10.7%	6	10.7%	0	0.0%	1	4.2%
n total =	56		56		24		24	

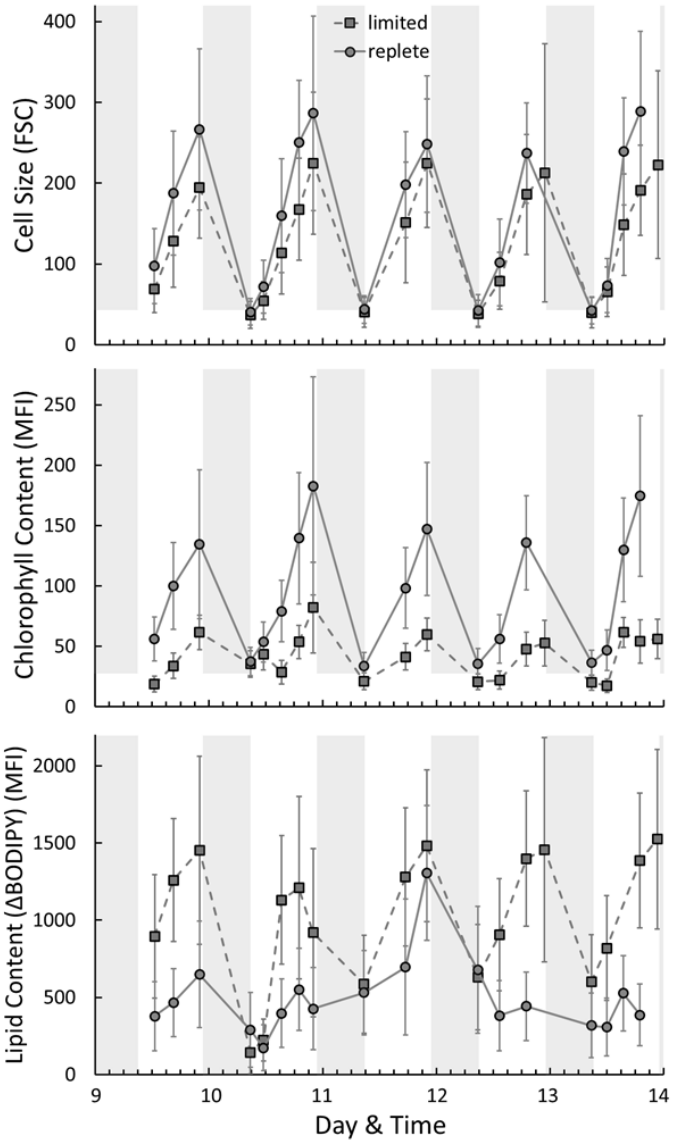

Supp. Fig. 6: Flow cytometry phenotyping of samples from individual cultures across 5 steady-state periods (expt. 3). A) cell size measured as forward scatter; B) chlorophyll content measured via autofluorescence; C) normalized lipid content measured via BOPIDY 495/505 staining. Median values from a single culture from replete and limited are shown with error bars representing the coefficient of variation of the population spread. Replicate cytograms files from each sample tube were merged to obtain the values shown.

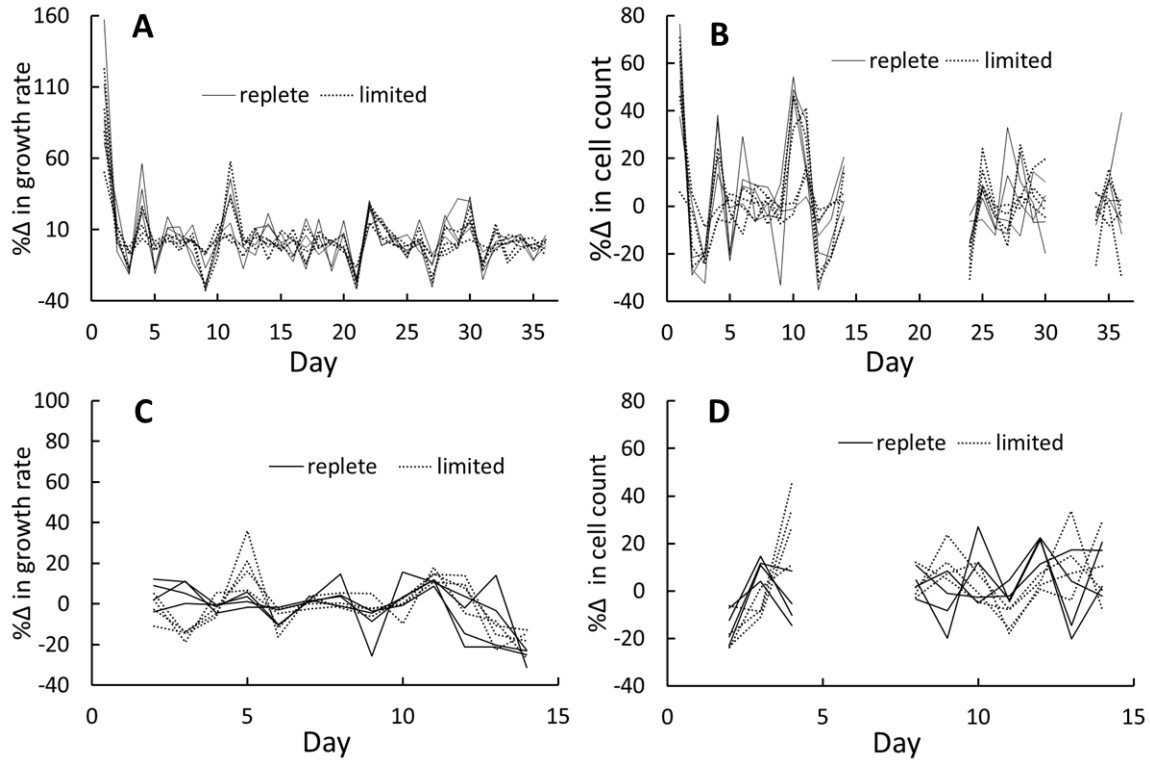

Supp. Fig. 7: Daily percent change in culture parameters for individual cultures in expt. 2 (panel A, B) and expt. 3 (panel C, D).

CHAPTER II

Evidence of Multiple Fission in Asynchronous Continuous Cultures of *Picochlorum oklahomense* Suggest Clustered Rounds of DNA Replication

Abstract:

Empirical evidence of multiple fission in *Picochlorum oklahomense* (Chlorophyta, Trebouxiophyceae) grown in light-saturated turbidostats and in semi-continuous cultures is shown. We provide a description and discussion of the methods used and explore future directions in the study of cell division in the class Trebouxiophyceae. We confirm that *Picochlorum oklahomense* is an autosporic species, and show it produces 2 to 4 daughter cells per mother cell via a multiple fission pathway. Furthermore, our data suggest that *P. oklahomense* undergoes multiple fission according to the clustered pattern, much like Chlorophyceae genus *Chlamydomonas* and the Trebouxiophyceae genus *Chlorella*. These results suggest that multiple fission and the number of resulting daughter cells is tied to both photon flux and resource availability, i.e., carbon and nitrogen supply. However, we hypothesize that phenology, or the timing of cell cycle events relative to the photoperiod, is an additional important factor in determining the incidence of multiple fission. In other words, the life history of individual cells, i.e., the timing of cell cycle events relative to the onset of the photoperiod/scotoperiod modulates the occurrence of multiple fission cell cycle stages, especially at growth rates exceeding 1 d^{-1}.

Keywords: cell cycle, Trebouxiophyceae, doublet discrimination, autosporulation

1.0 Introduction:

Green algae are a ubiquitous and diverse group of organisms whose taxonomic relationships are continually under investigation. Morphological characteristics remain an important tool in the designation of algal taxa [33, 38-40], and the use of modern phylogenetics offers molecular testing of these relationships [33, 38, 39, 41-43]. Meanwhile, our understanding of the eukaryotic cell cycle has seen incredible advancements in the last few decades with advancements in microscopy and the advent of modern genetic techniques. Notably, the discovery of the cell cycle regulation by kinase cascades received a Nobel Prize in 2001 and marked a burgeoning of cell cycle research across eukaryotic lineages [44-48].

There are three modes of cell division in eukaryotic algae: binary fission, autosporulation, and budding. Binary fission is the simplest and most common cell division strategy whereby a mother cell gives rise to two new daughter cells following cytokinesis – no mother cell wall is present after division. Autosporulation is characterized by the development of daughter cells inside the mother cell wall, giving rise to free-living daughter cells following the rupture of the mother cell wall. These modes stand in contrast to the budding-type cell division commonly found in fission yeast, whereby a daughter cell develops as a small bulb-like projection from the mother cell. Multiple fission is a more complex cell cycle pattern whereby mother cells give rise to more than two daughters cells via a number of routes [11, 13, 14]. This occurs through multiple iterations of genome duplication and mitosis, with or without cytokinesis depending on species, giving rise to cells containing multiple copies of the genome.

Multiple fission in green algae can be categorized into consecutive and the clustered models, which describe the sequence and arrangement of the S-phases of the multiple fission cell cycle. Yet this is an oversimplification, as the true pattern of cell division can differ even in closely related genera. Multiple fission patterns in green algae are therefore described using model genera such as *Chlamydomonas*, *Scenedesmus*, and *Chlorella*. It is hypothesized this adaptation is used

to separate the biomass growth and division phases of the cell cycle under optimal conditions on a light-dark cycle to focus on autotrophic growth throughout the photoperiod without stopping photosynthesis or diverting resources to genome duplication and cell division [11, 13, 14].

The genus *Picochlorum* (Chlorophyta, Trebouxiophyceae) was recently described by reassigning a group of species from the *Nannochloris*-like coccoid green algae [2]. This genus is gaining considerable attention in algal research programs due to its rapid growth rate and tolerance to heat and salinity [15-20]. Recent sequencing projects of *Picochlorum* species revealed exceedingly small, diploid genomes with intricate organization hypothesized to function in decreasing cell size in response to extreme conditions [7, 18]. This species is known to divide by autosporulation into two or more daughter cells though little investigation of its cell cycle patterns is present in the literature. Genomic studies have shown that certain *Picochlorum* spp. possess diploid genomes, thus one would expect to find cells of diploid genomes denoted as 2C as well as cells with double the genome copies that have yet to divide, denoted as 4C. If multiple fission cell cycles are present within a given population, one would also expect to find cells with more than two copies of the genome, or greater than 4C, i.e., 8C, 16C etc. If each genome copy is independently replicated, one may then expect to find a distribution of cells possessing an intermediate number of genomic copies, i.e., 6C, 12C or anywhere in between.

Here we present empirical evidence of multiple fission in *Picochlorum oklahomense* (Chlorophyta, Trebouxiophyceae) grown in light-saturated turbidostats, provide a description and discussion of the methods used, and explore future directions in the study of cell division in the class Trebouxiophyceae.

2.0 Methods:

2.1.1 Growth conditions and culture maintenance:

Cultures of *Picochlorum oklahomense* (Trebouxiophyceae) were maintained in artificial seawater (AS) containing 20 g NaCl L^{-1} (2% w/v), 5 mM $NaHCO_3$, 825 μM Tris buffer, f/2

vitamins, and a trace metals mix [21]. Cultures used to inoculate turbidostats were maintained in glass bottles, sparged with air, and stirred at 100 rpm under 150 μmol photons m^{-2} s^{-1} of illumination provided by 400-W metal halide lamps on a 14:10 h L:D cycle.

Rapid light curves (RLCs) were measured using a fiber optic Phyto-PAM EDF chlorophyll fluorometer (Heinz Walz GmbH, Effeltrich, Germany) to measure maximum quantum yield (F_v/F_m) and maximum relative electron transport rate ($rETR_{max}$) through PSII.

2.1.2 Turbidostat experiments:

The cyclo-turbidostat system used here was previously described [21, 22]. Briefly, computer-controlled peristaltic pumps delivered fresh AS medium to turbidostat bottles and removed culture from the bottles in equal amounts; culture volume was 300 mL. The system maintained a constant biomass density by averaging the turbidity signal at 15 sec intervals over a 5-minute period and triggering 1-minute pump cycles at a flow rate of 10 mL min^{-1} when the 5-minute average signal exceeded an arbitrary set-point voltage.

This setup was housed in a temperature-controlled growth room maintained at 25 ± 3 °C. Light was provided by 400W LED light banks (PhytoMAX 400, Black Dog LED, Niwot, CO) at *ca.* 750 – 850 μmol photons m^{-2} s^{-1} incident illumination on a 14:10 L:D cycle. Each culture was stirred at *ca.* 120 rpm and sparged continuously with air at *ca.* 10 mL min^{-1} at night and 1% CO_2 in air during the photoperiod. Sterile fresh medium was made in 2-L batches, fitted to luer-lock connections for the corresponding cultures, and stored at 4˚C. Culture effluent volume was measured each morning to determine dilution rate, which is equal to μ, over the previous day.

2.1.3 Semi-Continuous Experiment:

Semi-continuous turbidostat-mode cultures were maintained by diluting cultures at the same time each day to obtain an optical density (A_{750}) of 0.2 using fresh AS media containing 20 g NaCl L^{-1} (2% w/v), 1.5 mM NO_3, 300 μM PO_4, 5 mM $NaHCO_3$, 825 μM Tris buffer, f/2

vitamins, and a trace metals mix. Light was provided by two metal halide lamps at *ca.* 250 μmol photons m^{-2} s^{-1} incident illumination on a 14:10 L:D cycle. Each culture was stirred at *ca.* 300 rpm and sparged continuously with air at *ca.* 10 mL min^{-1}. A mixture of 1.0% CO_2 in air was supplied to half of the cultures at a flow rate of *ca.* 10 mL min^{-1} during the photoperiod. Half of the cultures were shaded to *ca.* 50 μmol photons m^{-2} s^{-1}. A 2x2 experimental setup was used with duplicate cultures under each condition high light or low light, with or without CO_2 supplementation denoted HL+, HL–, LL+, and LL–. A single healthy stock culture in semi-continuous mode was used to inoculate pre-experimental cultures which were maintained in semi-continuous mode and acclimated to the appropriate experimental conditions for 5 days before the experiment. Growth rate (μ) was calculated daily for 5 days after acclimation (8 days total) by the following equation:

$$\mu = \frac{\ln(\mathrm{OD}_{Final}) - \ln(\mathrm{OD}_{Initial})}{1\ day}$$

where OD is the optical density (A_{750}) at a given timepoint and μ is growth rate.

Division rate per day (D) was calculated by the following equation:

$$\mathrm{D} = \frac{\mu}{\ln(2)}.$$

2.1.4 Flow cytometry:

One-mL culture samples were gathered at designated time-points from pre-dawn through late photoperiod. Samples were transferred to 1.7-mL centrifuge tubes and centrifuged at 12,000 x rpm for 3 min. Pelleted cells were fixed in 0.2 μm filtered neutralized methanol and stored at -20˚C. On the day of analysis, samples were centrifuged at 12,000 rpm for 5 min, re-extracted in 0.2 μm filtered methanol, and pelleted again by centrifuging at 12,000 rpm for 5 min. This pellet was resuspended in 2 mL of PBS buffer and stained with 8 μL of SYBR Green 1 (Thermo-Fisher,

Waltham, MA) (diluted 25:1 in Tris-EDTA buffer), then vortexed for 10 seconds and incubated in darkness for 10 minutes before processing [23, 24].

The 488-nm argon laser of the FACSCalibur® (BD Biosciences, San Jose, CA) excited green SYBR Green 1 fluorescence, which was detected in the FL2 channel (560–640 nm). A total of 10,000 events were gathered and cells were filtered first by size in a FSC vs. SSC gate and then using the doublet-discrimination (DDM) method. Briefly, events were plotted on a FL2-A by FL2-H plot and a gate was built to include only cells that fall on the diagonal i.e., their FL2 area and width increase proportionally. These filtered events were then displayed on a FL2-A (which is equal to DNA content) vs. cell size plot. A logarithmic scale for FSC-H was chosen in order to differentiate cell size more precisely, as *Picochlorum* is very small (< 2 μm), making it difficult to distinguish between cells of interest and bacterial contamination or cell debris; methanol fixation may also marginally shrink cells, exacerbating this issue. These filtered events were then subjected to doublet-discrimination (DDM) using dimensions of the FL-2 signal by plotting events in an FL2-Area vs FL2-Width plot and gating for events that fall on the diagonal. This eliminates events where the proportion of FL2-Area and FL2-Width values deviate from the diagonal (Supp Fig. 1).

To distinguish and quantify multiple fission populations, events were further split according to FL2-Area, which is proportional to total DNA content [23, 24]. An additional gate including only diploid (2C) and tetraploid (4C) cells only was used to model cell cycle phases via built-in multicycle models in FCS Express Multicycle (De Novo Software, Pasadena, CA) (Supp Fig. 1 & 2). Multiple fission populations, i.e., hexaploid (6C) and octoploid cells (8C), were gated based on DNA content, i.e., the number of copies (C) of the genome each cell holds as per SYBR Green I fluorescence. Histograms of each population with median values can be found in Supp Fig. 3. All flow cytometer settings were constant for all samples. Refer to Franks et al. for further details on cytometry methods [22].

2.1.5 Microscopy

The agar pad method was utilized for epifluorescence microscopy to prevent cells from moving during imaging. Briefly, clean glass microscope slides were arranged forming a 1 cm trough between slides, with a slide below the trough and a slide above. A mixture of 1% low-melt agar was mixed with 2% AS salts and microwaved for 30 seconds. Once cool, the agar was pipetted into the trough and allowed to harden. The slides were carefully removed, and 1 cm square agar pads were cut and transferred to clean slides. Pelleted cells were thawed, washed once with PBS buffer, and resuspended in 0.5 mL of PBS buffer, then stained with 2 µL of SYBR Green I. Cells were incubated for 10 min., then pipetted onto the agar pads in darkness and imaged using a Nikon Eclipse 80i microscope equipped with a UV-excitation and fluorescence imaging system. All DIC images were taking using a Nikon Eclipse Ni-U.

2.1.5 Statistics

The turbidostat experiment consisted of eight total cultures in two groups (n = 4, 4) that were inoculated and operated at their respective nutrient regimes for the duration of the experiment. Groups of replicate cultures were evenly distributed in relation to the light source to control for discrepancies in photon flux. Multiple fission populations percentages were obtained using triplicate cytograms from individual cultures (one replete and one limited culture) over 5 consecutive days. The semi-continuous experiment consisted of duplicate cultures for the four different treatments: high light with CO_2 (HL+), high light without CO_2 (HL-), low light with CO_2 (LL+), low light without CO_2 (LL-). Multiple fission populations percentages were obtained using triplicate cytograms from duplicate cultures over 2 consecutive days. All growth and physiological parameters are reported as mean ± standard deviation of replicate cultures.

3.0 Results:

3.1 Turbidostat experiment:

We previously used replicate cycloturbidostat cultures of *Picochlorum oklahomense* to quantify the minimum nitrogen cell quota supporting maximum growth rate and to study the physiological effects of mild nitrogen limitation at near-μ_{max} [22]. Mildly N-limited, steady-state cycloturbidostat cultures grew rapidly (87% μ_{max}) and maintained near optimal physiology, while also accumulating neutral lipids during the photoperiod. N-replete cultures exhibited a specific growth rate of 2.41 d^{-1} compared to 2.09 d^{-1} for N-limited cultures, but no difference in fluorescence properties was evident despite the difference in N cell quota ($Q_{N, cell}$) between the replete (6.68 ± 0.67 pmol $cell^{-1}$) and limited treatment (5.11 ± 0.55 pmol $cell^{-1}$).

Flow cytometry was employed to characterize the distribution of individual cellular properties over the course of the photoperiod in these cycloturbidostat cultures. While pre-dawn cell size, chlorophyll and lipid content were roughly equivalent, populations at mid-day and late in the photoperiod showed clear differences between the replete and limited treatments. Populations in the limited treatment at mid-day had reached only 85% of the cell size and exhibited only 52.3% of the chlorophyll content exhibited by the replete populations but showed 188% of the lipid content exhibited by replete populations, indicating uncoupling of nitrogen and carbon assimilation in N-limited populations.

Flow cytometry was also employed to monitor the progression of the cell cycle over the course of two consecutive days in individual cultures under both the replete and limited treatment (Fig. 10). The replete treatment showed phased cell division beginning late in the photoperiod and gradually progressed into its division cycle, with peak S-phase populations at 54.7% ± 4.0 and the lowest %G1 population at 29.6% ± 12.0 occurring after the onset of the dark period. In contrast, the limited culture exhibited increased %S-phase and decreased %G1 9 hrs into the 14-hr photoperiod with peak S-phase populations at 60.2% ± 12.6 and the lowest G1 population at 39.1% ± 11.3. Notably, G2/M population in the replete culture never fell below 11%, but the G2/M population fell to near-zero in the limited culture 9 hrs into the photoperiod.

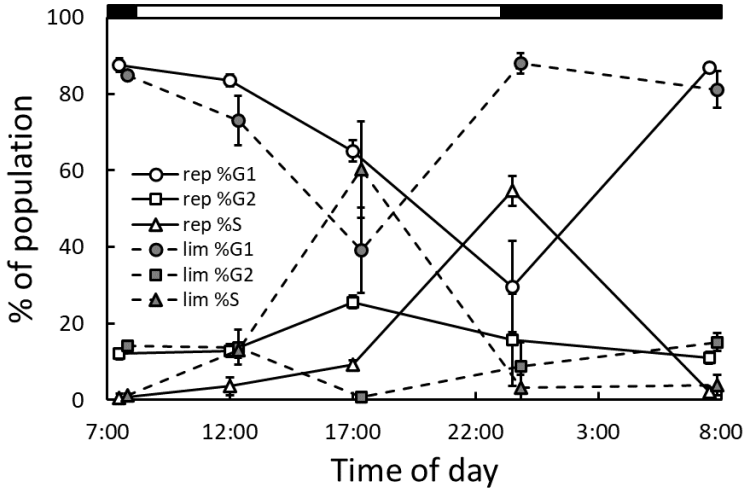

Fig. 10: Cell cycle data from replicate cytograms across 3 days in N-replete and N-limited cycloturbidostats. Cell cycle models were calculated by FCS Express Multicycle. Error bars represent standard deviation of $n \geq 3$ replicate cytograms over 3 consecutive days in two individual cultures, one each under the replete and limited treatment. X-values for the limited treatment are offset for clarity. Black bar represents the 14:10 hour light:dark cycle.

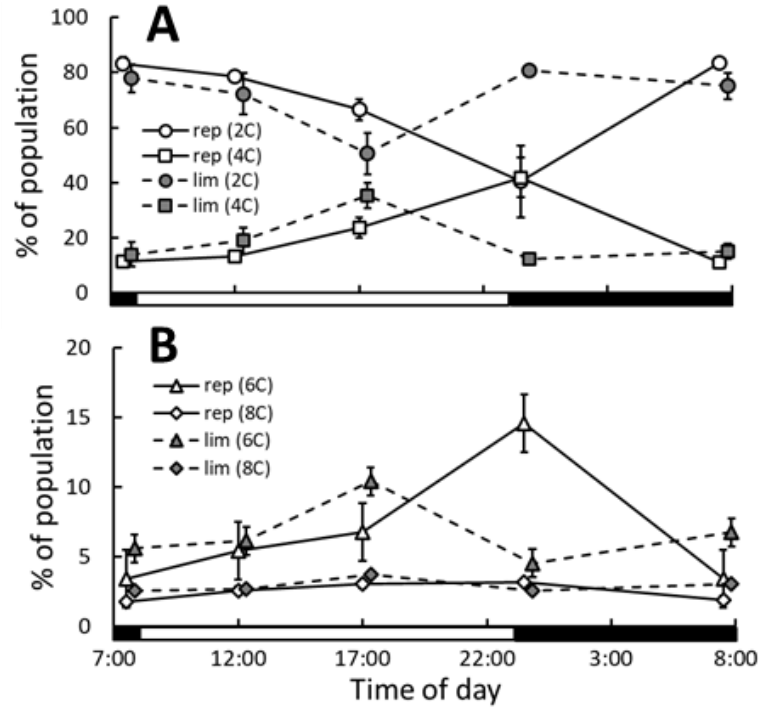

Fig. 11: Cell cycle data from replicate cytograms across 3 days in N-replete and N-limited cycloturbidostats. Populations were calculated using custom gates after performing doublet-discrimination in FCS Express. A) Populations of replete and limited 2C and 4C cells, B) populations of replete and limited 6C and 8C cells. Error bars represent standard deviation of $n \geq 3$ replicate cytograms over 3 consecutive days in two individual cultures, one each under the replete and limited treatment. X-values for the limited treatment are offset for clarity. White/black bar represents the 14:10 hour light:dark cycle.

A series of cytograms depicting the gating framework for multiple fission populations is shown in Supp. Fig. 8. Representative histograms with fitted multicycle models for binary fission populations are given in Supp. Fig. 9, and representative histograms of manually-gated multiple fission populations are given in Supp. Fig. 10. Manual gating of DNA content showed the expected 2C (diploid) and 4C (tetraploid) populations that mirror the patterns modelled in Fig. 10 and Fig. 11A. However, additional multiple fission populations were detected including

hexaploid (6C) and octoploid (8C) cells. Figure 11B shows that the replete culture exhibited a peak incidence (15%) of hexaploid cells just after the onset of the dark period. Likewise, the limited culture showed an increased incidence (10%) of hexaploid cells 9 hrs into the photoperiod. Octoploid cells were relatively rare in both the replete and limited treatment, making up ca. 3% of the total population (Fig. 11B).

3.2 Semi-continuous experiment:

To investigate how light and carbon supply affect the incidence of multiple fission, duplicate semi-continuous cultures were grown under high and low light (450 and 80 µmol photons m^{-2} s^{-1}) on a 14:10 L:D cycle, with and without supplemental 1% CO_2. Growth was monitored via optical density and chlorophyll fluorescence, and flow cytometry was used to monitor the progression of the cell cycle.

The primary effects of both light and CO_2 and their interaction significantly affected specific growth rate (2-way ANOVA, $F_{3,20} = 13.4$, $p = 0.0016$) (Supp. Table 5). Cultures supplied with high light and supplemental CO_2 grew faster than all other conditions, followed by cultures supplied with low light and supplemental CO_2 (Tukey's HSD, Table 3). Quantum yield (F_v/F_m) did not differ among treatments and was not affected by either of the primary factors (2-way ANOVA, $F_{3,20} = 0.040$, $p = 0.843$; Supp. Table 6). However, the primary effects of both light and CO_2 and their interaction significantly affected relative electron transport rate ($rETR_{max}$) (2-way ANOVA, $F_{3,20} = 11.5$, $p = 0.0029$; Supp. Table 7). Significant treatment differences for $rETR_{max}$ are shown in Table 3 (Tukey's HSD Test).

Table 3: Growth summary from semi-continuous experiment.
HL+: High light, with CO_2, HL-: High light, without CO_2,
LL+: Low light, with CO_2, LL-: Low light, without CO_2

	Specific growth rate (d^{-1})	F_v/F_m	rETRmax
HL+	1.38 ± 0.14^a	0.68 ± 0.03^a	34.0 ± 6.4^a
HL–	0.77 ± 0.15^b	0.69 ± 0.02^a	29.5 ± 7.4^b
LL+	0.90 ± 0.05^b	0.69 ± 0.01^a	34.9 ± 4.4^a
LL–	0.60 ± 0.09^c	0.71 ± 0.02^a	23.2 ± 5.0^c

Flow cytometry was also employed to monitor the progression of the cell cycle over the course of two consecutive days in duplicate semi-continuous cultures (Fig. 12). Different patterns of phased cell division were evident in the different conditions. HL+ showed phased cell division beginning late in the photoperiod with peak %S at 76.4% ± 8.9 and the lowest %G1 at 17.1% ± 8.8 occurring 9 hours into the photoperiod. In contrast, the second-fastest growing cultures LL+ showed peak %S at 42.6% ± 5.16 and the lowest %G1 at 54.7% ± 17.9 occurring just after the onset of the dark period. The HL– and LL– treatments showed consistently high %G1 and low %S, where %S populations never exceeded 25%.

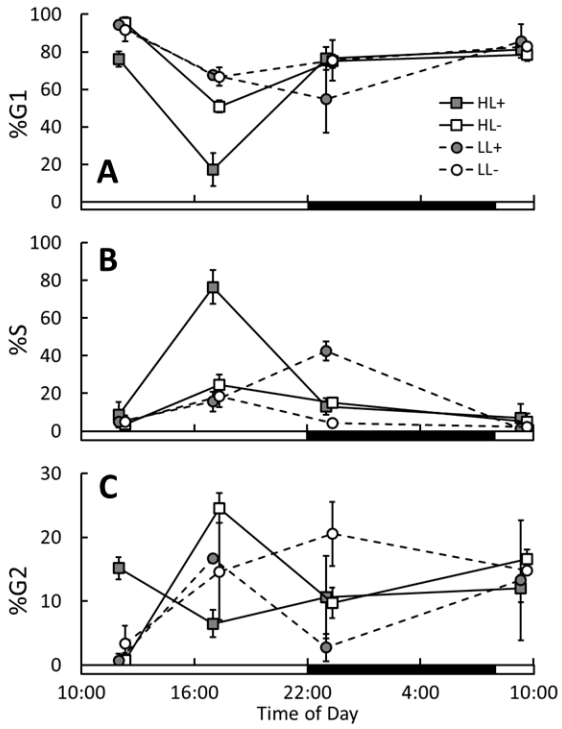

Fig. 12: Cell cycle data from replicate cytograms across consecutive days in semi-continuous cultures. Values were calculated by built-in FCS Express Multicycle models. Error bars represent standard deviation of n ≥ 3 replicate cytograms over two consecutive days in duplicate semi-continuous cultures. X-values for the $–CO_2$ treatments are offset for clarity. Black bar represents the 14:10 hour light:dark cycle.

Manual gating of DNA content revealed differences in patterns of multiple fission between treatments in semi-continuous cultures. Populations of 2C and 4C cells showed decreased incidence of 2C cells and an increased incidence of 4C cells at the onset of the scotoperiod in HL- and LL+ cultures (Fig. 13A, B). This is consistent with patterns shown by built-in cell cycle models (Fig.12). 6C and 8C populations were more prevalent in cultures supplied with CO_2, and 8C cells appear consistently high in LL+ cultures, highlighting the potential role of light intensity on the incidence of multiple fission.

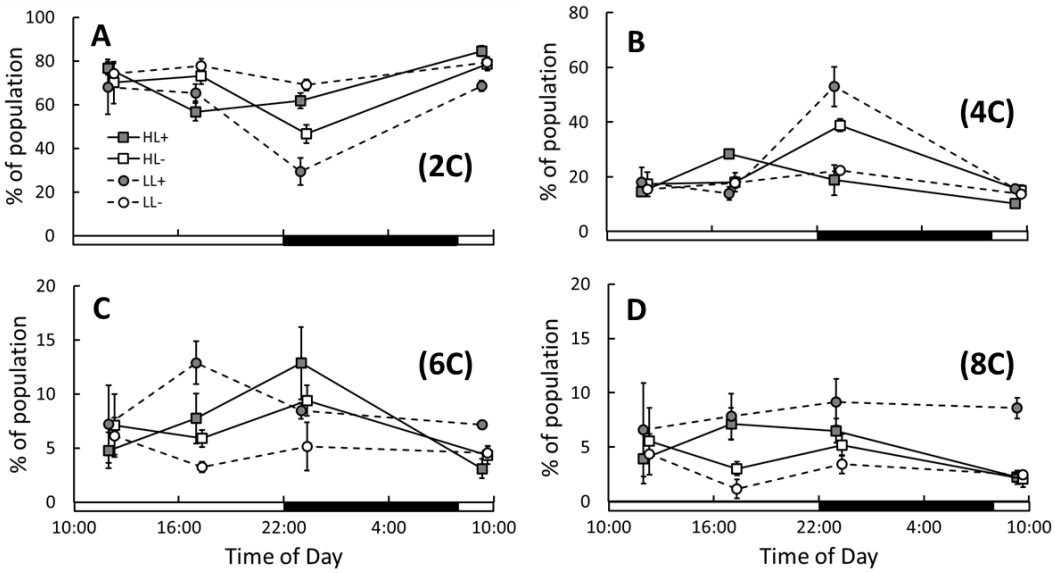

Fig. 13: Cell cycle data from duplicate semi-continuous cultures across two consecutive days. Values were calculated using manually-gated populations following doublet-discrimination in FCS Express. A) Populations of replete and limited 2C and 4C cells, B) populations of replete and limited 6C and 8C cells. Error bars represent standard deviation of $n \geq 3$ replicate cytograms over 3 consecutive days in two individual cultures, one each under the replete and limited treatment. X-values for the limited treatment are offset for clarity. White/black bar represents the 14:10 hour light:dark cycle.

3.2 Microscopy and Morphology:

Epifluorescence imaging of methanol-fixed cells shows the number and placement of nuclei in cells, while DIC microscopy better shows cellular orientation and morphology. Cells with two, three, and four nuclei can be seen in various stages of cell division in Fig. 14. Some multinucleate cells appear to lack cleavage furrows (Fig. 14A, D) where others show clear separations between daughter cell compartments (Fig. 14B, C, E, F). In some instances, nuclei appear close together but on opposite sides of a cleavage furrow, suggesting that the process of mitosis was completed just before imaging (Fig. 14C, E). As well, some nuclei exhibit fluorescence in a very defined area where others appear much more diffuse, which could also reflect timing relative to mitosis.

A DIC image in Fig. 15 shows the broken sheaths of mother cell walls surrounding autospores following its rupture. Cells imaged in DIC show detailed cellular architectures including defined nuclei and cleavage furrows (Fig. 16). Small individual cells presumably in the G1-phase (Fig. 16C), and cells undergoing cytokinesis into two daughter cells (Fig. 16A) are evident. Also shown are large cells prior to cytokinesis (Fig. 16B), and a group of 4 daughter cells in a tetrahedral orientation (one behind the other three and not visible; Fig. 16D).

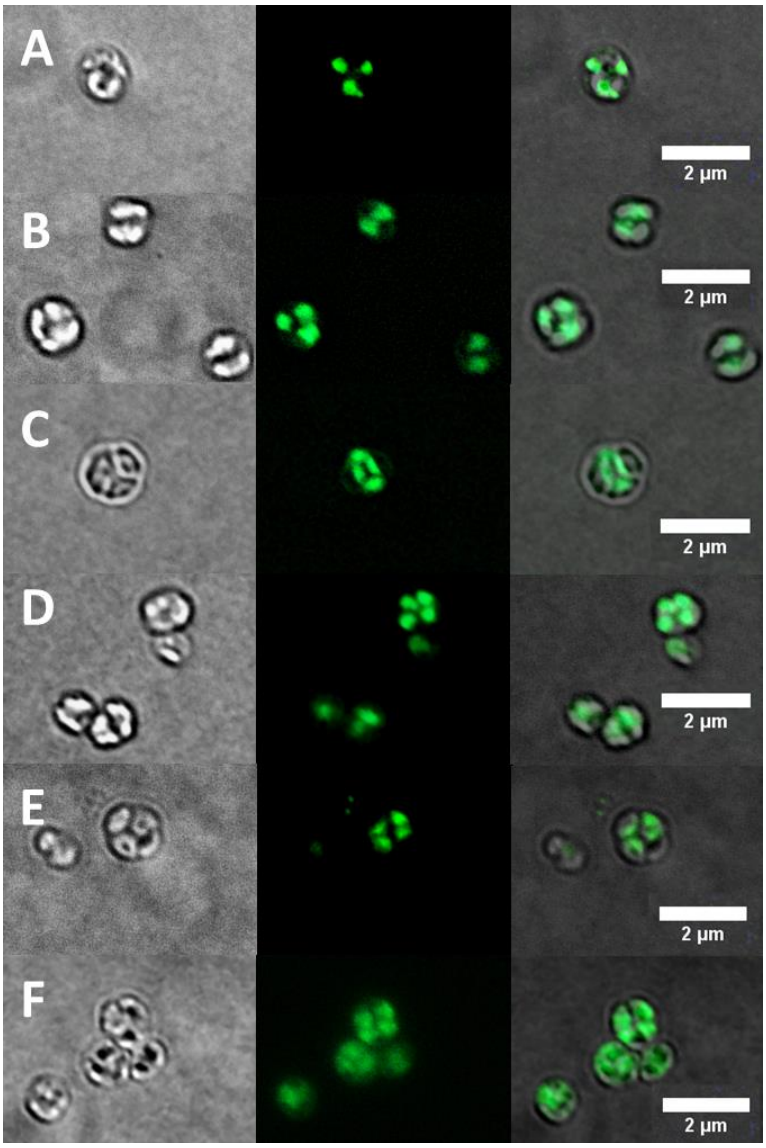

Fig. 14: Epifluorescence micrographs showing SYBR Green fluorescence of stained DNA in methanol-fixed cells (center) with bright field images (left) overlayed (right) to show cell positions. Cells were imaged from pooled samples across days, timepoints, and replicates in cycloturbidostat cultures. Letters A-F indicate individual image sets. Cells may have shrunk due to methanol fixation. Scale bar is 2 µm.

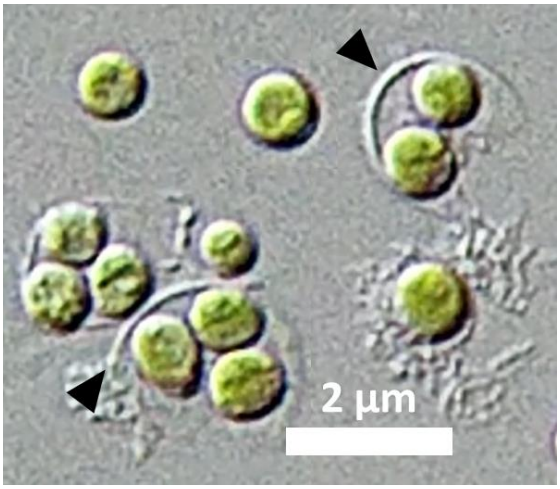

Fig. 15: DIC image showing broken mother cell wall debris and the resulting daughter cells. Arrowheads indicate ruptured mother cell walls. Scale bar is 2 µm.

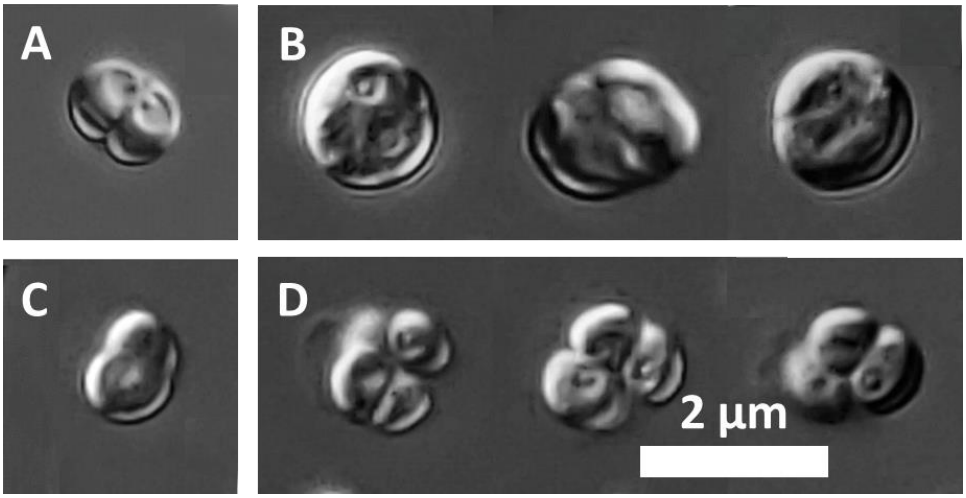

Fig. 16: DIC images of four individual cells (A-D). Cells B and D are shown in various orientations with respect to the camera. Scale bar is 2 µm.

4.0 Discussion

4.1 Evidence of multiple fission in *Picochlorum oklahomense*

We observed relatively high incidence of multiple fission cell cycle stages in our nitrogen-replete and deplete cycloturbidostat cultures, as well as in our semi-continuous cultures supplied

with supplemental CO_2. While these fast-growing cultures exhibited an increased incidence of multiple fission, all cultures exhibited some hexaploid and octoploid populations, but at lower quantities and with different temporal patterns in slower growing cultures. Multiple fission has been defined to occur under optimal conditions on a light-dark cycle [11, 13, 14, 25, 26]. This would seem to suggest that cycloturbidostats, and to a lesser extent semi-continuous cultures, provide ideal conditions enabling multiple fission; whether slower-growing batch cultures do so as well was not investigated here.

In our cycloturbidostats, N-replete cultures showed phased cell division with peak S-phase populations at night, in contrast to N-limited cultures showing peak S-phase populations midway to late in the photoperiod. In our semi-continuous cultures, LL+ showed constitutively high (ca. 8%) incidence of octoploid cells, where HL+ cultures showed a cyclical pattern of octoploid incidence increasing through the photoperiod and decreasing at night.

These results suggest that multiple fission and the number of resulting daughter cells is tied to both light availability and interval, as well as resource availability, i.e., light, carbon and nitrogen supply. However, we hypothesize that phenology, or the timing of cell cycle events relative to the light interval, is an additional important factor in determining the incidence of multiple fission cell cycle stages. Furthermore, we hypothesize that the appearance of 4, 6 and 8C throughout the photoperiod reflects variability in the population as to when cells reach the critical size to begin the process. In other words, phenological traits and the life history of individual cells, i.e., the timing of cell cycle events relative to the onset or end of the photoperiod modulates the occurrence of multiple fission cell cycle stages.

4.2 *Picochlorum* cell cycle biology

The genus *Picochlorum* (Chlorophyta, Trebouxiophyceae) was a recently described by reassigning a group of halotolerant species from the *Nannochloris*-like coccoid green algae [2]. This genus is gaining considerable attention in algal research programs due to its rapid growth

rate and tolerance to heat and salinity [6, 15-20, 27]. It divides by autosporulation into two or more daughter cells, though little investigation of its cell cycle is present in the literature [2, 4].

The data here show a non-zero level of multiple fission and confirm that *P. oklahomense* is an autosporic species capable of producing two to four daughter cells per mother cell via a multiple fission pathway. Furthermore, *P. oklahomense* appears to undergo multiple fission according to the clustered pattern, as nuclear division appears to be directly followed by cytokinesis of individual daughter cells [11, 13, 28, 29].

It is hypothesized this adaptation is used to separate the growth and division phases of the cell cycle under optimal conditions on a light-dark cycle to focus on autotrophic growth throughout the photoperiod without stopping photosynthesis or diverting resources to genome duplication and cell division. That both small and large cells are present in all multiple fission populations suggests that individual cells begin the day at each respective stage before progressing through the next S-phase cycle. Additionally, that multiple fission phenotypes are present throughout the photoperiod suggests that the hypothesized purpose of multiple fission as separating growth and the dark period is not absolute, perhaps especially at very high growth rates [13].

Multinucleate cells are short-lived in the clustered pattern [11, 13, 29]. The low incidence of octoploid cells may simply be due to the low likelihood of these events occurring, or it could be explained by the punctuated nature of these events as the mitotic stage in the clustered pattern, i.e., genome duplication is directly followed by cell division. Multinucleate cells are present but very short-lived, making it difficult to image these events.

Figure 17 depicts a contour plot of pooled cytograms from samples taken across days and timepoints. This illustrates the range of cell cycle (DNA content) populations present in the culture over the course of the day and shows that these cell cycle patterns are repeated day-to-day in our steady-state cycloturbidostat cultures. In this merged contour plot, time is implicit; as cells increase in size over the day, they follow a lower left to upper right ‘trajectory’ with the most common routes to division shown by the densest regions in the innermost contour lines. In this

way, cell size offers a convenient way to track cells as they progress through the photoperiod and cell cycle, which is a well-established measure in phycological research [10, 28, 30].

Figure 17 also depicts hypothesized cell trajectories in green and orange lines. Standard one-cycle autosporic cell cycle trajectories (i.e., 4C cells resulting in two 2C daughter cells) are depicted with solid green lines and circles. In these populations, cells increase in size moving from left to right along the x-axis before increasing DNA content during the S-phase, evident in the upward trajectory leading to the 4C checkpoint. In this case, cells increase in size and double their genome before dividing into two daughter cells of half the size. Multiple fission populations (i.e., those with DNA content >4C) are depicted with orange lines and circles. These hypothesized trajectories show cells with a DNA content of 4C entering hexaploid (6C) and tetraploid 8C) stages by several routes. If cells reach the 4C checkpoint but do not progress through cell division, they lose biomass (i.e., cell size) during the dark period to respiratory loss and continue their lower-left to upper-right trajectory at the onset of the next photoperiod from 4C onward. The presence of two populations at both the 6C and 8C level, one exhibiting large and one with relatively smaller cell sizes, suggests that some cells begin the photoperiod at both the 6C and 8C levels. These cells continue their lower-left to upper-right trajectories, beginning their day at the 6C or 8C level, until they attain the final checkpoint and progress through cell division and cleavage. Yellow dotted lines and arrows represent the process of cell division and cleavage resulting in newly formed diploid daughter cells, which is more a punctuated event rather than a phase, i.e., the process of cell division is not a simple cycle but a progression of events ending with the final event of daughter cell separation [11, 13].

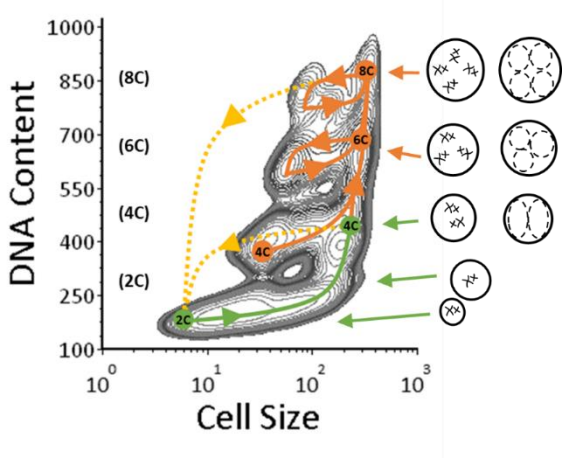

Fig. 17: Contour plot of merged cytograms including all data for both replete and limited cycloturbidostat cultures with annotations of hypothesized cell cycle trajectories. The densest regions are found in the innermost contour lines. Green lines and circles depict cell trajectories and checkpoints for a standard one-cycle autosporic cell cycle (2C & 4C). Orange lines and circles depict cell trajectories for multiple fission cell cycles (6C & 8C). Yellow dashed lines represent the process of cell division and cleavage resulting in newly formed diploid daughter cells. Same data as Supp. Fig. 8D in contour plot form.

4.3 Using flow cytometry to monitor the cell cycle of Trebouxiophytes

We analyzed individual cytograms using both built-in cell cycle models and by manually-gating cell cycle populations according to DNA content. Manually-gated multiple fission patterns mirror those modelled in the 2C-4C populations via a single-phase cell, i.e., peak S-phase populations coincided with peak 4C populations, as expected.

A logarithmic scale for FSC-H was chosen in order to differentiate cell size more precisely. *Picochlorum* is very small, making it difficult to tune the instrument to that size; this compresses the cell size ranges and may marginally decrease accuracy. However, given the defined cell size ranges for the 4C, 6C and 8C groups, it is unlikely that these cells represent doublets or aggregates of multiple cells. Aggregates only constitute <2% of all cells (Supp. Fig. 8, 11, 13).

The use of doublet discrimination in cell cycle analysis via flow cytometry is essential. Cell aggregates must be filtered out, leaving only single cells, which are then normalized to the DNA content exhibited at the beginning of the cell cycle – 1C for haploid species, 2C for diploid. Doublet discrimination relies on the fundamentals of signal detection. As cells pass through the laser, the fluorescence signal is detected as a pulse with a height (H), width (W), and total area (A). A single cell in G1 will have a unit H, W, and A equal to one. A doublet (two cells stuck together) will have a H equal to one but double the area and width. Thus, cells that have a DNA content greater than 2C will exhibit a proportional increase in the H and A of the fluorescent signal but not width, offering a convenient way to gate out doublet or cell clumps. Additionally, results show multiple cell sizes within one gated DNA content population (small early in the day, large later in the day); thus, cell size plays little role in the DNA content signal. Cell debris from both our cycloturbidostat and semi-continuous cultures is visualized in Supp Fig. 6.

It should be noted that trajectories in between the high and low cell sizes would likely be filled with more comprehensive diel sampling. Likewise, sampling during the dark period would reveal further details regarding the transition from multinucleate/multicellular states to diploid daughter cells. Finally, it is difficult to model multiple fission cycles. Species-specific models using open-access coding tools would greatly improve the ability to record multiple fission characteristics in diverse green algal genera. In particular, modelling the S-phases between levels is difficult given their overlapping nature.

Our understanding of the cell cycle, in particular atypical cycles, continues to develop and many questions remain. In the case of *Picochlorum*, perhaps leveraging its small genome size (*ca.* 13.5 Mbp) to allow for rapid S-phases is a favorable strategy [6, 16, 31, 32]. This could explain its rapid growth rate and may be a contributing factor to the evolution of an exceedingly small genome. Little data regarding the effect of cell and genome size on the incidence of multiple fission exist in the literature, but it would be an interesting future study to compare similarly sized and closely related species/strains that have significantly different genome sizes. Studies

investigating the cessation of the cell cycle have made strides in understanding the genetic basis of quiescence and the subsequent hyper-accumulation of lipids [8, 10, 28, 30, 33-36], which could be connected to multiple fission pathways. Identifying novel genetic elements that play a role in regulating multiple fission could have significant potential in increasing biomass productivities if incorporated into a wholistic metabolic engineering framework and cultivation protocol.

5.0 Conclusion

These results suggest that multiple fission and the number of resulting daughter cells is tied to both photon flux and resource availability, i.e., carbon and nitrogen supply. However, we hypothesize that phenology, or the timing of cell cycle events relative to the photoperiod, is an additional important factor in determining the incidence of multiple fission cell cycle stages. Furthermore, we hypothesize that the appearance of 4, 6 and 8C throughout photoperiod reflects variability in the population as to when cells reach the critical size to begin the process. In other words, phenological traits and the life history of individual cells, i.e., the timing of cell cycle events relative to the onset or end of the photoperiod modulates the occurrence of multiple fission cell cycle stages, especially at specific growth rates exceeding 1.0 d^{-1}.

Supplemental Figures:

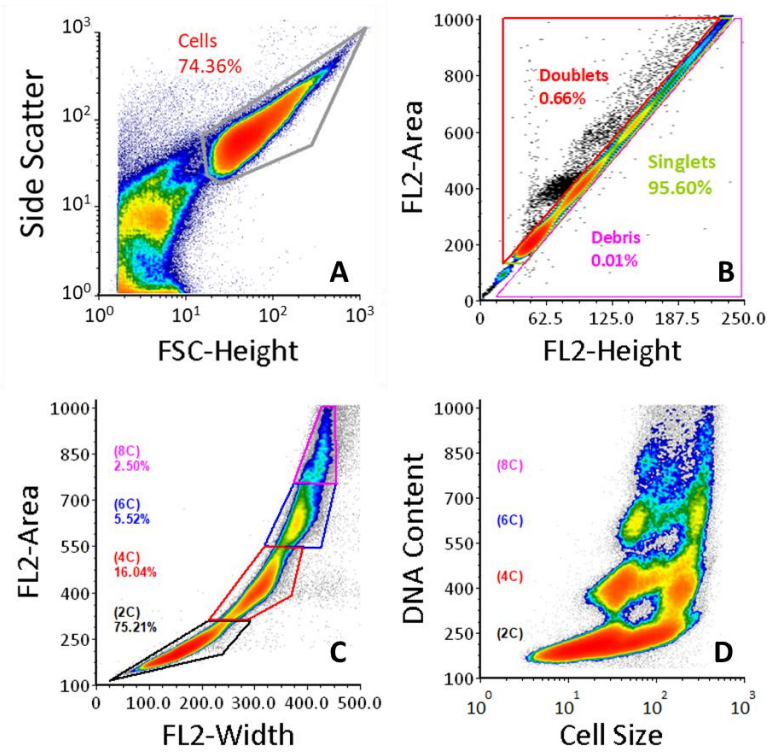

Supp Fig. 8: Comparative cell cycle data of merged replicate cytograms across 5 days in replete and N-limited cycloturbidostats. Dot plots from individual samples were merged to illustrate the range of cellular properties throughout the photoperiod. A) Gating of *P. oklahomense* cells by forward and side scatter. B) Doublet discrimination of particles within the gate shown in panel A. The gate for singlets lies along the diagonal between gates for doublets (black dots upper left) and debris (black dots lower right). C) Construction of gates dividing different multiple fission population according to DNA content. D) Dot plot of multiple fission stages with DNA content plotted against cell size. All dot plots show the densest regions in red and most sparsely populated state in blue.

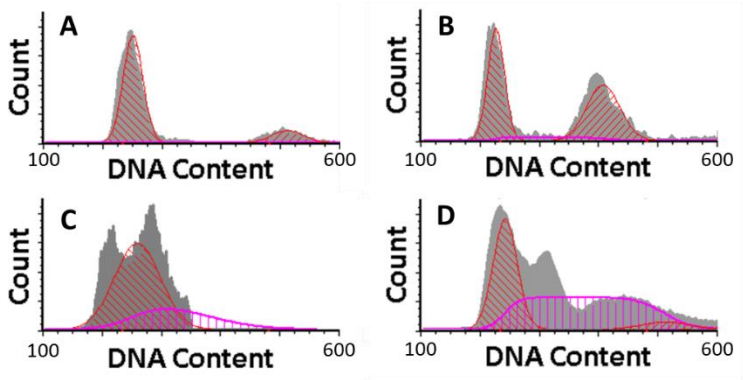

Supp Fig. 9: Example DNA content histograms from cycloturbidostat cultures of 2C and 4C populations. A) Most of the population is in G1 with a small G2/M population, B) A population split evenly between G1 and late S-phase, C) a population with a large group of S-phase cells, D) a mixed population with a peak in the G1, S, and G2/M phases. Red lines depict fitted models for the G1 and G2/M phases, magenta lines depict the fitted model for the S-phase. Cell counts on the y-axis are scaled-to-fit. Mean fluorescence intensity (MFI) values on the x-axis calculated by the multicycle model were ca. 240 and ca. 500 for the G1 and G2/M populations, respectively.

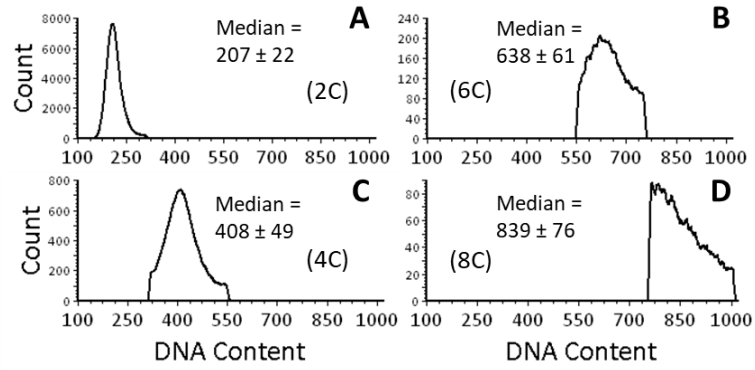

Supp Fig. 10: Respective DNA content histograms for different multiple fission populations in replete and N-limited cycloturbidostat cultures. A) 2C, B) 4C, C) 6C, D) 8C cells.

Supplemental Table 5: Two-way ANOVA with replication.
Growth rate (μ) in semicontinuous experiment.

Source	*SS*	*df*	*MS*	*F*	*P-value*	*F crit*
Light	0.62808	1	0.62808	55.1666	3.6E-07	4.35124
CO_2	1.22774	1	1.22774	107.836	1.7E-09	4.35124
Light + CO_2	0.15257	1	0.15257	13.4012	0.00155	4.35124
Within	0.2277	20	0.01139			
Total	2.2361	23				

Supplemental Table 6: Two-way ANOVA with replication.
Quantum yield (F_v/F_m) in semicontinuous experiment.

Source	*SS*	*df*	*MS*	*F*	*P-value*	*F crit*
Light	0.00135	1	0.00135	0.81081	0.3786	4.35124
CO2	0.00282	1	0.00282	1.69169	0.20817	4.35124
Light + CO2	6.7E-05	1	6.7E-05	0.04004	0.84342	4.35124
Within	0.0333	20	0.00167			
Total	0.03753	23				

Supplemental Table 7: Two-way ANOVA with replication.
Electron transport rate ($rETR_{max}$) in semicontinuous experiment.

Source	*SS*	*df*	*MS*	*F*	*P-value*	*F crit*
Light	40.8204	1	40.8204	5.823239	0.02553	4.35124
CO2	389.62	1	389.62	55.58132	3.4E-07	4.35124
Light + CO2	80.3004	1	80.3004	11.45526	0.00294	4.35124
Within	140.198	20	7.00992			
Total	650.94	23				

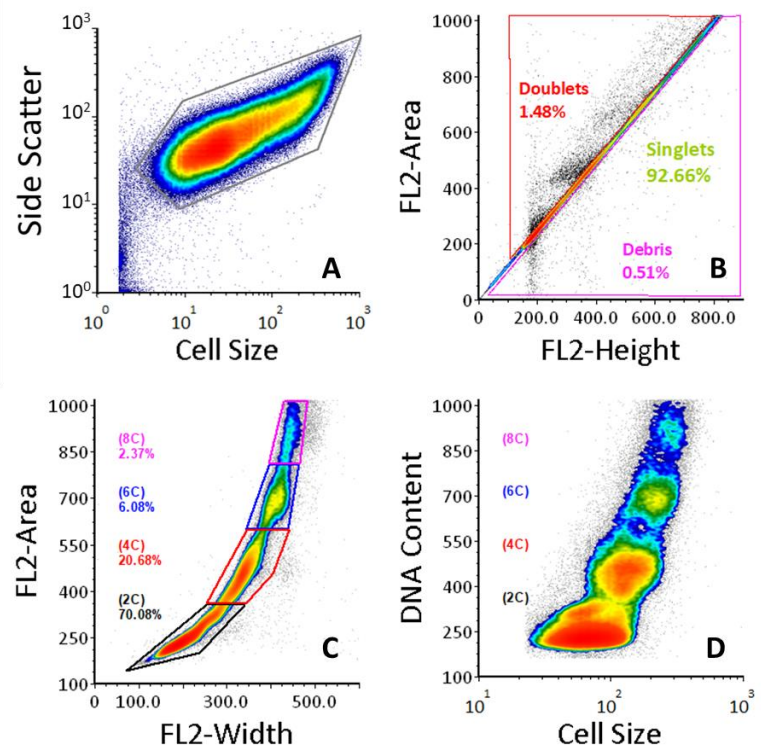

Supp Fig. 11: Comparative cell cycle data of merged replicate cytograms across two days in duplicate semi-continuous cultures. Dot plots from individual samples were merged to illustrate the range of cellular properties throughout the photoperiod. A) Gating of cells by forward and side scatter. B) Doublet discrimination of particles within the gate shown in panel A. The gate for singlets lies along the diagonal between gates for doublets (black dots upper left) and debris (black dots lower right). C) Construction of gates dividing different multiple fission population according to DNA content. D) Dot plot of multiple fission stages with DNA content plotted against cell size. All dot plots show the densest regions in red and most sparsely populated state in blue.

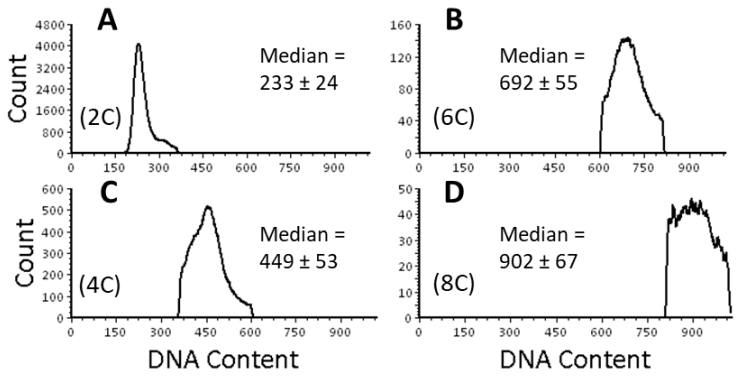

Supp Fig. 12: Respective DNA content histograms for different multiple fission populations in semi-continuous cultures. A) 2C, B) 4C, C) 6C, D) 8C cells.

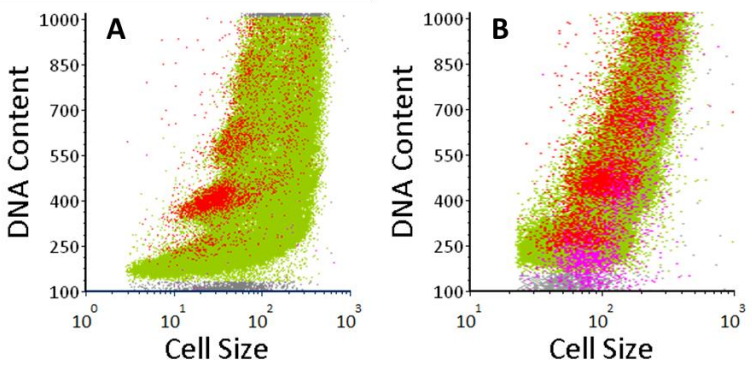

Supp Fig. 13: Merged dot plot of all data depicting filtered singlet cells in green, and cell aggregates filtered via doublet-discrimination in red; gray and magenta dots represent debris. Most aggregates fall in the 4C region likely representing cell doublets. A) Cycloturbidostat experiments; B) Semi-continuous experiment.

CHAPTER III

Lessons from the Lab: The Utility of Cycloturbidostats in Microalgal Biotechnology

Abstract:

Turbidostats are an underappreciated tool in experimental phycology and recent advances now allow for affordable and simple assembly of continuous cultures at the laboratory-scale. These systems are uniquely fit for the continuous and reliable cultivation of microalgae that will be an essential piece in decoding algal biology and in building valuable year-round supply-chains. Here I provide an outline of cycloturbidostat fundamentals, a brief summary of its use in lab-scale experiments and will use unpublished data from preliminary or less-than-successful trials to describe potential issues one may encounter when utilizing cycloturbidostats in the laboratory, particularly in nutrient-limitation studies.

1.0 Introduction

Photosynthetic microalgae are a diverse group of organisms that have received considerable attention in recent years for their potential to mitigate climate change, generate renewable energy, and help feed the world's growing population. These organisms require ample light and CO_2, can be grown using brackish water on marginal lands, and can be fertilized using inexpensive

agricultural inputs [6-8, 35-37, 65-68]. They are also gaining traction as a sustainable biomanufacturing platform alongside industry-standard heterotrophic systems utilizing bacteria or yeast/fungi, which require exogenous carbon, costly inputs, and produce CO_2 as waste [69-75].

However, low photosynthetic efficiency and contamination in outdoor cultures continues to plague commercial algal biomass production [6-8, 35-37, 66-68]. Likewise, the vast array of species, physiologies, and potential uses of microalgae present a daunting amount of explorative research necessary to valorize algae's potential. While numerous studies have enhanced our technical understanding of the nutritional, metabolic, and genomic requirements for large-scale production of algal biomass, more advancements are needed to make these ventures both environmentally and economically sustainable [76-79].

Continuous culture of photosynthetic microalgae is used to maintain stable growth rate and nutrient supply via frequent replacement of culture volume with fresh media. This is achieved utilizing pumps and a microcontroller under one of two classic modes: the turbidostat or the chemostat; a cyclostat refers to the operation of these culture modes under a photoperiod. Chemostats supply media at a constant rate to set an experimentally fixed growth rate and equilibrium cell/biomass density decreases with increasing dilution rate. In contrast, turbidostats use an arbitrary turbidity setpoint to maintain a constant biomass density and growth rate according to the organism and conditions [9, 11, 80-83].

The algal research field and its adjacent industries utilize batch cultures for the majority of research and biomass production. However, the computer-age and wide-spread application of microcontrollers coupled with low-cost manufacturing has led to many advancements in culturing practices and equipment at the laboratory-scale [7, 9, 11, 35, 65-68, 84-86]. Likewise, decades of experience in algal culturing and improvements in infrastructure now allow near year-round semi-continuous production of microalgal biomass at the commercial-scale given the proper conditions and controls; a feat previously thought too costly and labor-intensive to be sustainable [8, 35-37, 66-68, 87]. In the past, continuous culture was used only at the laboratory-scale due to its cost and

complexity, but today some large-scale systems successfully operate in semi-continuous mode at specific growth rates exceeding 1 d^{-1}.

one doubling per day for very long periods [4, 66-68, 87]. If the algae industry is to come to fruition at-scale, continuous and reliable cultivation systems will be an essential piece in building valuable year-round supply-chains. Turbidostats in particular are uniquely fit for this task as they allow for the control of light penetration into the culture and maintain culture health via dilution [13, 14, 53, 84, 87, 88].

Here I provide an outline of cycloturbidostat fundamentals, a brief summary of its use in lab-scale experiments and will use unpublished data from preliminary or less-than-successful trials to describe potential issues one may encounter when utilizing cycloturbidostats in the laboratory, particularly in nutrient-limitation studies.

1.1 Cycloturbidostat Fundamentals

Turbidostats are designed to operate at nutrient-replete growth rates by maintaining a constant biomass density via frequent replacement of culture volume with fresh media at a user-defined photometric setpoint. The dynamics of any individual turbidostat system will exhibit different equilibria as the turbidity setpoint and resulting biomass density is arbitrary. This setpoint along with light and nutrient levels, temperature, and species present all work to determine the equilibrium-state (i.e., balanced growth state) of the system, and thereby the maximum growth rate (μ_{max}) and operating cell quota (Q_{cell}) for a particular limiting nutrient under the given experimental conditions [9-11]. In this way, turbidostats represent an internally-controlled system where the organism sets the growth rate and thereby the dilution rate of the system.

In contrast, chemostats are externally-controlled, operating at a growth rate set by the user, as determined by the amount of limiting nutrient entering the system as well as light and temperature. This makes chemostats remarkably consistent and uniquely suited for studies focusing on growth rates < 1.0 d^{-1} and for studies techniques such as pulse-chase type

experiments that require low variability [20]. However, equilibrium biomass density in chemostats varies with dilution rate (D) in a non-linear fashion and may not be independently controlled [9-11]. Chemostats are also constrained by the risk of washout, which may occur at high μ/μ_{max}, i.e., 90% of μ_{max}. Thus, turbidostats are distinct from chemostats in two important ways: biomass density is uncoupled from dilution rate, and they operate at μ_{max} without the risk of washout.

The internally-controlled nature of the turbidostat adds considerable complexity as biomass density, light intensity and penetration into the culture, nutrient supply, and growth rate are all inter-related. This goes for cycloturbidostats in particular, as the addition of diurnal physiological cycles will introduce further variability from culture-to-culture and day-to-day. Specifically, when the photoperiod ends and lights are turned off total biomass begins to decrease due to respiration and the turbidity signal will begin to fall; as a result, predawn turbidity will be below the setpoint, and cultures must begin growth at the onset of the photoperiod to return back to their starting point without the addition of nutrients. These patterns and parameters will vary in the approach to steady-state until they reach equilibrium when given the correct conditions cycloturbidostat cultures can achieve remarkable consistency.

Physiological status in continuous cultures is classically monitored by daily specific growth rate (μ, d^{-1}) and cell density, and chlorophyll content or chlorophyll fluorescence measures are commonly added as a proxy for photosynthetic performance. Steady-state balanced growth is then defined by less than a 10% change growth rate, cell count, and photosynthetic performance over a 3-day period. The maximum quantum yield (F_v/F_m) and maximum relative electron transport rate ($rETR_{max}$) through PSII are the canonical proxies for photosynthetic performance. Nutrient supply rate in a continuous culture is equal to the concentration of limiting nutrient in the influent media multiplied by the dilution rate; further dividing this value by the cell density of the cultures yields moles per cell or the operating cell quota (Q_{cell}). While chemostats run the risk of washout, the risk of failure due to a slippery slope of decreasing growth rate and media supply is

an important vulnerability of cycloturbidostats at near-limiting nutrient supply rates. If for instance a perturbation leads to decreased nutrient supply thereby exacerbating any nutrient limitation, cultures may slow their growth to the point that they receive insufficient levels of nutrient to sustain growth and the turbidostat system breaks down, i.e., turbidostats only perform under nutrient-replete growth. This highlights the importance of monitoring not the bulk but the more biologically relevant cell-specific nutrient supply rate, as this is what sets the growth rate.

Even small perturbations to a cycloturbidostat's equilibrium-state may take more than a day to resolve and can illuminate the hysteresis and interplay between the aforementioned factors, i.e., the previous day's growth will influence the growth rate of subsequent days. If, for example, something decreases the growth rate of a cycloturbidostat culture, dilution rate and media supply will also decrease; because cells are not starved but only limited for nutrients they will continue to grow and divide for a time, resulting in increased cell count the following morning. This inadvertently decreases the cell-specific supply of nutrients, thereby decreasing growth rate. However, these issues usually resolve themselves and result in a congruent equilibrium balanced-growth state despite the perturbation. This demonstrates a self-regulatory feedback mechanism that re-equilibrates turbidostat cultures to their steady-state equilibria, a process inherent in the development of a balanced growth-state.

All this to say, cycloturbidostats are complex systems that are sensitive to perturbations. This may disqualify turbidostats for outdoor use unless appropriate measures are taken to reduce the effects of fluctuations in the weather, but if measures to decrease variability are taken their remarkable consistency also allows for carefully controlled studies of physiological phenomena.

1.2 Cycloturbidostat in Notable Literature

The use of continuous cultures in lab-scale physiological studies of algae has long been overshadowed by less-laborious and less-complex batch cultures, but the non-steady-state nature of batch culture where decelerating growth rate, nutrient depletion, and light penetration leave the

associated phenomic behaviors irresolvably confounded. Continuous systems are thus superior in certain studies and are gaining traction as the reduction in cost and widespread adoption of microcontrollers make these systems more affordable and easier to build. Still, turbidostats and cyclostats are underrepresented in the literature highlighting the need for more basic research regarding continuous culture systems [9].

Conceptually, turbidostats are intended to study nutrient-replete growth but recent studies have utilized them in novel ways and in new contexts. Specifically, recent studies focused attention on nutrient limitation techniques to enhance biomass productivity and product yield and utilized turbidostats or cyclostats to investigate nitrogen limitation at high growth rates ($\mu \geq 1\ d^{-1}$) by supplying just enough N to grow rapidly and maintain division [12-17, 53]. This is only possible in cycloturbidostats (not in batch, semi-continuous, or chemostat cultures), due to their sensitivity and unique dynamics.

Though they are less common than simple batch-mode cultures, continuous culture systems have a rich history in the literature. Many early studies of microalgal growth that established growth rate benchmarks, quantified nutrient uptake, mapped out nutrient quota curves and investigating patterns of ecophysiological importance utilized continuous cultures [2, 3, 10, 65, 80-83, 85, 86, 89-94]. Likewise, many investigations of growth rate-dependent metabolic patterns necessitate the use of chemostats [20]. The dynamics of chemostats and turbidostats have been extensively explored in the biochemical engineering and biological modelling fields [2, 11, 80, 81, 85, 92]. Some have taken this further to compare batch and continuous modes of production in terms of product yield and process efficiency [17, 84, 95] and models to compare these modes have been explored [12, 14]. Patterns of cells division, photoperiodism, circadian clocks, and diurnal patterns also necessitate continuous cultures [30, 47, 55].

Recently, a novel fast-growing species of *Picochlorum* was isolated using a semi-continuous? turbidostat system via high-light selection. In this case, enrichment cultures under constant high irradiance in continuous culture identified several rapidly-growing cell lines that are very resilient

to inhibition by light and exhibit doubling times as short as 2.0 h [26, 59, 96]. Other studies have focused on aspects of competition between species in polyculture scenarios [97, 98] and contaminant washout as a commercial production consideration [88, 99-101].

These studies highlight the utility of turbidostats in experimental phycology particularly in nutritional and comparative studies, but also as versatile tools for the microalgal biotechnology field. This rich history of cyclostat studies has contributed much to the field of phycology, oceanography, and to plant science writ large. The untapped potential in the future of biotechnology is manifest, thus there is a need to articulate and disseminate the hurdles and potential of cycloturbidostat studies to future practitioners.

2.0 Lessons from repeated cycloturbidostat cultures

We used replicate cycloturbidostat cultures to identify the threshold of N limitation in *P. oklahomense* and defined a scantly explored concept in the study of N limitation: the threshold of N cell quota necessary to support μ_{max} below which cells are forced to re-allocate resources and slow growth, denoted $Q_{N,T}$ [13, 53, 98]. This proved challenging in practice as any perturbation (e.g., accidental pause in media supply) can cause individual cultures to become unstable and lead to a slippery-slope of decreasing growth rate. Nearly all published studies using continuous cultures employ a single photobioreactor that is subjected to different treatments sequentially, i.e., there is neither replication nor concurrent control cultures. Building a cyclo-turbidostat system with replicate culture bottles required multiple iterative preliminary trials that helped to improve not only the culturing systems to decrease variability but also develop workflows to streamline the labor-intensive nature of maintaining and monitoring these cultures.

2.1 Cycloturbidostat Mechanics and Operation

The most basic considerations in cycloturbidostat design relate to the mechanics of the system, i.e., sensors, pumps, and tubing. The most fundamental aspect of the turbidostat is the sensing of

culture turbidity which was classically achieved using manual spectrophotometry via culture sampling. Today numerous turbidity sensors are available with varying applications. Ideally, a turbidity sensor needs little cleaning, has a wide range of sensitivity, and does not suffer from optical obstruction. If a senor is submerged in the culture a biofilm will inevitably accumulate leading to signal drift. In contrast, sensors that point through the culture from outside the bottle may be obstructed by biofilm inside the bottle or more commonly by oxygen bubbles that form on the walls of the bottle during peak hours of photosynthesis. Any artificial inflation of the turbidity signal will lead to a dilution event and the culture must grow back to the setpoint in order to restart turbidostat operation.

Turbidity sensors should be calibrated to minimize discrepancies between cultures. A two-point calibration using pure water for the minimum, and a culture near intended biomass density or a neutral density filter for the maximum turbidity is adequate for calibration - some sensors also include a 'span' function that modulates the range of signal, this should also be calibrated between units (Fig. 18). Optimizing the microcontroller code and computer interface is another important consideration, i.e., signal reporting intervals, pump cycle duration and frequency, data accessibility, time-stamped notation, etc., but this is outside the scope of this article.

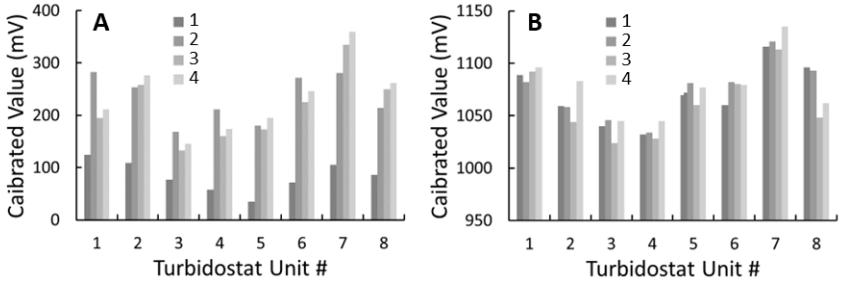

Fig. 18: Turbidity sensor calibrations over four experiments. A) turbidity value with deionized water; B) turbidity value with neutral density filter.

Old and under-powered pumps not only fail but can introduce discrepancies in flow rates between the influent and effluent leading to changes in culture volume - this may argue for culture outflow by gravity overflow rather than pumping, which should be more consistent within and between units. Likewise, designing the system to reduce tubing length and keep the lines organized will help to eliminate leaks and airlocks that decrease or interrupt flow; durable medical-grade tubing can withstand rounds of autoclaving and acid-washing without degrading.

Finally, human error is an obvious driver of variability so precautions should be taken to limit its influence by streamlining workflows, optimizing protocols, and ample note taking. Human error can be the culprit of dilution events or more commonly, failure to refill media supply resulting in cultures growing past their setpoint. These events not only negate results from the current day but also a number of subsequent days following the perturbation as discussed above.

2.2 Physiological Drivers of Variability

Other aspects of variability can be attributed to discrepancies in abiotic environmental factors between cultures. Mixing media in large batches before aliquoting into bottles connected to the system is a good way of preventing nutritional differences between cultures. Attention should be paid to both media and culture pH to ensure proper buffering – we opted for bicarbonate as a buffer in addition to CO_2 supplementation in lieu of other additives. Likewise, reducing hotspots from overhead lighting that provided higher irradiance to individual cultures is paramount as this will affect chlorophyll content and fluorescence properties used for the determination of steady-state and as proxies for physiological status. Interestingly, hotspots in irradiance showed differences in F_v/F_m and $rETR_{max}$ (Fig. 19), slight differences in chlorophyll content and cell count, but had no measurable effect on growth rate because all units received saturating irradiance (data not shown); this highlights the importance of multiple independent physiological measures in monitoring continuous cultures.

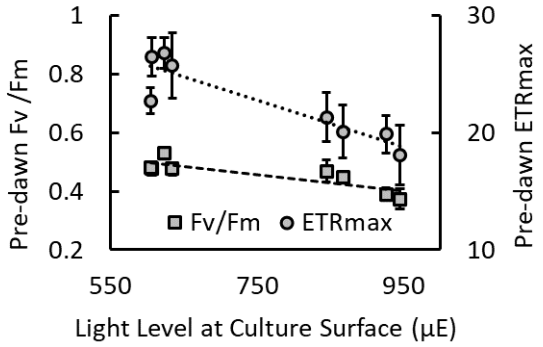

Fig. 19: Difference in predawn F_v/F_m and $rETR_{max}$ of *Picochlorum oklahomense* cultivated in replicate cycloturbidostats due to irradiance discrepancies averaged over 10 days.

One very important but easy to overlook issue is the inoculation protocols used in initiating continuous cultures. This can introduce more cryptic aspects of variability and improved inoculation protocols are central to reducing discrepancies among replicate cycloturbidostat cultures. Experienced operators of continuous cultures may speculate that inoculation plays a non-zero role in the development of the equilibria, which seems to run counter to continuous culture theory – same environment, different outcome. However, subtle differences in inoculation biomass density, inoculation nutrient concentration, and the life-history of the inoculum all play a role in the development of an equilibrium balanced-growth state.

Removing this variability entails operating an inoculum culture in semi-continuous mode under the experimental light source and fed moderate levels of nutrients that do not increase chlorophyll content – this is especially important if your intended limiting nutrient is subject to potential luxury uptake. Substantially fewer transient phenomena in the approach to steady-state will occur if inoculum cultures are properly pre-acclimated. Additionally, the best way to inoculate multiple replicate cultures is to mix a large axenic batch at the intended biomass density and then aliquot into culture bottles. Cultures that are not properly inoculated and/or were fed excess N and P will see high chlorophyll content that give rise to wide swings in growth parameters in the beginning days of the trial.

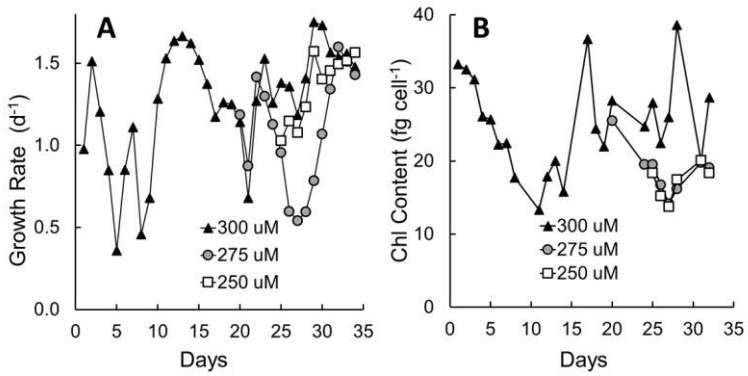

Fig. 20. A) Daily specific growth rates and B) predawn chlorophyll content of *Picochlorum oklahomense* cultivated in replicate cycloturbidostats. Means are given for each influent [NO_3^-] group. 300 μM: n = 8 until day 20 then n = 2; 275 μM and 250 μM: n = 3.

The risk of failure due a slippery slope can also be related to improper acclimation of inoculum – cultures fed high N that exhibit high chlorophyll content have a greater need for N than properly acclimated cultures. In the trial shown in Figure 20, it is likely that this situation resulted in an inadequate cell-specific N supply and cultures crashed through day 5 when supplemental N and P was manually added to the cultures to restart growth and restore turbidostat operation.

This trial also demonstrates how cultures held at near-limiting nutrient supply rates will likely exhibit higher variability as cells are supplied just enough N to grow rapidly and maintain division but are vulnerable to incipient N limitation if supply is disturbed or decreased. Likewise, discrepancies in cell density between units likely led to confounding results, i.e., cultures in the 275 μM treatment suffered more from low growth rate on days 25-30 than cultures in the 250 μM treatment (Fig. 20A).

A different experimental trial also illustrates the vulnerability of cycloturbidostats under near-limiting nitrate supply rates. While duplicate replete cultures achieved and maintained a steady-

state through day 7 and on, the duplicate limited cultures began to fail on day 3 until supplemental N and P was added on day 5 (Fig. 21A). These nitrate-limited cultures then slowly make their way towards a steady-state that more closely resembles replete growth with a slightly reduced growth rate. Cell count is significantly more variable in the limited cultures until a steady-state is reached (Fig. 21B). As in other trials, there is no difference in either F_v/F_m or $rETR_{max}$ (Fig. 21C).

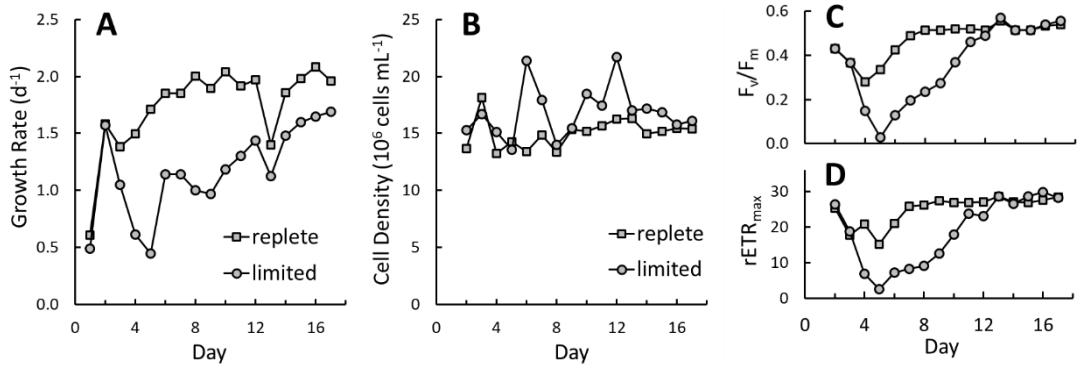

Fig. 21. A) Specific growth rates, B) predawn cell density, C) predawn F_v/F_m, D) predawn $rETR_{max}$ of *Picochlorum oklahomense* cultivated in duplicate cycloturbidostats at replete (300 μM) and limited (250 μM) [NO_3^-] conditions.

An interruption in CO_2 supply can be another source of perturbations when cultures are fed supplementally – having an extra full tank at the ready is a simple mitigation strategy (Fig. 20, day 21; Fig. 21, day 13). However, interruptions in CO_2 supply seem to resolve quickly and have less of an effect on growth parameters than interruptions in media supply or changes in irradiance.

All the facets discussed above: system mechanics, abiotic environmental factors, inoculation and inoculum life-history, nutrient regime, etc., drive variability between cultures and between days to varying degrees and are important considerations for any future cycloturbidostats studies.

2.3 Cycloturbidostat Experimental Design

Designing continuous culture experiments is not trivial – they are long, laborious, and detailed. So, experiments will benefit from ample planning, organized notation via datasheets etc., and by streamlining workflows. Trials should be designed in a manner that maximizes replication and cultures should be arranged so as not to introduce bias from subtle lighting or temperature differences. The trial depicted in Fig. 20 utilized two controls bottles and three bottles for each of the two treatment groups; this not only made for a less-than-ideal arrangement for the randomization of cultures but also diminished statistical power by spreading out cultures among three groups. Likewise, if the differences between treatments is too subtle the signal from experimental treatments may get lost in the noise; this trial assumed the difference between 300 μM, 275 μM, and the 250 μM treatments would be significant enough to measure – this was not the case. Subsequent trials benefited from having four controls bottles and four treatment bottles.

The species to be cultured is obviously an important choice in continuous culture experimental design. Nutritional needs between distinct algal lineages can be quite different and small nutritional deficiencies in culture media will be quickly exacerbated at high growth rates and by dilution over time. Likewise, pH can vary widely in rapidly growing cultures and may affect growth depending on species and media formulation.

We utilized our system to successfully grow a number of species including *Picochlorum oklahomense, Picochlorum* SENEW3, *Dunaliella* spp., and co-cultures of *Dunaliella* sp. GSP-980625-1E with either the cyanobacterium *Aphanothece* or the diatom *Phaeodactylum tricornutum* (CCMP 1327). We trialed other bioprospected strains of *Chlorella* sp. but found filamentous contaminants and abandoned this strain for other readily culturable strains. Filamentous contamination will inevitably lead flocculation of biomass which invalidates turbidity measurements and clogs tubing. This highlights the importance of not only species and inoculum choice, but tubing and bottle material as well. Certain plastics and rubbers tend to form

biofilms. Some species also tend to stick to bottle walls, whether because of extracellular secretions, large flagella, or benthic growth forms.

We also trialed the diatom *Thalassiosira pseudonana* but found issues with attaining reliable steady-states (Fig. 22). This species has a tendency towards lower temperatures, lower light, and requires available silica to build its frustule. We suspected temperature, light, and media formulation was the cause of slow growth and culture crash. After the addition of Tris buffer and some alterations to media preparation and formulation, we were able to maintain growth with this species; the addition of selenium to the media and a water bath to cool the culture bottles were other important changes. An additional factor could be that centric diatoms like *Thalassiosira* exhibit complex cell cycle where frustule size decreases over generations giving rise to unpredictable patters. Likewise, the presence of ammonia has been shown to induce the sexual cell cycle in *Thalassiosira* [102]. Not surprisingly, we confirmed the presence of sexual cell-types like oogonia in our cycloturbidostat cultures. As such, even after troubleshooting, unpredictable cycloturbidostat behavior continued with this species – when some units were growing fine, others were inexplicably stalled or began to crash as on days 15 – 22 (Fig. 22A).

However, these trials did show diel cycling of cell count and chlorophyll content in fast growing cultures (Fig. 22B). Interestingly, while *Thalassiosira pseudonana* exhibits a diel cycle of C:N (Fig. 22C), we detected little difference in C:N molar ratio over the diel cycle in *Picochlorum oklahomense* (data not shown). These limited results from a less-than-successful trial illuminate physiological differences between species and thereby highlight the utility of the cycloturbidostat system.

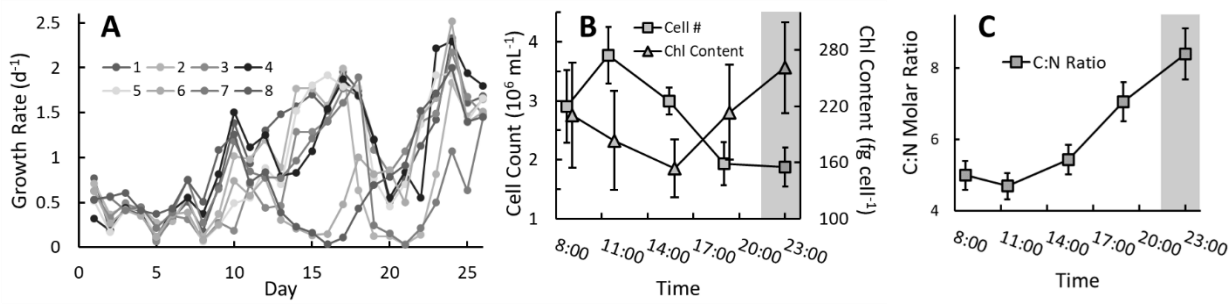

Fig. 22. A) Daily specific growth rates, B) predawn cell density and chlorophyll content, and C) C:N molar ratio of *Thalassiosira pseudonana* cultivated in replicate cycloturbidostats. Means in panels B and C are from cultures growing at >1 d^{-1} over a three-day period.

The determination of steady-state is a central issue in continuous culture studies. Some have defined steady-state balanced growth as less than a 10% change in growth parameters over a 3-day period. However, this is not a universal benchmark, it is somewhat arbitrary, and was set by studies utilizing turbidostats under continuous light, which vastly decreases the variability in growth parameters. If the photoperiod is not central to a study, considerable variability may be avoided by removing the photoperiod, but this limits the ecological applicability of the conclusions.

One important operational limitation of turbidostats is the restricted ability to sample from the without perturbing the equilibrium – decreased culture volume will result in an elevated concentration of limiting nutrient at the same nutrient supply rate until the full culture volume is restored. This means that destructive assays of biomass or any measure requiring large volumes of culture are limited and must be planned accordingly ahead of time.

Another difficulty in sampling relates to gathering time-sensitive measures such as chlorophyll fluorescence from multiple replicate cultures over multiple time-points. These samples may need to be incubated in the dark for a time further complicating data acquisition. An additional difficult-to-control consideration for physiological measures is the interplay between nutrient

supply and physiological status. Anecdotally, we found that F_v/F_m and $rETR_{max}$ fluctuated during the day in accordance with pump cycles, i.e., nutrient supply. Measures of $[NO_3]$ showed that levels after a pump cycle averaged *ca*. 10 μM before falling to 0 μM before the next pump cycle – this complicated obtaining chlorophyll fluorescence measure during the day. All of this complexity in cycloturbidostat dynamics complicates the interpretation and analysis of the resulting data.

4.0 Conclusion:

Be it comparative trials between strains or conditions, pilot-scale production trials, or novel applications, there is no doubt of the versatility of continuous cultures. While performing these experiments is daunting, their rhythm and routine can be a labor of love. It is my intent to inspire and inform those who wish to utilize continuous culture and in particular turbidostats in their studies and know they will contribute much to future research in microalgal biotechnology.

REFERENCES

[1] Berman-Frank, I., Dubinsky, Z., Balanced growth in aquatic plants: Myth or reality? Phytoplankton use the imbalance between carbon assimilation and biomass production to their strategic advantage, Bioscience, 49 (1999) 29-37, DOI: 10.2307/1313491.

[2] Flynn, K.J., Use, abuse, misconceptions and insights from quota models—the Droop cell quota model 40 years on, Oceanography and Marine Biology, CRC Press2008, pp. 7-30.

[3] Flynn, K.J., The importance of the form of the quota curve and control of non-limiting nutrient transport in phytoplankton models, Journal of Plankton Research, 30 (2008) 423-438, DOI: 10.1093/plankt/fbn007.

[4] Adams, C., Godfrey, V., Wahlen, B., et al., Understanding precision nitrogen stress to optimize the growth and lipid content tradeoff in oleaginous green microalgae, Bioresour Technol, 131 (2013) 188-194, DOI: 10.1016/j.biortech.2012.12.143.

[5] Li-Beisson, Y., Thelen, J.J., Fedosejevs, E., et al., The lipid biochemistry of eukaryotic algae, Prog Lipid Res, 74 (2019) 31-68, DOI: 10.1016/j.plipres.2019.01.003.

[6] Benemann, J.R., Woertz, I., Lundquist, T., Autotrophic microalgae biomass production: From niche markets to commodities, Industrial Biotechnology, 14 (2018) 3-10, DOI: 10.1089/ind.2018.29118.jrb.

[7] Borowitzka, M., Commercial-scale production of microalgae for bioproducts, Blue biotechnology: production and use of marine molecules, 1 (2018) 33-65, DOI: 10.1002/9783527801718.ch2.

[8] White, R.L., Ryan, R.A., Long-term cultivation of algae in open-raceway ponds: Lessons from the field, Industrial Biotechnology, 11 (2015) 213-220, DOI: 10.1089/ind.2015.0006.

[9] Henley, W.J., The past, present and future of algal continuous cultures in basic research and commercial applications, Algal Research, 43 (2019) 101636, DOI: 10.1016/j.algal.2019.101636.

[10] Chisholm, S., Stross, R., Phosphate uptake kinetics in *Euglena gracilis* (z)(Euglenophyceae) grown in light/dark cycles. i. Phased po4-limited cultures, Journal of Phycology, 12 (1976) 217-222.

[11] MacIntyre, H.L., Cullen, J.J., Using cultures to investigate the physiological ecology of microalgae, Algal Culturing Techniques, (2005) 287-326, DOI: 10.1016/B978-012088426-1/50020-2.

[12] Klok, A.J., Martens, D.E., Wijffels, R.H., et al., Simultaneous growth and neutral lipid accumulation in microalgae, Bioresour Technol, 134 (2013) 233-243, DOI: 10.1016/j.biortech.2013.02.006.

[13] Novoveská, L., Henley, W.J., Lab-scale testing of a two-stage continuous culture system for microalgae, Industrial Biotechnology, 10 (2014) 228-236, DOI: 10.1089/ind.2013.0034.

[14] Klok, A.J., Verbaanderd, J.A., Lamers, P.P., et al., A model for customising biomass composition in continuous microalgae production, Bioresour Technol, 146 (2013) 89-100, DOI: 10.1016/j.biortech.2013.07.039.

[15] Lacour, T., Sciandra, A., Talec, A., et al., Diel variations of carbohydrates and neutral lipids in nitrogen-sufficient and nitrogen-starved cyclostat cultures of *Isochrysis* sp., J Phycol, 48 (2012) 966-975, DOI: 10.1111/j.1529-8817.2012.01177.x.

[16] Lacour, T., Sciandra, A., Talec, A., et al., Neutral lipid and carbohydrate productivities as a response to nitrogen status in *Isochrysis* sp. (t-Iso; Haptophyceae): Starvation versus limitation, Journal of phycology, 48 (2012) 647-656, DOI: 10.1111/j.1529-8817.2012.01154.x.

[17] Wen, X., Geng, Y., Li, Y., Enhanced lipid production in *Chlorella pyrenoidosa* by continuous culture, Bioresour Technol, 161 (2014) 297-303, DOI: 10.1016/j.biortech.2014.03.077.

[18] Liu, J., Yao, C., Meng, Y., et al., The δ f/f m′-guided supply of nitrogen in culture medium facilitates sustainable production of tag in *Nannochloropsis oceanica* imet1, Biotechnology for biofuels, 11 (2018) 1-9.

[19] Edmundson, S.J., Huesemann, M.H., The dark side of algae cultivation: Characterizing night biomass loss in three photosynthetic algae, *Chlorella sorokiniana, Nannochloropsis salina* and *Picochlorum* sp, Algal research, 12 (2015) 470-476, DOI: 10.1016/j.algal.2015.10.012.

[20] Halsey, K.H., O'Malley, R.T., Graff, J.R., et al., A common partitioning strategy for photosynthetic products in evolutionarily distinct phytoplankton species, New Phytol, 198 (2013) 1030-1038, DOI: 10.1111/nph.12209.

[21] Hildebrand, M., Frigeri, L.G., Davis, A.K., Synchronized growth of *Thalassiosira pseudonana* (Bacillariophyceae) provides novel insights into cell-wall synthesis processes in relation to the cell cycle, Journal of Phycology, 43 (2007) 730-740, DOI: 10.1111/j.1529-8817.2007.00361.x.

[22] Porra, R., Thompson, W., Kriedemann, P., Determination of accurate extinction coefficients and simultaneous equations for assaying chlorophylls a and b extracted with four different solvents: Verification of the concentration of chlorophyll standards by atomic absorption spectroscopy, Biochimica et Biophysica Acta (BBA)-Bioenergetics, 975 (1989) 384-394, DOI: 10.1016/S0005-2728(89)80347-0

[23] Terashima, M., Freeman, E.S., Jinkerson, R.E., et al., A fluorescence-activated cell sorting-based strategy for rapid isolation of high-lipid *Chlamydomonas* mutants, The Plant Journal, 81 (2015) 147-159, DOI: 10.1111/tpj.12682.

[24] Van Wychen, S., Ramirez, K., Laurens, L.M., Determination of total lipids as fatty acid methyl esters (FAME) by in situ transesterification: Laboratory analytical procedure (LAP), National Renewable Energy Lab.(NREL), Golden, CO (United States), 2016, DOI: 10.2172/1118085.

[25] Schnetger, B., Lehners, C., Determination of nitrate plus nitrite in small volume marine water samples using vanadium (iii) chloride as a reduction agent, Marine Chemistry, 160 (2014) 91-98, DOI: 10.1016/j.marchem.2014.01.010.

[26] Weissman, J.C., Likhogrud, M., Thomas, D.C., et al., High-light selection produces a fast-growing *Picochlorum celeri*, Algal Research, 36 (2018) 17-28, DOI: 10.1016/j.algal.2018.09.024.

[27] Kolber, Z., Zehr, J., Falkowski, P., Effects of growth irradiance and nitrogen limitation on photosynthetic energy conversion in photosystem ii, Plant Physiol, 88 (1988) 923-929, DOI: 10.1104/pp.88.3.923.

[28] Dubinsky, Z., Berman-Frank, I., Uncoupling primary production from population growth in photosynthesizing organisms in aquatic ecosystems, Aquatic Sciences, 63 (2001) 4-17, DOI: 10.1007/PL00001343.

[29] Huppe, H., Turpin, D., Integration of carbon and nitrogen metabolism in plant and algal cells, Annual review of plant biology, 45 (1994) 577-607, DOI: 10.1146/annurev.pp.45.060194.003045.

[30] Bišová, K., Zachleder, V., Cell-cycle regulation in green algae dividing by multiple fission, Journal of experimental botany, 65 (2014) 2585-2602, DOI: 10.1093/jxb/ert466.

[31] Dahlin, L.R., Gerritsen, A.T., Henard, C.A., et al., Development of a high-productivity, halophilic, thermotolerant microalga *Picochlorum renovo*, Commun Biol, 2 (2019) 388, DOI: 10.1038/s42003-019-0620-2.

[32] Gonzalez-Esquer, C.R., Wright, K.T., Sudasinghe, N., et al., Demonstration of the potential of *Picochlorum soloecismus* as a microalgal platform for the production of renewable fuels, Algal Research, 43 (2019) 101658, DOI: 10.1016/j.algal.2019.101658.

[33] Henley, W.J., Hironaka, J.L., Guillou, L., et al., Phylogenetic analysis of the '*Nannochloris*-like'algae and diagnoses of *Picochlorum oklahomensis* gen. et sp. nov. (Trebouxiophyceae, Chlorophyta), Phycologia, 43 (2004) 641-652, DOI: 10.2216/i0031-8884-43-6-641.1.

[34] Steadman, C.R., Banerjee, S., Kunde, Y.A., et al., Inhibition of DNA methylation in *Picochlorum soloecismus* alters algae productivity, Front Genet, 11 (2020) 560444, DOI: 10.3389/fgene.2020.560444.

[35] Lammers, P.J., Huesemann, M., Boeing, W., et al., Review of the cultivation program within the National Alliance for Advanced Biofuels and Bioproducts, Algal research, 22 (2017) 166-186, DOI: 10.1016/j.algal.2016.11.021.

[36] Lee, P.A., White, R.L., Agronomic practices for photoautotrophic production of algae biomass, Grand challenges in algae biotechnology, Springer2019, pp. 111-156, DOI: 10.1007/978-3-030-25233-5_4.

[37] Unkefer, C.J., Sayre, R.T., Magnuson, J.K., et al., Review of the algal biology program within the national alliance for advanced biofuels and bioproducts, Algal research, 22 (2017) 187-215, DOI: 10.1016/j.algal.2016.06.002.

[38] Borowitzka, M.A., Siva, C.J., The taxonomy of the genus *Dunaliella* (Chlorophyta, Dunaliellales) with emphasis on the marine and halophilic species, Journal of Applied Phycology, 19 (2007) 567-590, DOI: 10.1007/s10811-007-9171-x.

[39] Krienitz, L., Bock, C., Present state of the systematics of planktonic coccoid green algae of inland waters, Hydrobiologia, 698 (2012) 295-326.

[40] Yamamoto, M., Nozaki, H., Miyazawa, Y., et al., Relationship between presence of a mother cell wall and speciation in the unicellular microalga *Nannochloris* (Chlorophyta), Journal of Phycology, 39 (2003) 172-184, DOI: 10.1046/j.1529-8817.2003.02052.x.

[41] Assunção, P., Jaén-Molina, R., Caujapé-Castells, J., et al., Phylogenetic analysis of its2 sequences suggests the taxonomic re-structuring of *Dunaliella viridis* (Chlorophyceae, Dunaliellales), Phycological Research, 61 (2013) 81-88, DOI: 10.1111/pre.12003.

[42] Foflonker, F., Mollegard, D., Ong, M., et al., Genomic analysis of *Picochlorum* species reveals how microalgae may adapt to variable environments, Molecular Biology and Evolution, 35 (2018) 2702-2711, DOI: 10.1093/molbev/msy167.

[43] Foflonker, F., Price, D.C., Qiu, H., et al., Genome of the halotolerant green alga *Picochlorum* sp. Reveals strategies for thriving under fluctuating environmental conditions, Environmental microbiology, 17 (2015) 412-426, DOI: 10.1111/1462-2920.12541.

[44] Cross, F.R., Regulation of multiple fission and cell-cycle-dependent gene expression by cdka1 and the rb-e2f pathway in *Chlamydomonas*, Current Biology, 30 (2020) 1855-1865. e1854, DOI: 10.1016/j.cub.2020.03.019.

[45] Zhang, W., Liu, H.T., Mapk signal pathways in the regulation of cell proliferation in mammalian cells, Cell Research, 12 (2002) 9-18, DOI: 10.1038/sj.cr.7290105.

[46] Umen, J.G., Goodenough, U.W., Control of cell division by a retinoblastoma protein homolog in *Chlamydomonas*, Genes & Development, 15 (2001) 1652-1661.

[47] Zachleder, V., Bišová, K., Vítová, M., The cell cycle of microalgae, The physiology of microalgae, Springer2016, pp. 3-46, DOI: 10.1007/978-3-319-24945-2_1.

[48] Fang, S.-C., Umen, J.G., A suppressor screen in *Chlamydomonas* identifies novel components of the retinoblastoma tumor suppressor pathway, Genetics, 178 (2008) 1295-1310.

[49] Ivanov, I.N., Vitova, M., Bisova, K., Growth and the cell cycle in green algae dividing by multiple fission, Folia Microbiol (Praha), 64 (2019) 663-672, DOI: 10.1007/s12223-019-00741-z.

[50] Foflonker, F., Ananyev, G., Qiu, H., et al., The unexpected extremophile: Tolerance to fluctuating salinity in the green alga *Picochlorum*, Algal Research, 16 (2016) 465-472, DOI: 10.1016/j.algal.2016.04.003.

[51] Becker, S.A., Spreafico, R., Kit, J.L., et al., Phased diploid genome sequence for the fast-growing microalga *Picochlorum celeri*, Microbiology Resource Announcements, 9 (2020) e00087-00020, DOI: 10.1128/MRA.00087-20.

[52] Wang, S., Shi, X., Palenik, B., Characterization of *Picochlorum* sp. Use of wastewater generated from hydrothermal liquefaction as a nitrogen source, Algal Research, 13 (2016) 311-317, DOI: 10.1016/j.algal.2015.11.015.

[53] Franks, D. T., Sabella, T. J., & Henley, W. J. (2022). Minimum nitrogen cell quota for maximal growth rate in cycloturbidostat cultures of Picochlorum oklahomense. Algal Research, 67, 102818.

[54] Hlavová, M., Vítová, M., Bišová, K., Synchronization of green algae by light and dark regimes for cell cycle and cell division studies, Plant cell division, Springer 2016, pp. 3-16, DOI: 10.1007/978-1-4939-3142-2_1.

[55] Vítová, M., Bišová, K., Hlavová, M., et al., *Chlamydomonas reinhardtii*: Duration of its cell cycle and phases at growth rates affected by temperature, Planta, 234 (2011) 599-608, DOI: 10.1007/s00425-011-1427-7.

[56] Cross, F.R., Umen, J.G., The *Chlamydomonas* cell cycle, The Plant Journal, 82 (2015) 370-392.

[57] Koren, I., Boussiba, S., Khozin-Goldberg, I., et al., *Chromochloris zofingiensis* (Chlorophyceae) divides by consecutive multiple fission cell-cycle under batch and continuous cultivation, Biology, 10 (2021) 157, DOI: 10.3390/biology10020157.

[58] Umen, J.G., The elusive sizer, Current opinion in cell biology, 17 (2005) 435-441.

[59] Becker, S.A., Spreafico, R., Kit, J.L., et al., Phased diploid genome sequence for the fast-growing microalga *Picochlorum celeri*, Microbiology Resource Announcements, 9 (2020) e00087-00020, DOI: doi:10.1128/MRA.00087-20.

[60] Krasovec, M., Vancaester, E., Rombauts, S., et al., Genome analyses of the microalga *Picochlorum* provide insights into the evolution of thermotolerance in the green lineage, Genome Biology and Evolution, 10 (2018) 2347-2365, DOI: 10.1093/gbe/evy167.

[61] Li, X., Umen, J.G., Jonikas, M.C., Waking sleeping algal cells, Proceedings of the National Academy of Sciences, 111 (2014) 15610-15611.

[62] Li, Y., Liu, D., Lopez-Paz, C., et al., A new class of cyclin dependent kinase in chlamydomonas is required for coupling cell size to cell division, Elife, 5 (2016) e10767.

[63] Tsai, C.-H., Warakanont, J., Takeuchi, T., et al., The protein compromised hydrolysis of triacylglycerols 7 (cht7) acts as a repressor of cellular quiescence in *Chlamydomonas*, Proceedings of the National Academy of Sciences, 111 (2014) 15833-15838.

[64] Takeuchi, T., Sears, B.B., Lindeboom, C., et al., *Chlamydomonas* cht7 is required for an effective quiescent state by regulating nutrient-responsive cell cycle gene expression, The Plant Cell, 32 (2020) 1240-1269.

[65] Rhee, G.-Y., Gotham, I.J., Chisholm, S.W., Use of cyclostat cultures to study phytoplankton ecology, Continuous culture of cells, 2 (1981) 159-187.

[66] Knoshaug, E., Laurens, L., Kinchin, C., et al., Use of cultivation data from the algae testbed public private partnership as utilized in NREL's algae state of technology assessments, National Renewable Energy Lab.(NREL), Golden, CO (United States), 2016.

[67] McGowen, J., Knoshaug, E.P., Laurens, L.M., et al., The Algae Testbed Public-Private Partnership (ATP3) framework; establishment of a national network of testbed sites to support sustainable algae production, Algal Research, 25 (2017) 168-177.

[68] Knoshaug, E.P., Wolfrum, E., Laurens, L.M., et al., Unified field studies of the Algae Testbed Public-Private Partnership as the benchmark for algae agronomics, Scientific data, 5 (2018) 1-10.

[69] Berndt, A.J., Smalley, T.N., Ren, B., et al., Recombinant production of a functional sars-cov-2 spike receptor binding domain in the green algae *Chlamydomonas reinhardtii*, PloS One, 16 (2021) e0257089.

[70] Gregory, J.A., Li, F., Tomosada, L.M., et al., Algae-produced pfs25 elicits antibodies that inhibit Malaria transmission, PloS One, 7 (2012) e37179.

[71] Jones, C.S., Luong, T., Hannon, M., et al., Heterologous expression of the c-terminal antigenic domain of the malaria vaccine candidate pfs48/45 in the green algae *Chlamydomonas reinhardtii*, Applied microbiology and biotechnology, 97 (2013) 1987-1995.

[72] Rasala, B.A., Mayfield, S.P., Photosynthetic biomanufacturing in green algae; production of recombinant proteins for industrial, nutritional, and medical uses, Photosynthesis Research, 123 (2015) 227-239.

[73] Rosales-Mendoza, S., Solís-Andrade, K.I., Márquez-Escobar, V.A., et al., Current advances in the algae-made biopharmaceuticals field, Expert Opinion on Biological Therapy, 20 (2020) 751-766.

[74] Specht, E., Miyake-Stoner, S., Mayfield, S., Micro-algae come of age as a platform for recombinant protein production, Biotechnology Letters, 32 (2010) 1373-1383.

[75] Surzycki, R., Greenham, K., Kitayama, K., et al., Factors effecting expression of vaccines in microalgae, Biologicals, 37 (2009) 133-138.

[76] Borowitzka, M.A., Techno-economic modeling for biofuels from microalgae, Algae for biofuels and energy, Springer 2013, pp. 255-264.

[77] Judd, S.J., Al Momani, F., Znad, H., et al., The cost benefit of algal technology for combined co2 mitigation and nutrient abatement, Renewable and Sustainable Energy Reviews, 71 (2017) 379-387.

[78] Panis, G., Carreon, J.R., Commercial astaxanthin production derived by green alga *Haematococcus pluvialis*: A microalgae process model and a techno-economic assessment all through production line, Algal Research, 18 (2016) 175-190.

[79] Tan, W., Roi-integrated commercialization: An adaptive pathway for microalgae technology, Industrial Biotechnology, 14 (2018) 17-24.

[80] Bull, A.T., The renaissance of continuous culture in the post-genomics age, Journal of Industrial Microbiology and Biotechnology, 37 (2010) 993-1021.

[81] Tamiya, H., Synchronous cultures of algae, Annual review of plant physiology, 17 (1966) 1-27.

[82] Chisholm, S., Stross, R.G., Nobbs, P.A., Light/dark-phased cell division in *Euglena gracilis* (z)(Euglenophyceae) in PO_4-limited continuous culture, Journal of Phycology, 11 (1975) 367-373.

[83] Frisch, H., Gotham III, I., On periodic algal cyclostat populations, Journal of Theoretical Biology, 66 (1977) 665-678.

[84] de Vree, J.H., Bosma, R., Wieggers, R., et al., Turbidostat operation of outdoor pilot-scale photobioreactors, Algal Research, 18 (2016) 198-208.

[85] Droop, M., The nutrient status of algal cells in continuous culture, Journal of the Marine Biological Association of the United Kingdom, 54 (1974) 825-855.

[86] Tamiya, H., Mass culture of algae, Annual Review of Plant Physiology, 8 (1957) 309-334.

[87] Posewitz, M., Pace: Producing algae for coproducts and energy, Colorado School of Mines, Golden, CO (United States), 2022.

[88] Rusch, K.A., Christensen, J.M., The hydraulically integrated serial turbidostat algal reactor (HISTAR) for microalgal production, Aquacultural engineering, 27 (2003) 249-264.

[89] Droop, M.R., 25 years of algal growth kinetics a personal view, (1983).

[90] Gotham, I.J., Rhee, G.Y., Comparative kinetic studies of phosphate-limited growth and phosphate uptake in phytoplankton in continuous culture, Journal of Phycology, 17 (1981) 257-265.

[91] Hase, E., Morimura, Y., Tamiya, H., Some data on the growth physiology of *Chlorella* studied by the technique of synchronous culture, Archives of Biochemistry and Biophysics, 69 (1957) 149-165.

[92] Laws, E.A., Bannister, T., Nutrient-and light-limited growth of *Thalassiosira fluviatilis* in continuous culture, with implications for phytoplankton growth in the ocean, Limnology and Oceanography, 25 (1980) 457-473.

[93] Rhee, G.Y., A continuous culture study of phosphate uptake, growth rate and polyphosphate in *Scenedesmus* sp., Journal of Phycology, 9 (1973) 495-506.

[94] van Liere, L., MUR, L.R., Growth kinetics of *Oscillatoria agardhii* Gomont in continuous culture, limited in its growth by the light energy supply, Microbiology, 115 (1979) 153-160.

[95] Remmers, I.M., Hidalgo-Ulloa, A., Brandt, B., et al., Continuous versus batch production of lipids in the microalgae acutodesmus obliquus, Bioresource technology, 244 (2017) 1384-1392.

[96] Cano, M., Karns, D.A.J., Weissman, J.C., et al., Pigment modulation in response to irradiance intensity in the fast-growing alga *Picochlorum celeri*, *Algal Rese*arch, 58 (2021) 102370, DOI: https://doi.org/10.1016/j.algal.2021.102370.

[97] Mayfield, S.P., Consortium for algal biofuel commercialization (CAB-Comm) final report, Univ. of California, San Diego, CA (United States), 2015.

[98] Novoveská, L., Franks, D.T., Wulfers, T.A., et al., Stabilizing continuous mixed cultures of microalgae, Algal Research, 13 (2016) 126-133.

[99] Benson, B.C., Rusch, K.A., Investigation of the light dynamics and their impact on algal growth rate in a hydraulically integrated serial turbidostat algal reactor (HISTAR), Aquacultural Engineering, 35 (2006) 122-134.

[100] Rusch, K.A., Malone, R.F., Microalgal production using a hydraulically integrated serial turbidostat algal reactor (HISTAR): A conceptual model, Aquacultural engineering, 18 (1998) 251-264.

[101] Theegala, C., Malone, R., Rusch, K., Contaminant washout in a hydraulically integrated serial turbidostat algal reactor (HISTAR), Aquacultural Engineering, 19 (1999) 223-241.

[102] Moore, E.R., Bullington, B.S., Weisberg, A.J., et al., Morphological and transcriptomic evidence for ammonium induction of sexual reproduction in *Thalassiosira pseudonana* and other centric diatoms, PLoS One, 12 (2017) e0181098.

VITA

Dylan Taylor Franks

Candidate for the Degree of

Doctor of Philosophy

Dissertation: MAINTAINING NITROGEN-LIMITED BALANCED-GROWTH STATES IN A CYCLO-TURBIDOSTAT

Major Field: Plant Science

Biographical:

Education:

Completed the requirements for the Doctor of Philosophy in Plant Science at Oklahoma State University, Stillwater, Oklahoma in May 2023.

Completed the requirements for the Bachelor of Science in Chemistry & Biochemistry at Colorado School of Mines, Golden, Colorado in 2012.

Experience:

Graduate Teaching Assistant for Dr. Donald French in the Department of Integrative Biology at Oklahoma State University from 2013 – 2020.

Undergraduate Researcher for Dr. Matthew Posewitz in the Department of Chemistry & Geochemistry at Colorado School of Mines from 2010-‘12.

Professional Memberships:

Algae Biomass Organization Member since 2014, Communications Committee 2018, Planning Comm. 2020-‘22, and Summit Co-Chair 2023.